

# AUBURN RESEARCH

*A Showcase of Research and Creative Scholarship*  
Proceedings of the 2020  
Virtual Student Symposium



# TABLE OF CONTENTS

Letter from the Vice President for Research & Economic Development..... 4

Research Symposium Committee Members..... 5

## RESEARCH SUMMARIES

**Nutrigenomics Approach to Dampen the Negative Effects of Endophyte-Infected Tall Fescue on Beef Cow-Calf Pair Performance**  
*Gastón Alfaro, Russell Muntifering, Soren Rodning, Julie Gard, Robert Cole, Wilmer Pacheco, and Sonia Moisés*.....6-7

**Design and Optimization of a Continuous Bioreactor for Enhanced Cell Culture**  
*Rithvija Avvari, Paul Todd, and Thomas Hanley*.....8-9

**Preparation of Phenol-Formaldehyde Resins Using the Lignocellulosic Biomass (Lignin, Lignin and Lignocellulosic Pyrolysis Bio-Oil) for Use as a Wood Adhesive**  
*Archana Bansode, Mehul Barde, Osei Asafu-Adjaye, John Hinkle, Vivek Patil, Brian Via, Sushil Adhikari, Thomas Elder, Ramsis Farag, and Maria L. Auad* .....10-11

**Puerto Rico’s Iron Deposits: Developing a Genetic Model Through Field Observations and Geochemical Analyses**  
*Marisa Barefoot, Laura Bilenker and Thomas Hudgins* .....12-13

**Using an Interactive Phonetics Learning Management System and User-Centered Design to Inform Phonetics Education Methods**  
*Abigail Bennett and Marisha Speights Atkins*.....14-15

**Monitoring of Pastured Poultry for Parasites**  
*Maria Tereza Bethonico Terra and Ruediger Hauck*.....16-17

**Estimating Soil Phosphorus Storage Capacity of Major Soil Areas of Alabama: Implications for Environmental Loss Risk Assessment**  
*Anjan Bhatta, Rishi Prasad, and Debolina Chakraborty*.....18-19

**E. coli Bacteriophage PF-2 Displays a Reduction in Infectivity Following Treatment with Hydrogen Peroxide**  
*Madeleine Bruderer, Harrison Smith, Keah Higgins, and Elizabeth Hiltbold- Schwartz* .....20-21

**Evaluation of the Effects of Work and Heat Exposure on Cognitive Function in Firefighters**  
*Abigail Campbell, Angela Burns, Kaitlin Lyons, Oluwagbemiga Dademathews, Aaron Parks, Paige McHenry, and JoEllen Sefto*.....22-23

**Testing and Developing Recycled 3-D Printing Filament for Use in Space**  
*Rylee Cardon and Asha-Dee Celestine*.....24-25

**Investigating Ribosomal Protein Duplication in Yeast *S. cerevisiae***  
*Mary C. Carlton, Rosaleny Orie, Caleb Thomas, and Alexey Petrov*.....26-27

**Analyzing the Parameters That Influence Soft Tissue Artifact Frequencies**  
*Scot Carpenter, Michael Zabala, and Jacob Larson*.....28-29

**The Effect of Load Magnitude on Muscle Activation During Unilateral Overhead Dumbbell Carries**  
*Molly Cassidy, Nicole Bordelon, Kyle Wasserberger, and Gretchen Oliver*..... 30-31

**Targeting p38 MAPK as a Novel Approach for the Treatment of Aggressive Form of Human Prostate Cancer**  
*Sayak Chakravarti, Suman Mazumder, Taraswi Mitra-Ghosh, Robert D. Arnold, and Amit K. Mitra*.....32-33

**Effectiveness of Distinguishing Soil Types Using Unoccupied Aerial Vehicles (UAVs)**  
*Brett Clark, Stephanie Rogers, and Lorraine Wolf*.....34-35

**ACEs, Mindfulness, and Romantic Self-Efficacy’s Influence on Relationship Functioning: A Risk and Resilience Approach**  
*Erin Cooper, Francesca Adler-Baeder, and Julianne McGill* .....36-37

**Trunk Lateral Flexion Differences Between the Fastball and Curveball Pitch in Collegiate Softball Pitchers**  
*Abigail M. Cramer, Jessica Downs, and Gretchen Oliver* .....38-39

**Changing Land Use and Land Cover of Big Creek Lake Watershed, Mobile County, Alabama**  
*Eshita Eva and Luke Marzen*.....40-41

**“Connecting the Corridors”- Rethinking Parkerson Mill Creek, AU Campus**  
*Riffat Farjana* .....42-45

**Field and Laboratory Investigations of Groundwater Arsenic Sequestration in Biogenic Pyrite at an Industrial Site in Florida**  
*Alicia Fischer and Ming-Kuo Lee* .....46-47

**Binary Versus Ternary Metal Oxide Synthesis Pathways: A Study on Copper Oxide Formation Catalyzed by Group 13 Metals**  
*Noah Gibson, Alexandria Bredar, and Byron Farnum* .....48-51

**Effect of Load Magnitude on Muscle Activation During Unilateral Suitcase Dumbbell Carries**  
*Peyton Gober, Nicole Bordelon, and Gretchen Oliver*.....52-53

**Tiered Collaboration: Addressing the Impact of High Poverty School Culture on Novice Teachers**  
*Bertha Guilford and Mashika Tempero* .....54-55

**Development of a Novel Rotating Volumetric Velocimetry Technique for Rotor Flows**  
*Abhishek Gururaj, Mahyar Moaven, Zu Puayen Tan, Brian Thurow, and Vrishank Raghav* .....56-57

**Investigation of the Antibacterial Activity Against Foodborne Pathogens and Chemical Composition of Extracts and Partitions of *Psidium guajava***  
*Audrey Hall, Emefa Monu, and Angela Calderón*.....58-59

**The Effect of Trunk Kinematics on Net Normalized Shoulder Kinetics in Baseball Pitching**  
*Michael Hankes, Kevin Giordano, and Gretchen Oliver* .....60-61

**Racial Disparities in Sleep Among College Students**  
*William Illiano and Thomas E. Fuller-Rowell* .....62-63

**Off Campus Students’ Participation Gap Linked to Difficulties with Transportation and Parking**  
*Jhayla Isom and Sara Driskell* .....64-65

**Novel SIRT3 Agonist Alter Lipid Accumulation in Lipid Mediated Hepatic Steatosis**  
*Victoria Jimenez, Sieun Yoo, Ian Steinke, Jared Senfeld, Nila Ghanei, Taylor Schaedig, Manoj Govindarajulu, Forrest Smith, and Rajesh Amin*.....66-67

**Inventory and Characterization of Gulf Coast Salt Marsh Soil Resources**  
*Brooke Johnson and Joey Shaw*.....68-69

**Studying the Relevance of Stomatal Characteristics on Drought Tolerance in Peanut**  
*Seth Johnston and Alvaro Sanz-Saez*.....70-71

**Theoretical Studies on Non-Enzymatic Dipeptide Hydrolysis Reactions and Their Applicability to Other Therapeutics**  
*Katherine Lawson and Andrew Adamczyk*.....72-73

**Medicare Part D Prescription Payments by Prescriber Specialty Types in 2017**  
*Chao Li, Shahariar Fahim, Salisa Westrick, and Jingjing Qian*.....74-75

**Do Bark Beetle Associated Fungi Contribute to Loblolly Pine Decline and Mortality?**  
*John K. Mensah, Mary Sword Sayer, Ryan Nadel, George Matusick, Zhaofei Fan, and Lori Eckhardt*.....76-77

**The Effect of a pH-Dependent Arginine Switch on Protein-Based Cofactor Formation in Catalase-Peroxidase (KatG)**  
*Laura Minton, Hui Xu, Jessica Krewall, and Douglas Goodwin* .....78-79

**Petrographic and Geochemical Analyses to Elucidate the Genesis of Au-Ag Deposits on Florida Mountain Epithermal Deposit, Silver City District, Idaho**  
*Lucas Monroe, Laura Bilenker, Willis Hames, Raeann Garcia, and Will Ebbert*.....80-81

**The P2Y2 Nucleotide Receptor Mediates Tissue Factor Expression in Human Monocytes**  
*Qianman Peng and Jianzhong Shen*.....82-83

**Anthropometric Factors in Softball Hitting Performance**  
*Johann Phan, Kenzie Friesen, and Gretchen Oliver* .....84-85

**Gentamicin-Loaded 3D-Printed Metal Implants for Post-Surgical Infections**  
*Ishwor Poudel, Manjusha Annaji, Robert D. Arnold, Amal Kaddoumi, Nima Shamsaei, Seungjong Lee, Jonathan Pegues, Kayla Corriveau, and Jayachandra R. Babu* .....86-87

**Assessment of Angle of Repose as a Tool to Measure the Flowability of Different Particle Sizes of Ground Corn with and Without Added Soybean Oil**  
*Marc R. Presume, Jorge L. Sandoval, Gerardo A. Abascal-Ponciano, Allan J. Calderon, Danny B. Patino, Kevin E. Ordonez, Luis P. Avila, Samuel F. Leiva, Josh J. Flees, Wilmer J. Pacheco, and Charles W. Starkey*.....88-91

**Determining the Effect of Chinese Privet (*Ligustrum sinense*) Invasion on the Occurrence of Ground-Dwelling Herpetofauna Species**  
*Gabrielle Ripa, Christopher Anderson, and James Stiles*.....92-93

**High Chlorophyll Dietary Intervention in a High Red Meat Diet Caused No Significant Changes in Serum and Fecal Zonulin**  
*Aaron Riviere and Andrew Frugé*.....94-95

**Pore Network Modelling of Reactive Permeability Evolution**  
*Mollie Sabo and Lauren Beckingham*.....96-97

**Temperature Dependency of Magnetic Particle Characterization by Particle Tracking Velocimetry**  
*Abhinav Sannidhi, Thomas Hanley, and Paul Todd* .....98-99

**Assessment of Age and Region Differences in Health Beliefs and Dietary Habits Related to Colon Cancer Risk**  
*Megan Schaberg, Kristen Smith, Michael Greene, and Andrew Frugé*..... 100-103

**Engineering Lignin Transformation Mechanisms to Create Value-Added Products Using Atomistic Modeling**  
*Jonathan Schuler, Tanzina Azad, Maria Auad, Thomas Elder, and Andrew Adamczyk*..... 104-105

**Performance Enhancement of Ditch Check Practices During Highway Construction**  
*Jaime Schussler, Michael Perez, Bora Cetin, and Blake Whitman*.. 106-107

**3D Printing of Self-Healing Polymer Composites**  
*Vinita Shinde and Bryan Beckingham* ..... 108-109

**Study of the Vortex Interactions in the Near Wake of Coaxial Rotors in Hover**  
*Lokesh Silwal and Vrishank Raghav* ..... 110-111

**Enhancing Heat Transfer in Microgravity Through Vapor Mobility in Phase-Change Cooling**  
*Karthekeyan Sridhar, Ryan Smith, and Sushil Bhavnani*..... 112-113

**Development of MATLAB Trip/Slip Algorithms to Investigate the Effectiveness of Treadmill-Based Perturbation Training**  
*Jacob Stotser and Jaimie Roper*..... 114-115

**Investigating Late-Stage Polypeptide Diversification via Formation of Twisted Amides**  
*Xavier Streety, Mahesh Sriram, Victor Adebomi, and Monika Raj*..... 116-117

**Auburn University and the United Nations’ Sustainable Development Goals**  
*Hollen Terry and Alicia Powers*..... 118-119

**Effect of Different Inlet Velocity Profiles on Patient-Specific CFD Simulations of Healthy Trachea**  
*Bipin Tiwari, Tarun Kore, Zhenglun Alan Wei, Sandeep Bodduluri, Surya P. Bhatt, Vrishank Raghav*..... 120-121

**A Method of Containing Near-Source Undegraded Floating Plastic**  
*Zachary Wadzinski and Mark Dougherty* ..... 122-123

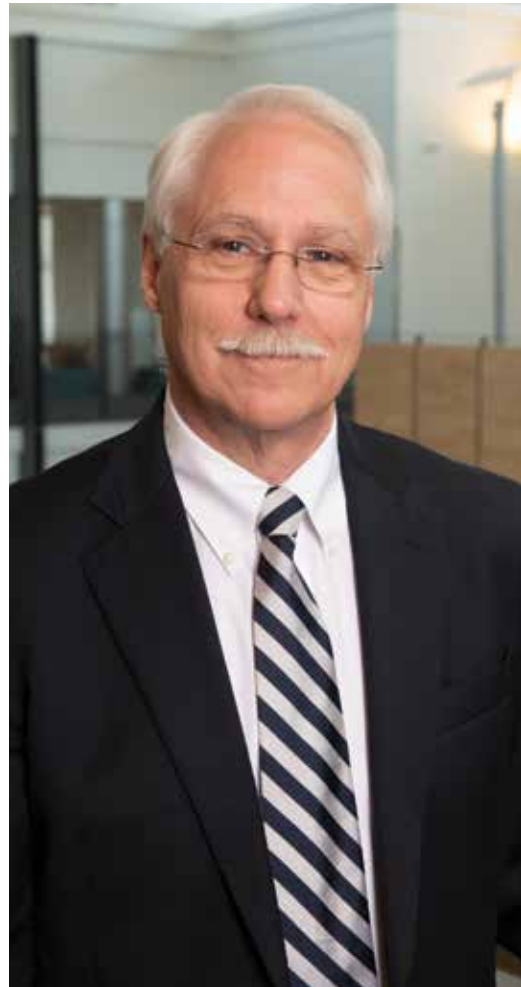
**Biocidal Properties of Europa Lander Solid Rocket Motor Adhesive, Loctite® EA9394, Against *Hypsibius dujardini***  
*Natalie Williams, Mark Liles, and Morgan Sisk* ..... 124-125

**Determining How Images of Different Exercise Contexts Are Spontaneously Registered in the Brain of Non-Exercisers via Electroencephalography (EEG)**  
*Victoria A. Zona, Juliana O. Parma, and Matthew W. Miller*..... 126-127

## SYMPOSIUM ABSTRACTS

Please [click here](#) to access symposium abstracts.

## LETTER FROM THE VICE PRESIDENT FOR RESEARCH & ECONOMIC DEVELOPMENT



James Weyhenmeyer, Ph.D.  
Vice President for Research  
& Economic Development

We are pleased to release the proceedings of the 2020 Auburn Research Virtual Student Symposium. With this publication, Auburn University takes a step forward in recognizing the academic and creative excellence of our graduate and undergraduate students in the midst of restrictions caused by the COVID-19 pandemic. The discoveries represented in the proceedings reflect the broad research expertise of our faculty coupled with the creative intuition and enthusiasm of many outstanding students.

The publication is divided into two sections: research summaries, consisting of extended abstracts that have been reviewed by faculty, and symposium abstracts that were originally accepted for presentation.

The summaries and abstracts contained in this volume represent only a small subset of our students' diverse intellectual endeavors and accomplishments. None of this research would have been possible without the commitment of our faculty to educating the next generation of scholars. We express our deepest appreciation for the faculty's efforts to extend our institution's research culture to our students.

We hope this publication will inspire readers to support and participate in the research process. Although often faced with obstacles, and sometimes even failure, students involved in research learn that success is the result of perseverance, hard work and creative passion.

**James Weyhenmeyer, Ph.D.**  
*Vice President for Research & Economic Development*

## RESEARCH SYMPOSIUM COMMITTEE MEMBERS

**Rodney Greer**  
*Assistant Dean for Research, College of Education (CHAIR)*

**Jennifer Kerpelman**  
*Associate Dean for Research, College of Human Sciences (past CHAIR)*

**Cynthia Bowling**  
*Associate Dean for Research, College of Liberal Arts*

**Jonathan Cullum**  
*Office of the Vice President for Research  
& Economic Development*

**Elizabeth Devore**  
*Graduate Student Council*

**Robert Holm**  
*Proposal Services and Faculty Support*

**Charles Martin**  
*Office of Communications and Marketing*

**Aaron Norris**  
*Graduate Student Council*

**Anthony Ventimiglia**  
*Proposal Services and Faculty Support*

**Lorraine W. Wolf**  
*Director of Undergraduate Research*

**Giovana Brannan**  
*Executive Assistant to the Vice President for Research  
& Economic Development*

# Nutrigenomics Approach to Dampen the Negative Effects of Endophyte-Infected Tall Fescue on Beef Cow-Calf Pair Performance

*Gastón Alfaro<sup>1</sup>, Russell Muntifering<sup>1</sup>, Soren Rodning<sup>1</sup>, Julie Gard<sup>2</sup>, Robert Cole<sup>2</sup>, Wilmer Pacheco<sup>3</sup>, and Sonia Moisés<sup>1</sup>*

Tall fescue (*Lolium arundinaceum* [Schreb.] Darbysh.) is a cool-season perennial bunch-grass originated in Western Europe and brought to the United States probably as a weed mixed with other grasses from Europe. Tall fescue is very popular among U.S. cattle producers because of different benefits such as good nutritional quality, long period of grazing, tolerance to high-density grazing, and the possibility to be used as a conserved forage (i.e. silage and hay) (Young et al., 2014). However, tall fescue is usually infected by *Epichloë coenophiala*, an endophyte fungus (Leuchtman et al., 2014). The mutualistic relationship between the plant and fungus produces secondary metabolites called ergot alkaloids. The ergopeptide ergovaline is the major alkaloid present in tall fescue, among other grasses. The negative effect of ergovaline in fescue utilization and cattle industry is fescue toxicity, which is a detrimental animal condition that causes a reduction of animal performance and it is associated with economic losses of approximately \$1 billion annually (Dillard et al., 2019). One of the physiological adverse effects of fescue toxicity is the vasoconstriction of peripheral vasculature and reduction in ovarian and uterine vessel area, causing a reduction in the blood flow of the gestating animals. Furthermore, vasoconstriction during gestation may lead to a reduction in offspring performance due to a lack of nutrients availability. The liver is the organ capable to detoxify the organism from ergot alkaloids thanks to the action of Cytochrome P450 and antioxidants.

Therefore, the objectives of this study were to assess the effect of a genetic test identifying animals resistant to fescue toxicity and the supplementation rumen-protected niacin, which is known as a vasodilator agent, on the performance of Angus-Simmental gestating dams receiving fescue seeds with high ergovaline concentration and to their offspring after weaning; and to analyze changes in the expression of genes related to oxidative stress in the liver due to ergot alkaloid

detoxification. Ninety days prior to calving, genotyped pregnant cows (n = 11) and heifers (n = 17) were stratified by body weight (BW; 540 ± 207 kg) and genetic resistance to fescue toxicity (susceptible or tolerant); and randomly assigned to dietary treatments: 1) Susceptible Control (SC); 2) Susceptible Niacin (SN); 3) Tolerant Control (TC); and 4) Tolerant Niacin (TN). Animals' BW and liver samples were obtained on days 0 and 29. Uterine arteries blood flow was measured using Doppler ultrasonography at treatment days 3, 10, 17, and 23. Messenger RNA was extracted from liver samples for RT-qPCR. Gene expression and BW data were analyzed using the PROC MIXED procedure of SAS, and uterine arteries blood flow was analyzed with the GLIMMIX procedure of SAS. Between day 0 and 29, *SOD1* and *CYP2E1* were upregulated (P < 0.05) in TC and SC, respectively. Furthermore, *SOD2* expression in SC was significantly lower (P < 0.05) on day 29. Genetic test and RPN did not affect uterine arteries' blood flow. TN animals had a greater decrease in BW compared with other treatments (P < 0.01). In conclusion, Doppler ultrasonography did not detect any changes in uterine arteries' blood flow, and supplementation with RPN may influence the oxidative status of cows' liver consuming endophyte-infected fescue seeds.

**Table 1.** Overall Least Mean Squares Values for Expression of Genes Analyzed in Liver of Angus-Simmental Dams. Treatment, time, and treatment × time P-values of expression of genes related to oxidative stress. Background: Pink color (P < 0.05), yellow (0.05 < P < 0.1)

Gene	DAY 0				DAY 29				SEM	P - value		
	SC	SN	TC	TN	SC	SN	TC	TN		Trt	Time	Trt*Time
SOD1	0.853	0.992	0.870	0.902	0.939	1.037	1.132	0.992	0.051	0.082	0.001	0.152
SOD2	0.697	0.861	0.905	0.938	0.856	1.067	1.135	1.184	0.073	0.001	0.001	0.986
CYP3A5	0.699	2.034	1.494	1.726	0.982	1.456	1.369	1.528	0.411	0.141	0.131	0.283
CYP2E1	0.701	1.273	1.040	1.812	1.591	1.286	1.162	0.872	0.286	0.200	0.163	0.032
CYP3A4	0.748	0.828	1.269	0.929	1.155	0.971	1.153	1.037	0.147	0.318	0.069	0.315
PON1	0.688	1.026	0.983	0.916	0.840	0.995	1.048	0.933	0.165	0.388	0.663	0.952
ATP5F1B	0.610	0.951	0.916	0.873	0.850	0.944	1.014	0.970	0.097	0.184	0.064	0.338

## References

- Dillard, L. S., Smith, S. R., & Hancock, D. W. (2019). Variability of ergovaline and total ergot alkaloid expression among endophytic tall fescue cultivars. *Crop Science*, 59(6): 2866-2875.
- Leuchtman, A., Bacon, C. W., Schardl, C. L., White, J. F., & Tadych, M. (2014). Nomenclatural realignment of *Neotyphodium* species with genus *Epichloë*. *Mycologia*, 106(2): 202-215.
- Young, C. A., Charlton, N. D., Takach, J. E., Swoboda, G. A., Trammell, M. A., Huhman, D. V., et al. (2014). Characterization of *Epichloë coenophiala* within the U.S.: are all tall fescue endophytes created equal?. *Frontiers in Chemistry*, 2:95.

## Affiliations

- <sup>1</sup> Department of Animal Sciences, Auburn University
- <sup>2</sup> Department of Clinical Sciences, Auburn University
- <sup>3</sup> Department of Poultry Sciences, Auburn University

# Design and Optimization of a Continuous Bioreactor for Enhanced Cell Culture

Rithvija Avvari<sup>1</sup>, Paul Todd<sup>2</sup>, and Thomas Hanley<sup>1</sup>

Researchers in the field of bioprocessing are investigating various biomanufacturing techniques to decrease capital costs, increase productivity and improve product quality. Continuous bioprocessing is emerging in upstream processing and is preferred over traditional batch processing. One important area of investigation is the design and operation of bioreactors. These devices are used extensively in STEM cell research (model systems, production of monoclonal antibodies and other proteins), cancer therapy, tissue engineering (scaffolds) and pharmaceutical industries (vaccines and antibiotics) on a large scale. Most bioreactors provide mixing with the use of impellers resulting in high shear that can cause cell death. A reactor environment that best provides low shear and high oxygen transfer along with controlled growth conditions will be suitable for cell cultures at a larger scale.

A rotating continuous bioreactor with an internal spiroid embedded on the outer wall was developed (Figure 1) using rapid prototyping for this purpose. The spiroid enhances oxygen transfer to the liquid phase. When the partially filled reactor is rotating, the spiroid picks up slugs of gas and liquid near the reactor exit and delivers them to the entrance of the reactor. The rotational rate of the reactor can be adjusted to control the flow of gas and liquid in the spiroid. The bioreactor is produced using rapid prototyping and can be operated in either batch or continuous mode. Based on this reactor design, our objective was to (1) model flow and oxygen transfer in the spiroid and optimize it and (2) conduct cell culture experiments optimizing reactor production for specific cell lines.

To address our first objective that the spiroid is pumping at an effective rate, dye experiments were conducted at different rotation rates in the scaled-up bioreactor. The reactor was filled up to two-thirds of its volume with water and the roller bed was activated. At each rotation rate, a food dye was introduced from the inlet of the reactor. Slugs of gas and liquid were clearly seen within the spiroid. This test was repeated at rotation rates of 4, 6, and 8 rpm. The flow observed in these experiments

was used for generating the simulation model. The optimization of spiroid is a major factor which will enhance the oxygen transfer in the bioreactor. The length and diameter of the spiroid must be optimum to provide the highest amount of oxygen transfer in the reactor.

ANSYS workbench 19.2 was used in this research to carry out the computation fluid dynamic (CFD) simulations. CFD simulations were performed as per a full factorial design of experiments (DOE) with rotation rates at three levels and diameter and length of spiroid at three levels. The spiroid geometry is complex and analyzing the flow through one turn (loop) alone is computationally expensive. Hence, the whole spiroid geometry is simplified to a straight tube. The simulation showed that the spiroid effectively pumps oxygen at higher rotation rates (8rpm). The turbulent eddy dissipation rates also indicated that the oxygen transfer was higher at 8rpm. In future studies, we plan to measure the actual increase in oxygen transfer to determine the efficiency of spiroid compared to the reactors already in use. Cell culture experiments using *Saccharomyces cerevisiae* will be conducted under various conditions to optimize the spiroid and reactor productivity. Based on these observations, changes to reactor design for better efficiency and performance will be made.

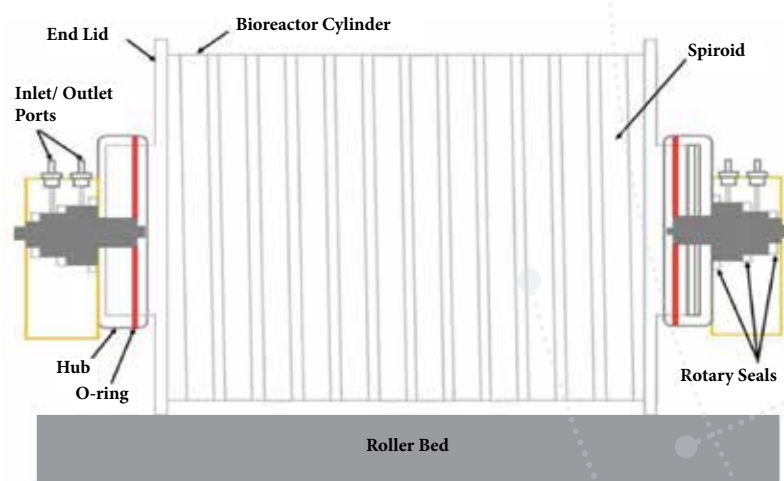


Figure 1. Bioreactor schematic (Fang et al., 2018).

## References

- Berson, R. E., & Friederichs, G. (2008). A self-feeding roller bottle for continuous cell culture. *Biotechnology Progress*, 24(1), 154–157.
- Fang, S., Todd, P. W., & Hanley, T. R. (2017). Enhanced oxygen delivery to a multiphase continuous bioreactor. *Chemical Engineering Science*, 170, 597–605.

## Affiliations

<sup>1</sup> Department of Chemical Engineering, Auburn University

<sup>2</sup> Magnaquant, LLC, Louisville, Kentucky

# Preparation of Phenol-Formaldehyde Resins Using the Lignocellulosic Biomass (Lignin, Lignin and Lignocellulosic Pyrolysis Bio-Oil) for Use as a Wood Adhesive

Archana Bansode<sup>1</sup>, Mehul Barde<sup>1</sup>, Osei Asafu-Adjaye<sup>2</sup>, John Hinkle<sup>1</sup>, Vivek Patil<sup>3</sup>, Brian Via<sup>2</sup>, Sushil Adhikari<sup>3</sup>, Thomas Elder<sup>4</sup>, Ramsis Farag<sup>1</sup>, Maria L. Auad<sup>1</sup>

Phenol-formaldehyde (PF) resin is the most commonly used adhesive in wood industries. It was used as the first synthetic adhesive for plywood in the mid-1930s (Yelle and Ralph, 2016), and is also used in the production of particleboard, oriented strand board (OSB), laminated veneer lumber (LVL), and medium-density fiberboard (MDF) by virtue of its good bonding, excellent moisture resistance, temperature stability, and durability (Seki et al., 2016; Spina et al., 2013). PF resin is also relatively inexpensive and easy to synthesize, being formed by the polycondensation polymerization reaction of phenol and formaldehyde solution (formalin). Depending upon reaction conditions, two types of PF resin can be obtained, novolac and resoles. Novolacs are thermoplastic resins produced with a molar ratio of formaldehyde (F) to phenol (P) less than one (F/P<1) under acidic conditions. Resoles are formed under alkaline conditions with a molar ratio of formaldehyde to phenol greater than one ((F/P >1) (Gardziella and Mueller, 1990; Holopainen et al., 2004). The advantages of PF resins notwithstanding, phenol is expensive, toxic, and is produced from nonrenewable petroleum-based resources, which are being depleted and have environmental consequences. With these growing concerns, there is ongoing interest in the development of sustainable and green alternatives for phenol-formaldehyde resins.

Modified phenol-formaldehyde resin was synthesized by substituting a significant fraction of the resin by lignocellulosic biomass. This research is divided into three parts. The first part of this study was performed to understand the structure of lignocellulosic biomass by phosphorus-31 nuclear magnetic resonance spectroscopy (<sup>31</sup>P-NMR), 2D [<sup>1</sup>H; <sup>13</sup>C] heteronuclear single quantum coherence (HSQC) analysis, gel

permeation chromatography (GPC) and pyrolysis-gas chromatography-mass spectrometry (Py-GCMS). In the second part of the research, phenolic (novolac) resins were produced by polycondensation reaction between phenol and formaldehyde under acidic conditions with a formaldehyde (F) to phenol (P) ratio less than one. Four types of phenolic resins were synthesized by using phenol, kraft lignin, bio-oil derived from wheat straw lignin and organic phase of bio-oil derived from lignocellulosic biomass. Further produced 100% phenol formaldehyde (100% PF) resin, 50% lignin phenol formaldehyde (50% LPF) resin, 50% lignin bio-oil phenol formaldehyde resin (50% LBPF) and 50% lignocellulosic bio-oil phenol formaldehyde resin (50% LCBPF) were characterized by fourier transform infrared spectroscopy (FTIR) analysis and proton nuclear magnetic resonance (<sup>1</sup>H-NMR) and carbon-13 nuclear magnetic resonance (<sup>13</sup>C-NMR) Spectroscopy analysis. These phenolic resins exhibit a linear or partially cross-linked structure, to achieve fully crosslinked structure they are cured with hexamethylenetetramine (HMTA) curing agent. Differential scanning calorimetry (DSC) was used to study the thermal behavior of physical mixture of resin with curing agent in order to obtain good bonding performance of adhesive by demonstrating curing temperature. In the third part of the research, adhesive strength of all phenolic resins cured with HMTA was studied under dry and wet condition along with water absorption and thickness swelling.

Our results from the chemical characterization of lignocellulosic biomass demonstrated that they have greater potential to partially substitute phenol in PF resin. The further characterization of modified PF resins was confirmed their successful synthesis with

cost-efficient and environmentally friendly properties. DSC analysis helps to understand the curing behavior of PF resin with a curing agent to improve the performance of the resin adhesive on wood. The tensile shear strength results indicate that the addition of curing agent HMTA shows the better impact on wood bonding except with PF resin of lignin this may be due to the highly branched structure of kraft lignin, however, the uncured PF resin shows lower tensile shear strength than the remaining ones. It can be noted that the water absorption and thickness swelling for uncured PF resin has the highest value than the cured PF resin due to the partially crosslinked structure faster than the hydrolysis.

## References

- Gardziella, A. & Mueller, R. (1990). Phenolic resins. *Kunststoffe, German Plastics*, 80(10), 66–68. <https://doi.org/10.4011/shikizai1937.64.710>
- Holopainen, T., Alvila, L., Savolainen, P., & Pakkanen, T. T. (2004). Effect of F/P and OH/P molar ratios and condensation viscosity on the structure of phenol-formaldehyde resol resins for overlays - a statistical study. *Journal of Applied Polymer Science*, 91(5), 2942–2948. <https://doi.org/10.1002/app.13511>
- Seki, M., Tanaka, S., Miki, T., Shigematsu, I., & Kanayama, K. (2016). Friction characteristics between metal tool and wood impregnated with phenol formaldehyde (PF) resin during exposure to high pressure. *Journal of Wood Science*, 62(3), 233–241. <https://doi.org/10.1007/s10086-016-1551-x>
- Spina, S., Zhou, X., Segovia, C., Pizzi, A., Romagnoli, M., Giovando, S., Pasch, H., Rode, K., & Delmotte, L. (2013). Phenolic resin wood panel adhesives based on chestnut (*Castanea sativa*) hydrolysable tannins. *International Wood Products Journal*, 4(2), 95–100. <https://doi.org/10.1179/2042645312Y.0000000020>
- Yelle, D. J., & Ralph, J. (2016). Characterizing phenol-formaldehyde adhesive cure chemistry within the wood cell wall. *International Journal of Adhesion and Adhesives*, 70, 26–36. <https://doi.org/10.1016/j.ijadhadh.2016.05.002>

## Affiliations

<sup>1</sup> Department of Chemical Engineering, Auburn University

<sup>2</sup> School of Forestry and Wildlife Sciences, Auburn University

<sup>3</sup> Department of Biosystems Engineering, Auburn University

<sup>4</sup> USDA-Forest Service, Southern Research Station

# Puerto Rico's Iron Deposits: Developing a Genetic Model Through Field Observations and Geochemical Analyses

Marisa Barefoot<sup>1</sup>, Laura Bilenker<sup>1</sup>, and Thomas Hudgins<sup>2</sup>

Puerto Rico has a complicated geologic history, which has resulted in the formation of diverse metal (ore) deposits. A mining ban restricts the exploitation of these mineral resources; as a result, these deposits are grossly understudied. Due to their variable geologic origins, ore deposits are more than potential economic resources, they are useful records of magmatic activity, metal transport, and fluid movement within the crust. By studying these deposits and developing their genetic models, we will gain valuable insight into the broader geologic history of the area and the dynamic geology of Puerto Rico as a seismically active, metal-rich island.

Puerto Rico's iron deposits are currently classified as skarns, which generally implies that they formed when a magma body intruded into a carbonate host rock. Heat and vapors leaving the magma chemically alter the host rock allowing for the concentration of economic minerals. Puerto Rico has several iron "skarn" deposits, including the Tibes and Keystone deposits, which are located in different geologic provinces of the island (Fig. 1; [Schellekens, 1998]). Interestingly, field observations of the Tibes deposit are not typical of a skarn; large bodies of magnetite appear to mirror the general northwest trend of the island's fault system. These observations sparked an investigation to determine the origin of the magnetite present at both deposits. Preliminary analyses of the iron in the magnetite indicate that these deposits have a higher temperature origin than previously thought. These data reveal a potential misclassification of these deposits and highlight the need for further study. Additional field work and geochemical analyses will allow us to create genetic models that will have implications for the geologic history of Puerto Rico.

I will travel to Puerto Rico to map the iron deposits in detail and extract strategic rock samples, which will be cut and made into thin sections. I will record and measure the geologic units present at the surface, including the magnetite bodies and their orientations.

These deposits have not been mapped recently, and these observations are required to provide context for new geochemical analyses. The thin sections will be imaged by microscope to identify minerals, characterize their textures, and assess patterns in their spatial relationships. This will provide useful information about the history of mineralization and fluid flow in the area.

Preliminary geochemical data for Tibes and Keystone were obtained by using an electron microprobe analyzer (EMPA) at Auburn University. EMPAs work by bombarding a sample with electrons and analyzing their interaction with the sample. By utilizing this technique, we are able to measure the concentrations of elements within magnetite samples to determine their origin (Dare et al., 2014). The elements titanium, vanadium, aluminum, manganese, and calcium were the focus of this analysis because they behave differently under specific conditions (e.g., within a magma versus a skarn environment) and can be used as indicators of formation conditions. These first trace element data support the hypothesis of a misclassification of these deposits. I plan to further analyze the magnetite using laser ablation inductively coupled plasma mass spectrometry (LA-ICP-MS) at Auburn to confirm the data and examine the variations of trace elements within individual magnetite grains. LA-ICP-MS works by striking the sample surface with a laser, heating the material that has been extracted to extreme temperatures, and separating each element by mass.

The use of iron isotopes to identify mineral formation processes is a relatively new technique but when combined with trace element data, it provides a direct fingerprint of formation conditions and magnetite origin (Knipping et al., 2015). Where the trace element data reveals the geologic environment of magnetite formation, the isotope data will provide detailed information about the processes that occurred during formation. After our field work, I will travel to the

University of British Columbia to analyze the iron isotope composition of magnetite from several ore bodies in both Puerto Rican iron deposits.

In addition to providing a potentially new perspective of the geologic formation of the island of Puerto Rico, this study will clarify the processes that formed its iron deposits. As society moves toward a future with more advanced technology and demand for renewable energy, iron will be a critical commodity. Iron is a major component in many technologies, including solar panels and wind turbines and is used to produce steel, which is integral for the growth of developing countries and the construction of infrastructure. This research will provide new insight into the formation of similar iron deposits elsewhere. Understanding these complicated systems will contribute to mineral exploration efforts around the world.

## References

Dare, S., Barnes, S. J., Beaudoin, G., Méric, J., Boutroy, E., & Potvin-Doucet, C. (2014). Trace elements in magnetite as petrogenetic indicators. *Mineralium Deposita*, 49.7, 785–796.

Knipping, J. L., Bilenker, L. D., Simon, A. C., Reich, M., Barra, F., Deditius, A. P., Lundstrom, C., Bindeman, I., & Munizaga, R. (2015). Giant Kiruna-type deposits form by efficient flotation of magmatic magnetite suspensions. *Geology*, 43(7), 591–594.

Schellekens, J. H. (1998). Geochemical evolution and tectonic history of Puerto Rico. *Special Paper of the Geological Society of America* 322.

## Affiliations

<sup>1</sup> Department of Geosciences, Auburn University

<sup>2</sup> University of Puerto Rico, Mayagüez

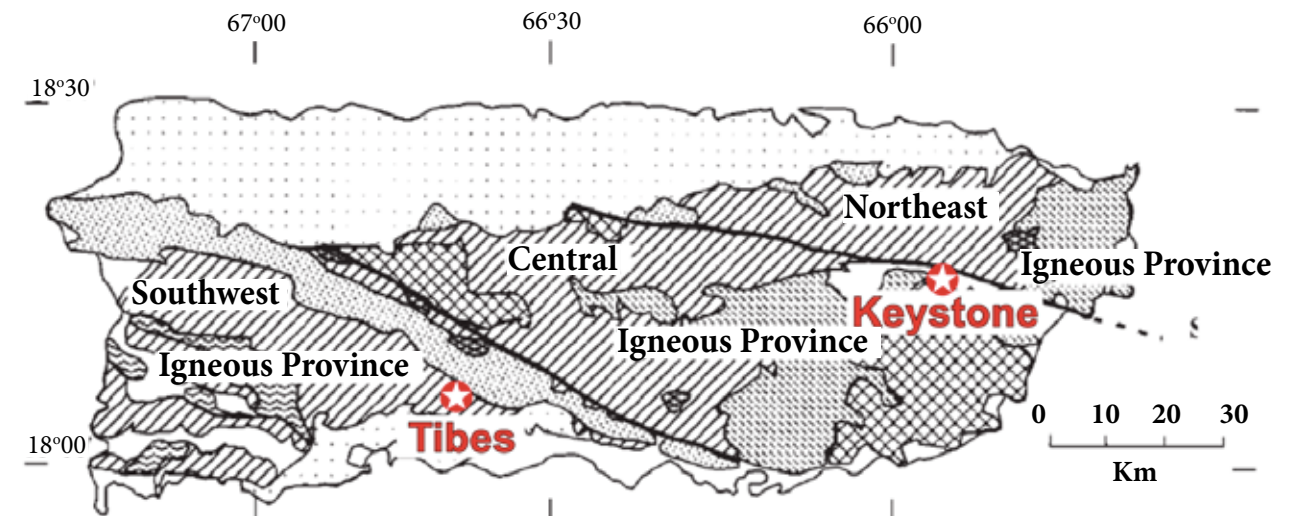


**Figure 1.** Map depicting different rock units across the island of Puerto Rico. Bold black lines indicate faults. The two study sites, the Tibes and Keystone iron deposits, are indicated by stars. Modified from Schellekens (1998).

# Using an Interactive Phonetics Learning Management System and User-Centered Design to Inform Phonetics Education Methods

Abigail Bennett and Marisha Speights Atkins

In the field of speech-language pathology, the understanding and use of phonetic transcription is a critical skill. The use of the International Phonetic Alphabet (IPA) for transcription allows speech-language pathologists (SLPs) to (1) create a visual representation of the status of speech production skills and (2) to interpret the coded speech in order to make diagnostic decisions for individuals at-risk for communication disorders (Knight et al., 2018). The goal of this research was to employ user-centered design principles to improve the functionality of the Automated Phonetic Transcription grading tool (APTgt) for teaching phonetics in a university setting.

## Research Questions

RQ1: What methods do instructors use to teach phonetic transcription?

RQ2: What methods of instruction have students taking phonetic transcription courses experienced?

RQ3: What is the user (instructors or students) experience when interacting with APTgt?

## Methods

The design had two parts, which were 1) a survey and 2) a usability study. Permission was obtained by the Auburn University Institutional Review Board. Surveys were designed in Qualtrics. 269 surveys were sent to instructors. A second survey was sent to 17 departments to forward to students for participation. Twenty-one instructor surveys and 24 student surveys were returned. The usability study was facilitated by the LUCIA lab through a secured Zoom web conferencing meeting. To date, seven students have been contacted through email and asked to participate in the usability study. Three students have completed the study so far.

## Survey

Surveys were sent to instructors and students of phonetics. The surveys queried teaching methods, technologies used, confidence in transcription after taking the class, and student outcomes. The survey was sent to instructors and students of phonetics across the country through direct e-mail, American Speech-Language Hearing Association members community website, and National Student Speech-Language and Hearing Association websites. Three primary questions of interest were (1) what types of technologies were used, (2) what type of transcription training is taught and received, and (3) how much practice students experienced with clinically relevant samples.

## Survey Results

Of the instructors queried, 35% said that they do not use any kind of technology when teaching phonetics courses. Of those that said they do use technology, the most popular choice was acoustic software, such as Praat or Wavesurfer. When asked how often their students transcribe real world, recorded, and non-typical speech, most instructors answered “sometimes” for all three questions. In the student version of the survey, 71% of students reported that their instructors did not use any kind of technology to teach phonetics. 62% reported only having 0-10 hours of practice with real-world transcription, while only 6% reported 60 hours or more.

## Usability Study

The second part of the study was a usability study that allowed participants to complete a module within the APTgt and give feedback about how easy or difficult the system was to use, along with suggestions for improving it. Again, the usability study was separated into instructor and student versions, with different modules and tasks in each. The participants were invited to talk aloud during the module, clarifying why

they were making certain decisions as well as voicing when something was difficult or confusing.

## Usability Study Results

A point of particular interest was the usability of the APTgt digital IPA keyboard. At the time of writing this project is ongoing. Preliminary analysis of the talk aloud responses from three students have provided insights for future improvement of the design. For example, one student remarked “...I did find myself struggling a little bit to find the correct symbols that I needed ‘cause I’m used to looking at like the QWERTY board...” Comments such as these are useful when updating the design of the APTgt, in order to make it a more effective tool for instructors and students alike.

## Conclusions

Data collection and analysis are still ongoing, since the experiment required modification to remote delivery and additional time for participant recruitment. From this two-part study, valuable information pertaining to phonetics instruction has begun to be gathered. Survey responses revealed that in many phonetics classrooms, technology is not used and transcription of real-world, recorded, or non-typical speech occurs only sometimes. The goal of the APTgt project is to provide instructors and students with a tool that can facilitate the use of technology for phonetics training and to increase the clinical relevance by making available training modules that include non-typical speech recordings.

## References

Knight, R. A., Bandali, C., Woodhead, C., & Vansadia, P. (2018). Clinicians’ views of the training, use and maintenance of phonetic transcription in speech and language therapy. *International Journal of Language & Communication Disorders*, 53(4), 776-787.

## Affiliations

Department of Communication Disorders,  
Auburn University

# Monitoring of Pastured Poultry for Parasites

Maria Tereza Bethonico Terra<sup>1</sup> and Ruediger Hauck<sup>1,2</sup>

There is an increasing market's demand for poultry meat and eggs that are produced in alternative and sustainable systems. These systems claim to be better for the environment, i.e. to be more sustainable, and to provide better animal welfare since they allow the birds to exercise natural behavior. However, on this type of rearing, the birds can come into contact with their excreta, increasing their chances of getting infected with endoparasites.

Pastured systems provide the animals with mobile houses that are moved every two or three days to a new patch on the pasture. While these systems offer little or no biosecurity, the low stocking density and the frequent change of location can reduce the concentration of feces on the ground and consequently decrease the infection pressure. Yet, these systems are rare and there is little literature evaluating and quantifying the prevalence of parasites in pastured production. The aim of the project was to systematically investigate and characterize the parasitological profile of birds in this type of system.

We did a parasitological surveillance on flocks of turkeys, broilers, and layers on a pasture farm. Fecal samples were collected at a two-week interval for one year. We sampled animals that were already at the pastures and were at least four weeks of age. At total, eight broiler and turkey flocks and four laying hen flocks were sampled. At each visit, two pooled fecal samples were collected. Parasite stages were counted under a microscope in a McMaster chamber. We were able to count oocysts of *Eimeria* spp. and eggs of *Ascaridia* spp. or *Heterakis* spp. *Eimeria* spp. were identified by next generation sequencing of PCR products. We used PCR followed by Sanger-sequencing to determine the worm species.

The broiler flocks had the highest mean of coccidia counts with 12,000 oocysts per gram of feces (OPG). The highest counts were also observed at their first week on pasture. For the turkey flocks, the average coccidia counts was 1,156 OPG with a cyclic peak at weeks 6, 10 and 14. For layer flocks, the average counts was close to 2,095 OPG, with two distinct peaks at weeks 25

and 68. There was no clear pattern of oocyst shedding related to age. However, there were different behaviors between species in terms of average coccidiosis counts between different seasons. Counts in broilers and layers were significantly higher in spring than in winter and summer.

We were able to detect the presence of *Eimeria acervulina*, *E. brunetti*, *E. maxima*, *E. mivatis*, *E. tenella* and *E. necatrix*. In addition, Operational Taxonomic Units (OTUs) Y and Z, possible new *Eimeria* species, about which is not much known at present were detected.

In turkeys, only once 50 eggs per gram (EPG) were present, while in layer flocks, the average counts were higher than 0 EPG in 80% of the samples and the mean counts was 509 EPG with no clear pattern related to age. There was an increase with the increase of temperatures during spring and summer with the peak reaching at mid-fall. Worm eggs from laying hens were identified as *A. galli*.

For all three types of birds, the counts of coccidia and *A. galli* were lower than published numbers in conventionally reared poultry (Höglund & Jansson, 2011), indicating the rotation system of the pastures might effectively reduce the infection pressure. In addition, the higher counts in the spring compared to winter and summer suggest that the parasites are sensitive to extreme environmental temperatures. Our results show the presence of *Eimeria* spp. commonly seen in conventionally reared broilers like *E. acervulina*, *E. maxima*, and *E. tenella* (Conway & McKenzie, 2007) as well as other species more commonly seen in backyard flocks. The final step in this project is to determine the *Eimeria* spp. in more samples of all three types of birds to broaden our data.

*A. galli* are the most commonly found worms in conventionally reared laying hens (Wuthijaree et al., 2017). The *A. galli* data showed that this parasite is a challenge mainly in older birds. It was consistently observed only in layer flocks; one positive sample of

roundworm eggs in one turkey flock does not indicate a substantial risk. Additionally, the seasonal differences suggest that higher temperatures might result in an increase of egg survival and sporulation in the environment since this process needs five weeks and the peak of egg counts was at mid-fall.

This study was able to identify and quantify the species of endoparasites that challenges three different poultry production birds in a pastured system. Moreover, we saw a possible interference of environmental conditions in the cycle of the worms.

## References

- Conway, D. P. & McKenzie, M. E. (2007). *Poultry coccidiosis* (pp. 77-164). Ames (IA): Blackwell Publishing Professional.
- Höglund, J. & Jansson, D. S. (2011). *Veterinary Parasitology* 180:267-273.
- Wuthijaree, K. C. et al. (2017). *Brit Poultry Sci* 58: 649-655.

## Affiliations

<sup>1</sup> Department of Poultry Science, Auburn University

<sup>2</sup> Department of Pathobiology, Auburn University

# Estimating Soil Phosphorus Storage Capacity of Major Soil Areas of Alabama: Implications for Environmental Loss Risk Assessment

Anjan Bhatta, Rishi Prasad, and Debolina Chakraborty

The poultry industry is the second largest agricultural industry in Alabama and contributes \$15 billion to the state economy annually. Besides, this intensive poultry production system also produces 1.5 million tons of poultry litter (PL) which contains approximately 19,000 tons of phosphorus (P). PL when applied to meet crop nitrogen requirement results in P build in the soil over time. Increase in soil test P level increases risk of P movement from soil to surface water bodies via runoff and leaching which can accelerate eutrophication of water bodies and reduce their water quality. Therefore, it becomes necessary to identify tools that can be used to predict risk of P loss from Alabama soils. Soil test phosphorus (STP) originally developed for agronomic purpose is also used as an indicator of environmental P loss risk. However, STP cannot be solely used for determining P loss risk as different soils have different critical STP values. Phosphorus saturation ratio (PSR) and soil phosphorus storage capacity (SPSC) can be potentially used in estimating environmental P loss risk from Alabama soils. Phosphorus saturation ratio is the molar ratio of P to [Al+Fe], calculated based on oxalate extraction. SPSC is defined as the amount of P that can be added to a given volume or mass of soil before the soil becomes an environmental concern. The objective of this research was to quantify SPSC and compare potential P loss risk for major soils areas in Alabama, namely Appalachian Plateau (AP), Coastal Plain (CP), Limestone Valleys (LV), and Piedmont Plateau (PP).

Soil samples were collected from several farms in Alabama representing four major soil areas that had a history of PL application. Each sample was separated into 0-5 cm, 5-15 cm, and 15-30 cm depths. Water soluble phosphorus (WSP) was determined by extracting soil with 1:10 soil: water ratio. Acid ammonium oxalate solution was used to extract P, iron (Fe) and aluminum (Al) from soil at 1:50 soil to solution ratio (Chakraborty et al., 2011). PSR and SPSC calculation was performed based on Nair and Harris (2004); 0.10 was used as PSR threshold for all soils.

$PSR_{ox} = \text{Extractable P} / \text{Extractable [Fe + Al]}$  (in moles)

$SPSC_{ox} = (0.10 - PSR) * \text{Extractable (Fe + Al)} * 31$  (mg P kg<sup>-1</sup>)

Results showed that WSP increased abruptly beyond 0.10 PSR for all soil (Figure A). The relationship between SPSC and WSP for soils indicated that when SPSC was positive, WSP was minimal (soil acted as P sink) and have very low P- release potential (Figure B). Water soluble P increased linearly with negative SPSC (soil acted as P source) and have high P release potential. Soil Phosphorus Storage Capacity of surface 0-5 cm and 5-15 cm soils were found to be negative for all four soil areas indicating that surface soils acted as a P source and have higher potential for P loss to the environment (Figure C). For 15-30 cm soil both AP and CP have negative SPSC while LV and PP have positive SPSC. Mean SPSC for all combined soils followed the order: AP (-108 mg kg<sup>-1</sup>) < CP (-67 mg kg<sup>-1</sup>) < PP (-44 mg kg<sup>-1</sup>) < LV (16 mg kg<sup>-1</sup>) and indicated that AP soils were found most vulnerable to P loss risk. Preliminary results showed that PSR and SPSC can potentially be used for environmental P loss risk assessment from Alabama soils.

## References

- Chakraborty, D., Nair, V. D., Chrysostome, M., & Harris, W. G. (2011). Soil phosphorus storage capacity in manure impacted Alaquods: Implications for water table management. *Agriculture, Ecosystems & Environment*, 142(3): 167–175. doi: 10.1016/j.agee.2011.04.019.
- Nair, V. D. & Harris, W. G. (2004). A capacity factor as an alternative to soil test phosphorus in phosphorus risk assessment. *New Zealand Journal of Agricultural Research*, 47(4): 491–497. doi: 10.1080/00288233.2004.9513616.

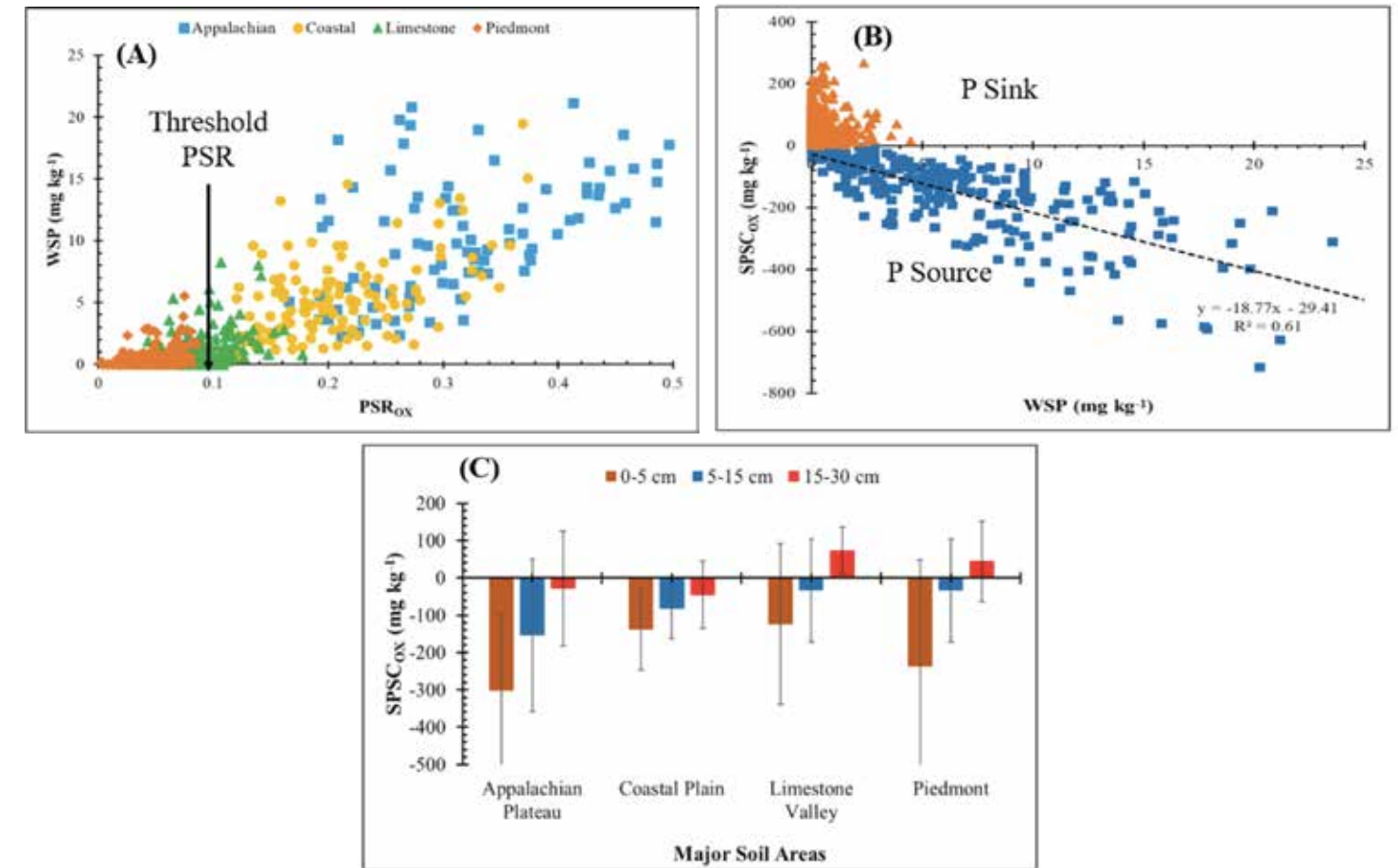


**Figure 1.** (A) Relationship between water soluble P (WSP) and P saturation ratio ( $PSR_{ox}$ ; calculated using P, Fe, and Al extracted in oxalate extractant) for four major soil areas of Alabama; (B) Relationship between soil phosphorous storage capacity (SPSC) and WSP for all soil in the study. SPSC was calculated using P, Fe, and Al in oxalate extractant; (C) Comparison of mean SPSC values of four major soil types of Alabama with 0-5 cm, 5-15 cm, and 15-30 cm soil depths.

## Affiliations

Department of Crop, Soil, and Environmental Sciences, Auburn University

# *E. coli* Bacteriophage PF-2 Displays a Reduction in Infectivity Following Treatment with Hydrogen Peroxide

Madeleine Bruderer, Harrison Smith, Keah Higgins<sup>2</sup>, and Elizabeth Hiltbold-Schwartz<sup>2</sup>

The enteric microbiota is a diverse and dynamic system of microorganisms that is partly composed of bacteria and bacteriophages. It is known that products of the immune system, in response to intestinal inflammation, can alter the bacteria residing in the enteric microbiome. However, the effects of immune products on the interactions between bacteriophages and bacteria are less widely understood. Therefore, the major objective of our research was to determine how immune system products, specifically hydrogen peroxide, impact the infectivity rate, the progeny production, and the timeline over which virulent bacteriophage infect their host.

To address this question, a modified one-step growth curve was utilized to measure the ability of a virulent, *E. Coli* targeting bacteriophage, PF-2, to adsorb and reproduce. The one-step growth curve called for six mono- and co-cultures of *E. Coli* and P-F2. The six cultures were designated E (*E. Coli*), EH (*E. Coli* and H<sub>2</sub>O<sub>2</sub>), P (PF-2), PH (PF-2 and H<sub>2</sub>O<sub>2</sub>), EP (*E. Coli* and PF-2) and EPH (*E. Coli*, PF-2 and H<sub>2</sub>O<sub>2</sub>). All six cultures were incubated for ten minutes to allow for adsorption. At the end of ten minutes, hydrogen peroxide treatments were added to the EH, PH, and EPH cultures. Three treatment concentrations were used; 0.5 mM H<sub>2</sub>O<sub>2</sub>, 1.0 mM H<sub>2</sub>O<sub>2</sub>, 2.0 mM H<sub>2</sub>O<sub>2</sub>. The cultures E, P, and EP functioned as controls. Samples were collected from each culture every five minutes for a total of 60 minutes. Samples without PF-2 (E and EH) were plated to calculate CFU/mL. Samples containing PF-2 (P, PH, EP, and EPH) were plated to calculate PFU/mL.

Findings showed that the timeline over which PF-2 replicated was rapid in control samples, with the first burst typically being observed around the 20-minute time point and a second burst being observed around the 30-minute time point. In samples treated with 0.5

mM H<sub>2</sub>O<sub>2</sub>, the latent period was increased significantly, delaying the burst in comparison with control samples. However, although the timeline of the burst was delayed, progeny production did not seem to be affected until the 55-minute time point of the experiment. In both samples treated with 1.0 mM H<sub>2</sub>O<sub>2</sub> and samples treated with 2.0 mM H<sub>2</sub>O<sub>2</sub>, a much more significant change in the infection timeline of PF-2 was observed. The latent period was increased significantly in the 1.0 mM H<sub>2</sub>O<sub>2</sub> and 2.0 mM H<sub>2</sub>O<sub>2</sub> treatments, resulting in delayed bursts. Some samples treated with 2.0 mM H<sub>2</sub>O<sub>2</sub> treatments did not even produce a burst in the 60-minute time frame of the experiment. In contrast to the 0.5mM H<sub>2</sub>O<sub>2</sub> treatment, in which progeny production was not significantly affected, progeny production was impacted in response to 1.0 mM H<sub>2</sub>O<sub>2</sub> and 2.0 mM H<sub>2</sub>O<sub>2</sub> treatments. As seen in Figure 1 below, bursts produced by 1.0 mM H<sub>2</sub>O<sub>2</sub> and 2.0 mM H<sub>2</sub>O<sub>2</sub> treatments were tenfold less than the control and the 0.5 mM H<sub>2</sub>O<sub>2</sub> treatments.

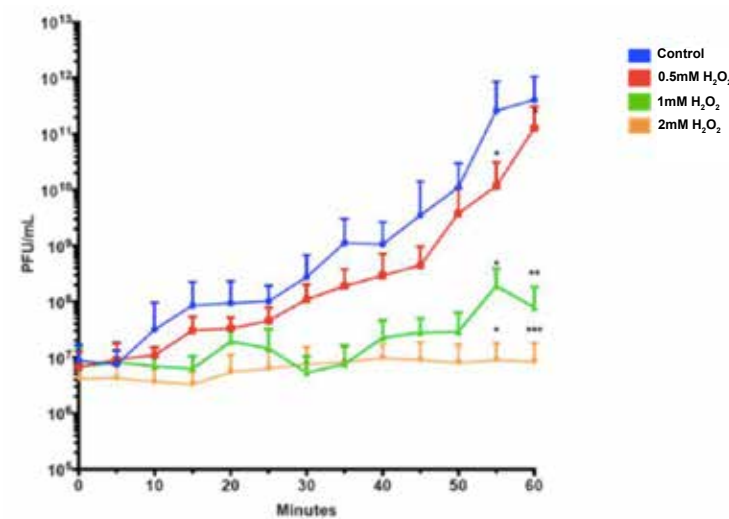


**Figure 1.** Impact of hydrogen peroxide concentrations on PF-2 infectivity rates over time.

In conclusion, hydrogen peroxide treatments resulted in a delayed and less efficient infection timeline of PF-2. Treatments at higher concentrations reduced progeny production, but it is unlikely the result of damage to PF-2. In addition, it should be noted that the delay in progeny production observed may be a response to damage to the host, *E. Coli*, rather than PF-2.

## References

Higgins, K. V. C. (2020). The inflamed gut: an integrative approach to understanding the impact of inflammation on bacteriophage-host dynamics., pp. 104–153.

## Affiliations

<sup>1</sup> Biomedical Sciences, Auburn University

<sup>2</sup> Department of Biological Sciences, Auburn University

# Evaluation of the Effects of Work and Heat Exposure on Cognitive Function in Firefighters

Abigail Campbell<sup>1</sup>, Angela Burns<sup>1</sup>, Kaitlin Lyons<sup>2</sup>, Oluwagbemiga Dademathews<sup>2</sup>, Aaron Parks<sup>2</sup>, Paige McHenry<sup>2</sup>, and JoEllen Sefton<sup>2</sup>

Firefighters regularly perform tasks requiring high levels of physical exertion under extreme environmental conditions. Firefighters respond to a variety of calls including house and vehicle fires, vehicle accidents, and medical aid including emergency medical services. Fire calls are the most highly regulated because of the inherent dangers and the requirement for compressed air carried in self-contained breathing apparatus (SCBA) (Fire-Related, 2019). The length of time firefighters are allowed to work during post-fire salvage/overhaul or during emergency medical services/extractions before taking a required break is not as highly regulated as fire extinguishing calls (Standards, 2015). Post fire salvage/overhaul takes place immediately after a fire has been extinguished. These operations take place in extreme environmental conditions, and firefighters are required to wear full PPE and SCBA (Standards, 2015).

Firefighters are confronted by difficult situations required quick decision making during all types of calls. Previous research has indicated that cognitive decline can result from physical exertion in environmental temperatures over 29.4°C (Hancock, 1982), which is well below the temperatures that firefighters encounter while extinguishing a fire. However, firefighters may regularly work in these environmental conditions on other calls such as vehicle accidents and emergency medical services. Although current research indicates the potential for cognitive decline (Rodrigues et al., 2018) and decreased reaction time (Morley et al., 2012) in firefighters, research to develop work to rest ratios for recovery/overhaul or EMS/extraction to minimize cognitive decline are minimal. The purpose of this study was to develop work to rest recommendations for firefighters working under three environmental conditions with the goal of maximizing safety and cognitive performance.

This study was a randomized control trial, using a 3x3 repeated measures single cohort design. The independent variables were heat with 3 levels (26.7°C,

40.6°C, and 46.1°C) and time with 3 levels (pre- and post-intervention and post-recovery). Exercise at each temperature lasted a maximum of 40 minutes and was performed in an environmental chamber that constantly regulates temperature and humidity, set to 50% for all trials. Participants were asked to walk on a treadmill at an incline of 2.5% and a speed of 4.5 kilometers/hour (2.8 miles/hour). This rate was used to simulate the sustained effort of firefighting. Participants walked for 5 minutes, got off the treadmill, and completed a deadlift of 40% of the participants body weight. Participants completed 3 lifts per minutes for a total of 15 lifts over the span of 5 minutes. They then returned to the treadmill to complete a total of 4 rounds of each exercise for a maximum total of 40 minutes. Participants stopped testing if they reached volitional fatigue, or they completed 4 rounds of each exercise. The researchers stopped the session if the participants core body temperature reached 39.4°C (103°F). Core temperature, heart rate, and perceived exertion were recording continuously during exercise and during the recovery period. During recovery, participants removed their jacket, gloves, and helmet, and were given water. The recovery period ended when participants returned to their resting core body temperature or at the end of 60 minutes.

Cognitive function was initially assessed with event-related brain potentials (ERP) captured using the MUSE 2 Brain Sensing Headband. Participants that used the MUSE 2 headband were asked to complete a game called One-Response OddBall on the iPad using the Portable EEG ERP Researcher (PEER) application. Preliminary data taken from the MUSE 2 headband indicated that during the sessions at 40.6°C participants had a tendency to have more negative brain voltages at the beginning of recovery and twenty minutes into recovery. A more negative voltage is indicative of lower ERP and inferior cognitive functioning. However, MUSE data from the other sessions was not sufficient to draw statistically significant conclusions.

The decision was made to use a go-no-go test for the remainder of the study. The go-no-go test collects data on decision making capabilities and reaction time and the participants were asked to complete the test before entering the chamber, upon completion of the exercise, twenty minutes into recovery, and at the end of recovery. Data collection using the go-no-go testing is still in progress.

## References

- Fire-Related Firefighter Injuries*. (2019). U.S. Fire Administration, 20(2):1-15
- Hancock, P. A. (1982). Task categorization and the limits of human performance in extreme heat. *Aviation, Space, and Environmental Medicine*, 53(8):778-84
- Morley, J., Beauchamp, G., Suyama, J., Guyette, F. X., Reis, S. E., Callaway, C. W., Hostler, D. (2012). Cognitive function following treadmill exercise in thermal protective clothing. *European Journal of Applied Physiology*, 112(5)1733-40 doi: 10.1007/s00421-011-2144-4
- Rodrigues, S., Paiva, J. S., Dias, D., Pimentel, G., Kaiseler, M., & Cunha, J. P. S. (2018). Wearable biomonitoring platform for the assessment of stress and its impact on cognitive performance of firefighters: An experimental study. *Clinical Practice & Epidemiology in Mental Health*, 14:250-62 doi: 10.2174/1745017901814010250 [published Online First: Epub Date]
- Standards on the Rehabilitation Process for Members During Emergency Operations and Training Exercises*. (2015). National Fire Protection Agency.

## Affiliations

<sup>1</sup> College of Science and Mathematics, Auburn University

<sup>2</sup> School of Kinesiology, Auburn University

# Testing and Developing Recycled 3-D Printing Filament for Use in Space

*Rylee Cardon and Asha-Dee Celestine*

Resources are dwindling and 3-D printing is leading the way into the future with customizable parts and reduced waste material. 3-D printing also offers the ability to test parts and materials in small batches. According to the Environmental Protection Agency (EPA), in 2017 only 8% of 35,370 tons of plastics generated were recycled. The rest were either combusted for energy recovery or put in a landfill, with the majority, 76%, going into a landfill (Plastics, 2019). The ability to reuse materials that are already available for 3-D printing, as well as the ability to create composite materials from these recycled materials is crucial in preventing more plastics from ending up in landfills where the average time to decompose 90% of the plastic is 287 years; with the longest being 573 years (e.g., polyethylene terephthalate) and the shortest being 105 years (e.g., low-density polyethylene) (Tansel, 2019). Applications of this research will benefit astronauts on longer missions farther away from Earth. They will have the ability to reuse material they already have available to engineer new inventions and solve problems they encounter while on these missions.

The material of choice for this study is recycled ABS mixed with other plastics from discarded printers and various other sources. First, the material must be cleaned and ground up in order for it to be used with an extruder because of oils and ink that may have contaminated the material. The grinder used is a Filabot Industrial Reclaimer (FB00070) and the material is washed in a hand-spun Filibot drum.

After the material has been cleaned and ground, it has to be dried, not just to be free of water on the outside, but it also has to have as little absorbed water as possible. Because plastic tends to absorb water and the experiment is being run in a very humid climate, the material is dried for at least 24 hours in a Slickvacseal aluminum vacuum chamber at 98.9 degrees Celsius.

In previous experiments, an exploration into how to remove or off-gas the fire-retardant chemicals from

recycled plastics has been performed. The best way to eliminate fire-retardant chemicals was to extrude the plastic at a high enough temperature to activate the fire-retardant chemicals without destroying the plastic molecules while using a vacuum hovering over the extruder to get rid of dangerous fumes. The best temperature so far for off-gassing fire-retardant material is 215 degrees Celsius on a Filibot single screw extruder with the extruder head screw taken off to allow for faster processing.

In addition, previous experimentation has identified how to extrude filament that is thin and consistent enough to put into a 3-D printer. The filament has to be between 2.75 and 3 mm thick for the 3-D printer to be able to use it. The filament is measured by a filament width sensor attached to a spooling device. The filament must be pulled by the spooler at a consistent speed in order for the filament to be the correct thickness.

Using these tools, a method for 3-D printing recycled plastics will be developed. A Monoprice MP Select Mini 3-D Printer V2 will be used to print a specimen for mechanical testing. 3-D printer parameters that may have to be adjusted are print speed, the temperature of the nozzle, and the temperature of the bed along with having to add a cover on the 3-D printer to keep the ambient temperature around the printed specimen constant. With continuing research, an ability to add carbon fibers and other additives to the fiber will be developed. The ability to extrude and print with filament at zero gravity will also be a part of future studies. This technology will not only provide great advances for space travel, but it will also provide a viable means to recycle and repurpose mixed plastics throughout the country and even the world.

## References

“Plastics: Material-Specific Data,” (2019, Oct. 30). EPA, [Online]. Available: <https://www.epa.gov/facts-and-figures-about-materials-waste-and-recycling/plastics-material-specific-data>. [Accessed: 30-Dec-2019].

Tansel, B. (2019). Persistence times of refractory materials in landfills: A review of rate limiting conditions by mass transfer and reaction kinetics. *Journal of Environmental Management*, 247, 88–103.

## Affiliations

Department of Aerospace Engineering,  
Auburn University

# Investigating Ribosomal Protein Duplication in Yeast *S. cerevisiae*

Mary C. Carlton, Rosaleny Orie, Caleb Thomas, and Alexey Petrov

This study represents a small portion within an overarching project designed to investigate specialized ribosomes, unique ribosomes designed for the translation of a specific subset of mRNAs (Segev & Gerst, 2018). The function of gene duplications within eukaryotes remains unclear but may be related to the formation of such ribosomes. Ribosomes can be considered the “builders” of a cell as they are responsible for synthesizing proteins required for cell composition, growth, and survival. Here, the focus is upon yeast cells, namely *Saccharomyces cerevisiae*. A genome wide duplication event occurred early in the evolution of *S. cerevisiae* wherein every gene was doubled (Wolfe, 2015). Of the 137 genes encoding ribosomal proteins in yeast, only 19 of these are unique genes, whereas the remaining 59 pairs of genes are duplicates: 59 genes with an almost genetically identical paralog (Ghulam et al., 2020). The purpose of these paralogs remains unclear. Recent studies favor the theory of functional specificity for paralogs encoding ribosomal proteins. This theory states that each gene in a pair of duplicates encodes for a unique protein that is regulated by paralog-specific mechanisms and results in unique expression profiles not shared by its ‘twin’ (Ghulam et al., 2020). Through this study, the role of gene duplication on the expression profiles of essential ribosomal complexes will be better understood.

To reveal timing and expression of ribosomal proteins, cells must be transformed with a metabolic marker that can be visualized. Transformation with the metabolic markers GFP and mScarlet allows direct viewing of the cells through flow cytometry, appearing green or red, respectively (Bindels et al., 2017). Transformation of yeast cells with fluorescent markers is a two-step process. First, cells were transformed with the URA3 gene that conferred selection of successfully transformed cells on media devoid of uracil (Goldstein et al., 1999). Universal forward and reverse primers allowed successful and robust PCR amplification of the URA3 gene from BY4742 yeast strain. Unique forward and reverse primers were then designed for each gene encoding ribosomal proteins. For example,

unique forward and reverse primers were designed for ribosomal protein S9A (S denotes the protein is of the small subunit, A denotes this is paralog A); another pair of unique forward and reverse primers was designed for ribosomal protein S9B (B denotes this is paralog A's duplicate). Another round of PCR amplification resulted in DNA used to transform cells and integrate the URA3 gene directly downstream of a desired ribosomal protein gene. After plating these cells on -URA media, only cells that successfully integrated the URA3 gene into the genome grew. Colony PCR primers that annealed within the URA3 gene and downstream of the ribosomal protein gene were used to confirm correct integration of the URA3 gene. The second step of this process was transformation of cells with GFP or mScarlet. GFP primers and mScarlet primers were designed to insert directly into the URA3 gene downstream of each ribosomal protein. A small ‘spacer’ sequence allowed the expression of fluorescent proteins after translation of each ribosomal protein. The final steps of the project will include visualizing these cell lines through flow cytometry and gathering data associated with paralog-specific events.

After focusing for months on optimizing primer design, PCR, and transformation protocols, successful transformation with mScarlet and GFP into a number of duplicate genes was obtained. The final steps of visualizing fluorescent cells remain before continuing further research. Cells will be viewed through flow cytometry, wherein those that express paralogs tagged with mScarlet will appear red and those that express paralogs tagged with GFP will appear green. If a cell expresses both paralogs, an orange color is emitted. Using these tags, timing and expression of these genes can be studied. The goal for future work will be to achieve the remaining necessary transformations for each duplicated and unique gene encoding ribosomal proteins in yeast, gather data for the inheritance patterns, timing, and expression of each gene and its duplicate, and begin to study the effect of duplicate deletions upon cells.

Previous studies showing that duplications aid in the cellular response to stress due to the presence of harmful drugs and nutrient deprivation imply that these genetic components play a significant role in cell survival and should be further studied (Parenteau et al., 2015). In fact, a number of mammalian cancers and human blood disorders have been previously associated with paralog deletions (Farrar et al., 2011). Paralog-specific effects on the phenotype, expression rates of other proteins within a cell, and the formation of specialized ribosomes may be elucidated utilizing the cell lines transformed with fluorescent tags from this project (Komili et al., 2017; Segev & Gerst, 2018). Researching genes encoding ribosomal proteins has implications in many other areas of study including epigenetics, cell growth and cell cycle progression, transcriptional and translational regulation, and treatment of diseases associated with ribosomal defects. A better understanding of how and why these genes are inherited will open the door for further study into the complex molecular mechanisms that govern cellular life.

## References

- Bindels, D. S., et al. (2017). MScarlet: A bright monomeric red fluorescent protein for cellular imaging. *Nature Methods*, U.S. National Library of Medicine.
- Farrar, J. E., Vlachos, A., Atsidaftos, E., Carlson-Donohoe, H., Markello, T. C., Arceci, R. J., Ellis, S. R., Lipton, J. M., & Bodine, D. M. (2011). Ribosomal protein gene deletions in Diamond-Blackfan anemia. *Blood*, 118(26), 6943–6951.
- Ghulam, M. M., Catala, M., & Abou Elela, S. (2020). Differential expression of duplicated ribosomal protein genes modifies ribosome composition in response to stress, *Nucleic Acids Research*, 48(4), 1954–1968.
- Goldstein, A. L., et al. (1999). Heterologous URA3MX cassettes for gene replacement in *Saccharomyces cerevisiae*. *Yeast (Chichester, England)*, U.S. National Library of Medicine.
- Komili, S., Farny, N. G., Roth, F. P., & Silver, P. A. (2007). Functional specificity among ribosomal proteins regulates gene expression. *Cell*, 131(3), 557–571.

Parenteau, J., Lavoie, M., Catala, M., Malik-Ghulam, M., Gagnon, J., & Abou Elela, S. (2015). Preservation of gene duplication increases the regulatory spectrum of ribosomal protein genes and enhances growth under stress. *Cell Reports*, 13(11), 2516-2526.

Segev, N., & Gerst, J. E. (2018). Specialized ribosomes and specific ribosomal protein paralogs control translation of mitochondrial proteins. *The Journal of Cell Biology*, 217(1), 117–126.

Wolfe, K. H. (2015). Origin of the yeast whole-genome duplication. *PLoS Biology*, 13,8.

## Affiliations

Department of Biological Sciences, Auburn University

# Analyzing the Parameters That Influence Soft Tissue Artifact Frequencies

Scot Carpenter, Michael Zabala, and Jacob Larson

Marker-based motion capture systems are commonly used for biomechanical analyses to measure human movement by tracking the positions of reflective markers placed on the surface of the skin. A 3-D model of the subject can be created using the data from the markers. This provides an approximate location of the position and orientation of the underlying bones during a given movement. A well-known limitation of this method of data collection, however, is the relative movement of skin and other soft tissue over the bone (Cappozzo et al., 1996). This type of error is known as *soft tissue artifact* (STA). In order to accommodate for this discrepancy, low-pass filters can be used to remove frequencies deemed to be too high for human volitional movement, thus lowering the likelihood of error due to STA. For general data collections, a common method of filtering at 6 Hz has been shown to be somewhat effective at removing STA (Nagano et al., 1998) and has been used as the standard kinematic data filter in biomechanical studies. However, the frequency at which data should be filtered has been shown to depend on the movement type as well as various subject characteristics (Peters et al., 2010). For this study, we hypothesized that STA frequency will be affected by muscle activation level. Thus, the objective of this study was to analyze how the STA frequencies of the thigh differ based on an activated and relaxed state of the thigh musculature.

Four human subjects participated in this study, having given IRB-approved informed consent. A 10-camera VICON motion capture system was used for data collection, and reflective markers were placed on each subject using a 79-marker set based on the point cluster technique (Andriacchi et al., 1998). The test consisted of subjects standing with their right foot on a platform which was raised to a height such that the knee was at 90 degrees of flexion. The subject was instructed to relax the thigh and perturb the skin by twisting the thigh with one hand about the femoral longitudinal axis to its maximum possible angle and quickly releasing, allowing the soft tissue to oscillate freely. The subject was then asked to repeat the procedure, while activating the musculature of the thigh. Three trials

were taken for both conditions. The marker trajectories were gap-filled in Nexus software and further processed in MATLAB by creating an anatomical reference frame on the thigh and tracking movement of the centroid of the 9-marker thigh cluster relative to the origin of the segment which was located at the distal femur. The angle of twist about the femur was calculated for each trial. This data was then converted to the frequency domain with a Fast Fourier Transform (FFT) to analyze the frequency components of the signal.

The angle of twist and frequency plot for a relaxed and activated state in one subject is shown in Fig. 1. The upper left plot shows the time history of the oscillations of the thigh's soft tissue when it is in a relaxed state. The upper right plot shows the FFT of this data. The lower plots show the same information for an activated thigh of the same subject. The results of the study indicated that the angular frequency of the thigh increased with muscle activation, where a relaxed and activated thigh had an average frequency of 4.04 and 5.60 Hz, respectively. The mean difference between the two sets of frequencies was 1.55 Hz and was shown to be statistically significant with a Student's T-test ( $p = 0.02$ ). More importantly, the average frequency was less than 6 Hz regardless of activation. This means that some STA might not be removed from motion capture data when the typical 6 Hz cut-off frequency is used.

The results of this study show that STA can still impact motion capture results while using a 6 Hz lowpass filter. Future work will investigate the relationship between STA and physical traits of the subject, such as age, weight, sex, and percent body fat. Determining respective STA of these subject categories could allow for subject specific filtering frequencies which could further reduce or eliminate the effect of STA in future biomechanical studies.

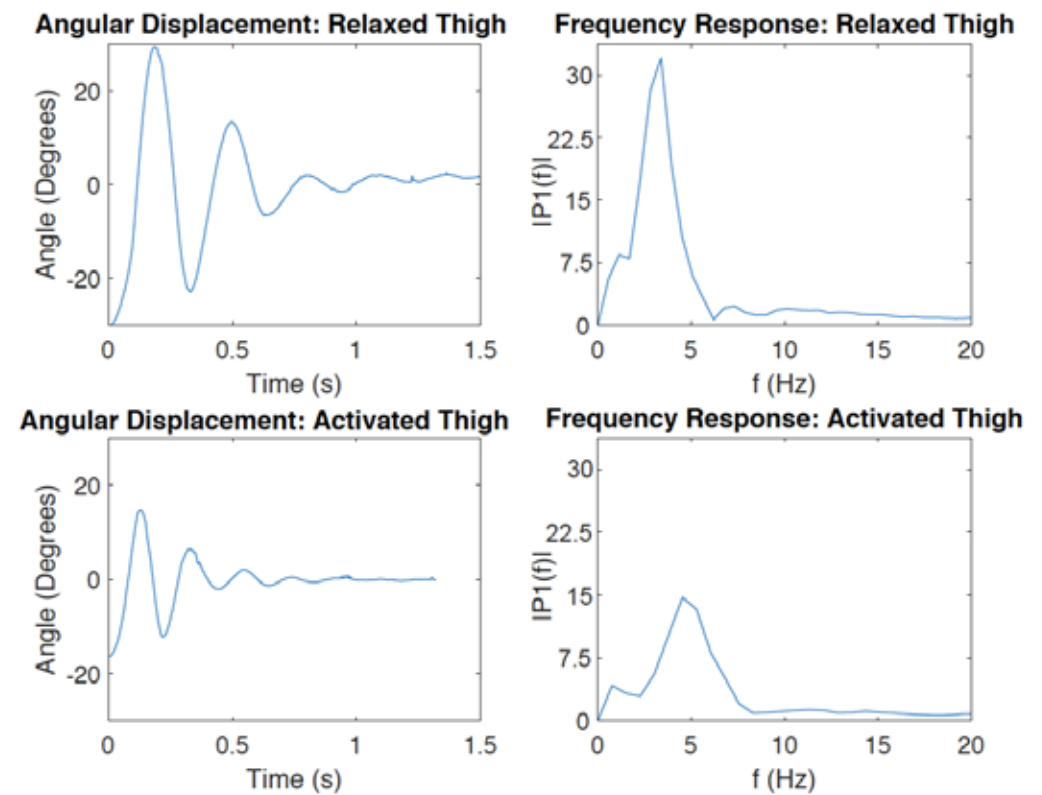


Figure 1. Time history and frequency response plot for a single subject with  $|P1(f)| = \text{peak amplitude (deg)}$ .

## References

- Andriacchi, T. P., et. al. (1998). *Journal of Biomechanical Engineering*, 120(6):743-749
- Cappozzo A., et al. (1996). *Clinical Biomechanics*, 11(2):90-100
- Nagano A., et. al. (1998). *Journal of Biomechanics*, 31(10):951-955
- Peters A., et. al. (2010). *Gait and Posture*, 31(1):1-8

## Affiliations

Department of Mechanical Engineering,  
Auburn University

# The Effect of Load Magnitude on Muscle Activation During Unilateral Overhead Dumbbell Carries

Molly Cassidy<sup>1</sup>, Nicole Bordelon<sup>2</sup>, Kyle Wasserberger<sup>2</sup>, and Gretchen Oliver<sup>2</sup>

## Introduction

Stability of the lumbo-pelvic hip complex (LPHC) and scapular stabilizing musculature allows for efficient proximodistal transfer of energy from the lower extremities to the upper extremities during dynamic sport tasks (Kibler et al., 2006; Kibler, 1998). Instability of these regions can result in less efficient energy transfer and require upper extremity compensation to maintain performance (Kibler et al., 2006). This is problematic since repeated compensation can increase risk of upper extremity overuse injuries (Kibler et al., 2006; Kibler, 1998). Therefore, strength and conditioning coaches can reduce susceptibility to injury by programming exercises that improve the stability of the LPHC and scapular stabilizers (Kibler et al., 2006). Although it is necessary to progressively include sport specific exercises, weighted carries can be used to develop a base of isometric LPHC stability in preparation for more dynamic tasks (McGill & Marshall, 2012). Unilateral carries may be especially advantageous for improving stability since the uneven load distribution enhances contralateral muscle activation to maintain trunk alignment (McGill & Marshall, 2012; McGill et al., 2012). However, load magnitude should be considered since variations may affect muscle activation (McGill & Marshall, 2012; McGill et al., 2012). Therefore, the purpose of this study was to examine the effect of load magnitude on muscle activation during unilateral overhead dumbbell carries.

## Methods

Eighteen individuals (22.6±2.6 y, 173.3±8.1 cm, 74.6±24.9 kg), all healthy and resistance trained, completed carries across a 12 m distance. Healthy was defined as musculoskeletal injury free for the past six months, and resistance trained was defined as lifting weights at least twice a week for the past six months. The participant performed carries on their dominant side in the overhead position. Three trials of three load conditions, relative to body weight

[10%(light), 15%(moderate), and 20%(heavy)], were performed. Muscle activation data were collected using electromyography during the middle 4 meters on the dominant upper and lower trapezius (UT, LT), latissimus dorsi (LD), and serratus anterior (SA), as well as bilateral gluteus medius (GM) and external oblique (EO). Maximum voluntary isometric contraction (MVIC) testing was used to establish baseline muscle activity to which subsequent trials were normalized. A 3 (load) x 8 (muscle) repeated measures ANOVA (RM-ANOVA) compared % MVIC between load conditions.

## Results

Analysis revealed a significant load by muscle interaction [F(4,799, 81.577)=7.834,  $p<0.001$ ] (Figure 1). Post hoc analysis revealed there were significant differences between light and moderate loads in the UT, LD, SA, dominant EO, non-dominant EO, and non-dominant GM ( $p=0.001-0.063$ ) with moderate loads showing greater activation. There were also significant differences between light and heavy loads in the UT, LD, SA, dominant EO, non-dominant EO, dominant GM, and non-dominant GM ( $p=0.001-0.031$ ) with heavy loads showing greater activation. There were also significant differences between moderate and heavy loads in the non-dominant EO ( $p=0.007$ ) and the dominant GM ( $p=0.048$ ) with heavy loads showing greater activation. There were no significant differences found in the LT ( $p > 0.05$ ).

## Conclusion

Lumbopelvic-hip complex and scapular muscle activation increased with load magnitude for all muscles except the lower trapezius; however, changes were muscle specific. The lack of muscle activation increase for the lower trapezius may be explained by the positioning of the external load which accomplishes scapular depression for the LT. Since the weight of the dumbbell was already applying an external

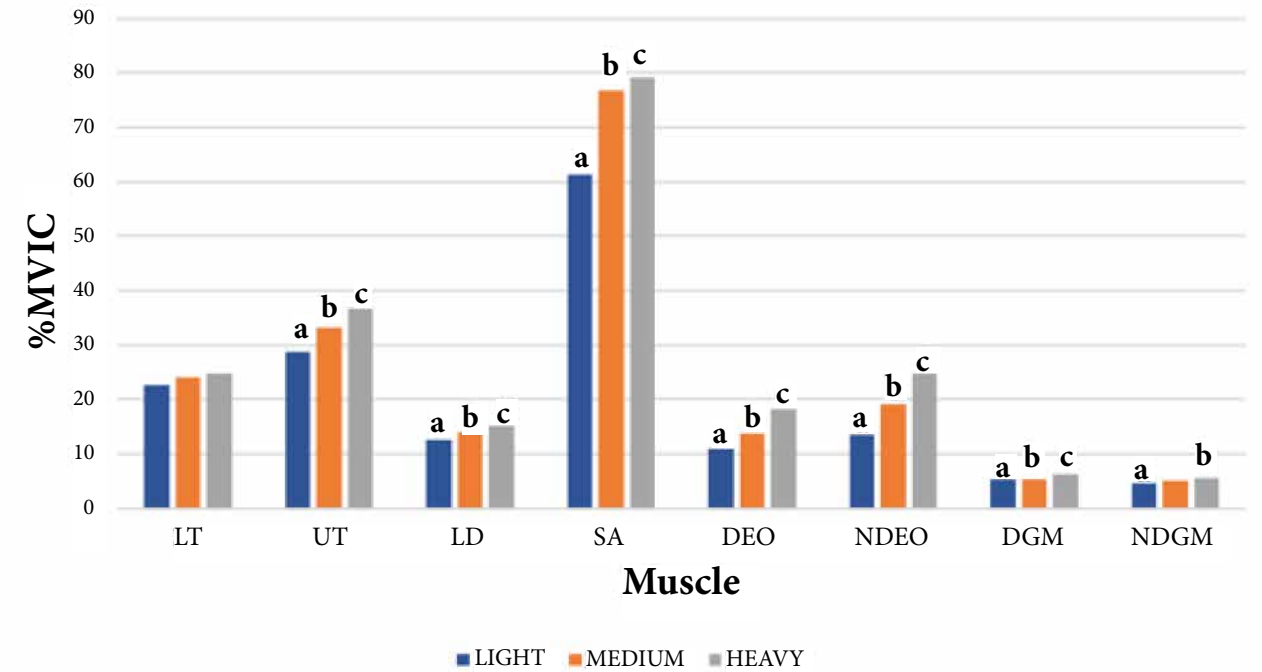


**Figure 1.** Muscle activation during load conditions. Note: \* denotes  $a < b < c$ ; LT = lower trapezius, UT = upper trapezius, LD = latissimus dorsi, SA = serratus anterior, DEO = external oblique, NDEO = non-dominant external oblique, DGM = dominant-gluteus medius, NDGM = non-dominant gluteus medius.

downward force, less activation was required from the lower trapezius to maintain scapular depression (19). Alternatively, there was high to very high activations in the serratus anterior. This is expected since the serratus anterior stabilizes the scapula during elevation and protraction which is required in the overhead position (3). In conclusion, unilateral overhead dumbbell carries do target activation of the LPHC and scapular musculature and may be used to improve isometric stability in preparation for more sport specific tasks. However, the effect of load on muscle activation should be considered during programming, and future research should analyze the training effects of unilateral overhead carries on stability.

## References

Kibler, W. B., Press, J., & Sciascia, A. (2006). The role of core stability in athletic function. *Sports Medicine*, 36(3): 189-98.

Kibler, W.B. (1998). The role of the scapula in athletic shoulder function. *American Journal of Sports Medicine*, 26(2): 325-37.

McGill, S. M., & Marshall, L. W. (2012). Kettlebell swing, snatch, and bottoms-up carry: Back and hip muscle activation, motion, and low back loads. *Journal of Strength and Conditioning Research*, 26(1): 16-27.

McGill, S. M., Marshall, L., & Andersen, J. (2012). Low back loads while walking and carrying comparing the load carried in one hand or in both hands. *Ergonomics*, 56(2): 293-302.

## Affiliations

<sup>1</sup> Biomedical Sciences Program, Auburn University

<sup>2</sup> School of Kinesiology, Auburn University

# Targeting p38 MAPK as a Novel Approach for the Treatment of Aggressive Form of Human Prostate Cancer

Sayak Chakravarti, Suman Mazumder, Taraswi Mitra-Ghosh, Robert D. Arnold, and Amit K. Mitra

Prostate cancer (PCa) is the 2nd-most common cancer and the 2nd leading cause of cancer deaths in US men with ~ 192,000 new cases (10.6 % of all new cancer cases) and ~ 33,300 new deaths (5.5% of all cancer deaths reported) in 2020 (<https://seer.cancer.gov/statfacts/>). Most of the early-stage PCa patients who receive standard therapy, i.e., Androgen deprivation therapy (ADT), show good initial response but later acquire ADT resistance and develop metastatic castration-resistant prostate cancer (mCRPC) (Crawford et al., 2019). mCRPC is a lethal disease state with a median survival <3 years and characterized by the continuous growth of tumor despite hormonal therapy and metastasis to the other organ like bones, lymph nodes (Moreira et al., 2017). Docetaxel (DTX)-based combination therapies, the standard-of-care regimen for mCRPC, have demonstrated success in both castration sensitive and castrate-resistant settings and thus remain the frontline therapeutic strategy for the treatment of advanced PCa and warrants continued development with the explicit goal to improve OS. However, most of these taxanes (TX)-based combination therapies show good initial response and improvement in overall survival (OS) followed by eventual relapse or resistance over time - progression-free survival (PFS) approaches almost 0% in 3 years (Petrylak et al, 2004). Moreover, extensive inter-individual variation in response and resistance to chemotherapy is a serious concern in the treatment of advanced-stage PCa. This warrants the development of novel combination therapy regimens based on robust biological rationale and aiming to exploit the potential synergism between different therapeutic classes with non-overlapping mechanisms of activity to treat mCRPC for its potential to enhance therapeutic efficacy (improve OS), ability to prevent drug resistance and reduce toxicity by simultaneous inhibition of multiple oncogenic factors.

We have developed a novel computational pipeline, the secDrug algorithm, that uses greedy algorithm-based set-covering computational optimization method followed by a regularization technique on large-scale pharmacogenomics databases, like Genomics of Drug Sensitivity in Cancer (GDSC), for the *in silico* prediction of novel secondary drugs to treat drug-resistant and advanced stage cancers, alone or in combination with respective standard-of-care drugs. Top among our *in silico* predicted drugs for CRPC and taxane-resistant PCa was the p38 MAPK inhibitor TAK715. *In vitro* validation studies using cell cytotoxicity assay on a panel of androgen-independent PCa cell lines PC3, PC3M, DU145, and DU145-TXR showed high potency of our predicted drugs both as single agents and in combination with taxanes (combination index or CI =  $0.68 \pm 0.2$ , Chao and Talalay's method; CI < 1 represents synergism). Synergistic effects were particularly profound in the DUTXR and PC3M - cell lines representing acquired taxane resistance and high metastatic property, respectively. Further, our results also showed that this DTX+ TAK715 combination lowered the effective dose of DTX required to achieve desired therapeutic response >10 times (Dose Reduction Index or DRI  $10.62 \pm 11.42$ ), thereby making the cell lines relatively more taxane-sensitive. Moreover, we observed significantly elevated levels of Caspase 3/7 activity in drug combination-treated cells compared to single-agent treated cells indicating higher apoptosis. Further, our *in vitro* live-cell imaging, cell proliferation, and cell migration assay data also corroborated with the *in vitro* cytotoxicity assay data. Next, we performed NGS-based mRNA sequencing (RNA-seq) of untreated and treated (single-agent and DTX+ TAK715 combination) PCa cell lines to derive baseline and kinetic differential gene expression profiles (GEP) for exploring the mechanism of drug synergism and to

reveal underlying molecular pathways using Ingenuity Pathway analysis (IPA). GEP results were validated using immunoblotting and enzyme activity assays.

Currently, we are performing single-cell transcriptomic analysis (scRNA-seq) to understand the intra-tumoral heterogeneity in drug response and to elucidate the mechanisms of drug synergy based on sub-clonal architecture. Our future plan is to perform *ex vivo* validation of our *in vitro* findings using patient-derived 3D/spheroidal models which closely mimic the clinical complexity of prostate tumors in terms of the tumor microenvironment and heterogeneity of the cell population.

Our study thus validates, characterizes, and repurposes TAK715 as potential novel secondary drug for mCRPC treatment. Together, this serves as a universal

prototype for the discovery of novel drug combination regimens using secDrug, which could ultimately lead to favourable treatment outcomes in mCRPC patients.

## References

- Crawford et al (2019). *Prostate Cancer and Prostatic Diseases*, 22, 24–38.
- Moreira et al (2017). *Clinical Genitourinary Cancer*, 15(1), 60–66.e2.
- Petrylak et al (2004). *New England Journal of Medicine*, 31:1513–20.

## Affiliations

Department of Drug Discovery & Development, Auburn University

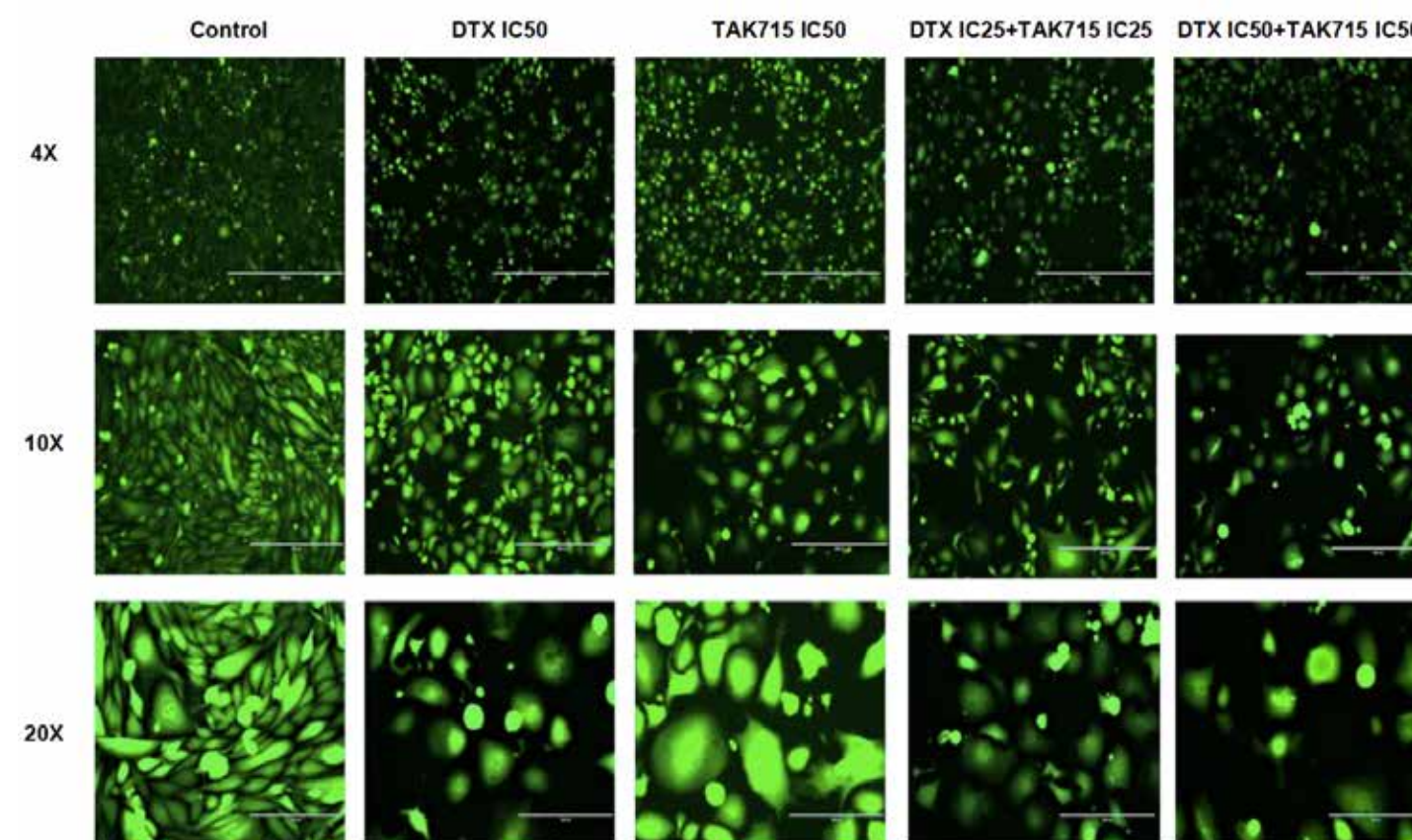


**Figure 1.** *In vitro* live cell imaging following Docetaxel and TAK715 treatment as single dose or in combination in human androgen independent/ castration resistant prostate cancers.

This representative image shows the androgen independent PCa cell Line PC3-GFP. Cells were treated for 48 hours with IC<sub>50</sub> doses of either Docetaxel (DTX) or TAK715 alone, and the following DTX+TAK715 combination doses - IC<sub>25</sub> of both the drugs; IC<sub>50</sub> of both the drugs. Significant changes in number and morphology of the cells were observed in response to the DTX+TAK715 drug combination treatment indicating high synergism.

# Effectiveness of Distinguishing Soil Types Using Unoccupied Aerial Vehicles (UAVs)

Brett Clark, Stephanie Rogers, and Lorraine Wolf

The study of earthquake-induced soil liquefaction deposits and their ages is of interest in the characterization of seismic sources and their history of faulting. Soil liquefaction occurs when saturated sandy soils are subjected to extreme stress in a manner that causes them to behave like a liquid. A common source of this extreme stress is shaking from earthquakes. In some cases, the liquefied soil may erupt through cracks in the ground, leaving above-ground deposits of sandy soils known as sand blows, many of which are quite large and remain visible hundreds of years after their deposit. Ages from liquefaction deposits associated with prehistoric earthquakes can be used to reconstruct the earthquake chronology of a seismic zone. Current methodology to identify potential sites for detailed study of these ancient deposits relies on relatively low-resolution satellite imagery. This study ultimately seeks to determine the effectiveness of using high-resolution multispectral imagery taken from unoccupied aerial vehicles (UAVs) to distinguish prehistoric liquefaction deposits from those caused by historic earthquakes. We hypothesize that high-resolution UAV-mounted multispectral imagery can be used to differentiate certain soil characteristics such as organic carbon content, which tends to be higher in older soils. This, in turn, would facilitate the identification of sites hosting prehistoric liquefaction deposits for further study and relative dating of adjacent sand blows.

To begin developing a methodology for distinguishing between soil characteristics, test flights were conducted on agricultural fields located at Auburn University's E.V. Smith Research Center in Shorter, AL.

A Parrot Sequoia multispectral sensor was used to capture aerial images in the green (550 nm), red (660 nm), red edge (735 nm), and near-infrared (790 nm) wavelengths. It was mounted on a DJI Phantom 4 Professional UAV. Flights were planned and executed using the Pix4Dcapture app on a tablet and were conducted in a single grid pattern at a height of 50 meters. The Sequoia captured images at an interval of

two seconds. The images were processed using Pix4D to generate output rasters for each of the green, red, red edge, and near-infrared wavelengths. These rasters were used in equations to calculate spectral indices. Each index is intended to highlight specific spectral soil characteristics, some of which may be useful for distinguishing younger soils from more well-developed soils (e.g., an index sensitive to soil organic carbon content). Figure 1 shows a sample of results from the test flights using one such index, the Brightness Index (BI) (Gholizadeh et al., 2020). The BI shows that a range of soil types may exist at the test site; however, to date, we have not empirically evaluated carbon content at this location.

The test flights conducted for this study served as an excellent way to become familiar with the equipment and processing software. Based on the evaluation of different indices for distinguishing different soil types or properties, the BI appears to hold the most promise. Future flights will be conducted at several sites in the New Madrid Seismic Zone (NMSZ), where the ages of earthquake-induced liquefaction deposits are known. Data acquired at these sites will directly test the effectiveness in differentiating prehistoric earthquake-induced liquefaction deposits from historic ones. If effective, this research will contribute to assessing seismic hazard by developing a methodology for large-scale mapping of earthquake-induced liquefaction deposits and for identifying prehistoric deposits that will constrain the ages of ancient earthquakes and refine the earthquake chronology of the NMSZ.

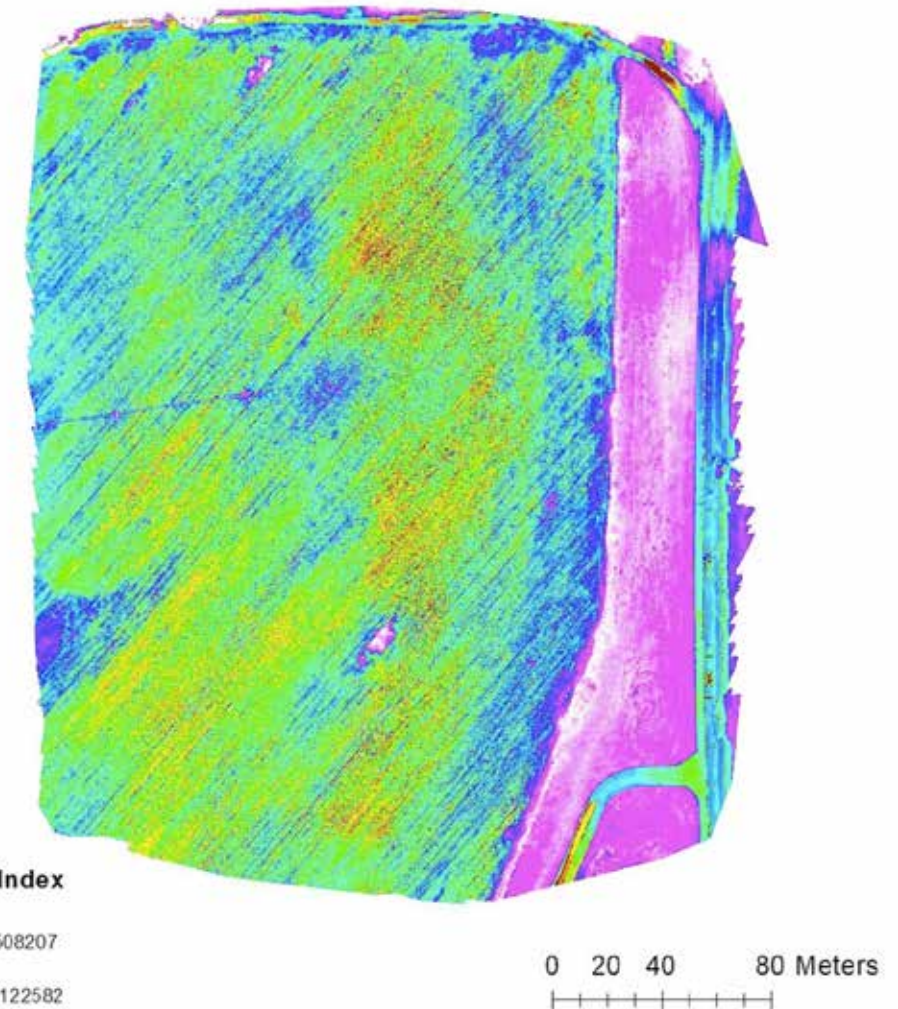


Figure 1. Map of Brightness Index  $\left( BI = \sqrt{\frac{Red^2 + Green^2}{2}} \right)$  calculated from UAV test flight.

The BI is sensitive to soil organic carbon content, which is higher in older, more developed soils. This index showed the best promise for distinguishing paleoliquefaction deposits from historic deposits.

## References

Gholizadeh, A., Saberioon, M., Viscarra Rossel, R. A., Boruvka, L., & Klement, A. (2020, January). Spectroscopic measurements and imaging of soil colour for field scale estimation of soil organic carbon. *Geoderma*, 357 : 113972. <https://doi.org/10.1016/j.geoderma.2019.113972>

## Affiliations

Department of Geosciences, Auburn University

# ACEs, Mindfulness, and Romantic Self-Efficacy's Influence on Relationship Functioning: A Risk and Resilience Approach

Erin Cooper, Francesca Adler-Baeder, and Julianne McGill

Adverse childhood experiences (ACEs) related to abuse, neglect, and household dysfunction are common in the United States (Felitti et al., 1998). Research shows that ACEs are associated with greater relationship distress in adulthood (e.g., Wheeler et al., 2019). Studies find positive effects of couples therapy for those with trauma history (Watson et al., 2018); however, less is known about preventative community-based couple relationship education (CRE) programs that likely serve individuals who have ACEs. The limited research exploring ACEs in the context of CRE demonstrate that ACEs are associated with lower couple relationship functioning before the program (Wheeler et al., 2019), and that individuals who report four or more ACEs report greater decreases in individual distress symptoms after participation than those who report fewer ACEs (Wheeler et al., 2020).

Taking a risk and resilience approach that assumes development of protective factors can mitigate the influence of risks, the current study provides a novel examination of the relative association between ACEs and couple relationship quality in the context of levels of mindfulness and romantic self-efficacy. The current study also is the first to examine the differential influence of ACEs on changes in couple relationship functioning after CRE participation.

The sample for this study ( $N = 1194$ ) was taken from a sample of couples recruited from the community to participate in a randomized control trial of two research-informed CRE programs. Before random assignment to a program group or the control group, participants completed baseline surveys and responded to a follow up survey approximately 2 months later.

A combination path and structural equation model was fit exploring the relative associations between ACEs, mindfulness, and romantic self-efficacy and a latent construct of relationship quality at baseline. Model fit indices demonstrate excellent model fit

( $\chi^2(16) = 40.31, p < .001$ ; RMSEA = 0.05,  $p = 0.45$ ; CFI = 0.99). As expected, results indicated a significant inverse link between cumulative ACEs and relationship quality for men ( $\beta = -.13, p < .01$ ) and women ( $\beta = -.09, p < .05$ ). In addition, mindfulness was positively associated with relationship quality for men ( $\beta = .10, p < .05$ ) and romantic self-efficacy had a positive—and the strongest—unique association with relationship quality for both men ( $\beta = .43, p < .01$ ) and women ( $\beta = .46, p < .001$ ), accounting for all else in the additive model.

We then conducted repeated measures analyses of covariance, separately for men and women due to data dependence, using only program participants ( $N = 793$ ) to explore differences in changes from pre- to post-program in couple relationship functioning between ACEs groups (i.e., participants who reported 0; 1-3; 4+). For men, results indicated differences in changes from pre- to post-program in relationship satisfaction between those who reported 1-3 and 4+ ACEs ( $F(1,201) = 4.55, p = .03$ ). For women, results indicated differences in changes in couple relationship skills between those who reported 0 and 4+ ( $F(1,210) = 9.93, p < .01$ ) as well as those who reported 1-3 and 4+ ACEs ( $F(1,268) = 6.79, p = .01$ ). For both men and women, those who report 4+ ACEs demonstrate greater improvements in couple functioning immediately after a CRE program compared to those who report fewer ACEs.

Results support continued efforts to promote self-efficacy as a protective factor in CRE, due to its stronger link with relationship quality compared to ACEs. Romantic self-efficacy may be modifiable through teaching relationship-enhancing skills (Riggio et al., 2013), and future research should explore the moderating role of self-efficacy in changes over time in CRE outcomes. Results also initially validate a “do no harm” approach for offering CRE to more vulnerable populations. Overall, this study supports the further use of a risk and resilience approach and the consideration

of ACEs of CRE participants in practice and research in order to better meet the needs of those in community-based CRE programs.

## References

- Felitti, V. J., Anda, R. F., Nordenberg, D., Williamson, D. F., Spitz, A. M., Edwards, V., & Marks, J. S. (1998). Relationship of childhood abuse and household dysfunction to many of the leading causes of death in adults: The Adverse Childhood Experiences (ACE) Study. *American Journal of Preventive Medicine, 14*(4), 245-258. [https://doi.org/10.1016/S0749-3797\(98\)00017-8](https://doi.org/10.1016/S0749-3797(98)00017-8)
- Riggio, H. R., Weiser, D. A., Valenzuela, A. M., Lui, P. P., Montes, R., & Heuer, J. (2013). Self-efficacy in romantic relationships: Prediction of relationship attitudes and outcomes. *The Journal of Social Psychology, 153*(6), 629-650. <https://doi.org/10.1080/00224545.2013.801826>
- Watkins, L. E., Sprang, K. R., & Rothbaum, B. O. (2018). Treating PTSD: A review of evidence-based psychotherapy interventions. *Frontiers in Behavioral Neuroscience, 12*, 258. <https://doi.org/10.3389/fnbeh.2018.00258>
- Wheeler, N. J., Daire, A. P., Barden, S. M., & Carlson, R. G. (2019). Relationship distress as a mediator of adverse childhood experiences and health: Implications for clinical practice with economically vulnerable racial and ethnic minorities. *Family Process, 58*(4), 1003-1021. <https://doi.org/10.1111/famp.12392>
- Wheeler, N.J., Griffith, S.M., Harris, H. & Kozachuk, L.A. (2020) Individual-Oriented Relationship Education: Exploring Adverse Childhood Experiences as a Moderator of Individual Distress Outcomes. *Journal of Couple & Relationship Therapy, 19*(1), 76-93. <https://doi.org/10.1080/15332691.2019.1661324>

## Affiliations

Department of Human Development and Family Studies, Auburn University

# Trunk Lateral Flexion Differences Between the Fastball and Curveball Pitch in Collegiate Softball Pitchers

Abigail M. Cramer, Jessica Downs, and Gretchen Oliver

In dynamic human movements such as the softball pitch, the ability of the trunk to provide stability and mobility is imperatively fundamental. The softball pitch is a full-body motion that requires the transfer of force from the lower extremities to the upper extremities. The primary link connecting the lower extremity segments to the upper extremity segments is the trunk. This linkage of segments that allows the transfer of force in a proximal to distal motion is commonly referred to as the kinetic chain. Since the trunk is central to the kinetic chain, trunk stability as well as controlled mobility allows for optimum force and energy transfer from the lower to the upper extremity. Therefore, any deficiencies in one segment can cause alterations in more distal segments, resulting in an increased risk for injury (Kibler et al., 2006).

Softball research has focused primarily on mechanics associated with performance and pain within a single pitch type. Variables such as trunk lateral flexion (TLF) and trunk rotation have previously been associated with pain (Oliver et al., 2018; Oliver et al., 2019). To the authors' knowledge, there are no studies investigating kinematic differences between pitch types in softball, thus it is unknown if those trunk kinematics associated with pain hold true across different pitch types. Therefore, the purpose of this study was to investigate trunk kinematics, specifically TLF, between the fastball (FB) and curveball (CV) in collegiate softball pitchers.

Thirty-one ( $20.10 \pm 1.81$  yrs,  $176.05 \pm 5.53$  cm,  $113.95 \pm 12.07$  kg) right-handed college softball pitchers participated. Inclusion criteria required participants to be free from injury and/or surgery for past six months and currently active as a pitcher on their team's roster at the time of testing. Eleven electromagnetic sensors were attached to the participants and a linked segment model was developed via a digitization process. Kinematic data were collected at 100Hz using an electromagnetic tracking system. Participants were instructed to throw three FBs and CVs for a strike to

a catcher at regulation distance. The average for the three trials for each pitch type was used for analysis. Two segments of the pitching motion were compared: foot contact (FC) and ball release (BR). A repeated-measures analysis of variance (ANOVA) was used to determine kinematic differences between pitch type; a priori was set  $p < .05$ . Statistical analysis revealed a significant difference in TLF at FC and BR between the two pitch types. At FC, there was greater TLF toward the glove arm side in the CV than in the FB. Likewise, at BR, the FB had greater TLF toward the pitching arm side than the CV (Figure 1).

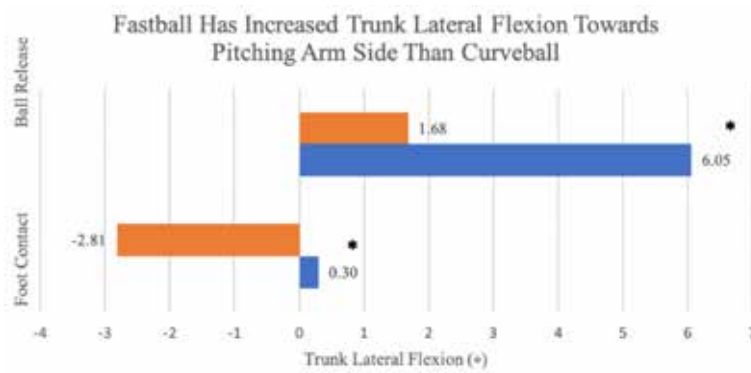


Figure 1. Trunk Lateral Flexion Differences Between the Fastball and Curveball

These results provide important information as they are one of the first to describe kinematic differences between pitch types in softball. Understanding the effects of different pitch types on trunk kinematics may enhance injury prevention strategies for softball pitchers. Because the lower and upper extremities are integrated within the kinetic chain, increased TLF towards the pitching arm site may result in a faulty kinetic chain link and increased susceptibility to upper extremity pain (Kibler et al., 2006). Further research will be needed to investigate this specific correlation between TLF and risk of injury.

## References

Kibler, W. B., Press, J., & Sciascia, A. (2006). The role of core stability in athletic function. *Sports medicine* (Auckland, NZ), 36(3):189-198.

Oliver, G. D., Friesen, K., Barfield, J. W., et al. (2019). Association of upper extremity pain with softball pitching kinematics and kinetics. *Orthopaedic Journal of Sports Medicine*, 7(8):2325967119865171.

Oliver, G. D., Gilmer, G. G., Anz, A. W., et al. (2018). Upper extremity pain and pitching mechanics in National Collegiate Athletic Association (NCAA) Division I softball. *International Journal of Sports Medicine*, 39(12):929-935.

## Affiliations

School of Kinesiology, Auburn University

# Changing Land Use and Land Cover of Big Creek Lake Watershed, Mobile County, Alabama

*Eshita Eva and Luke Marzen*

According to the U.S. Environmental Protection Agency (EPA), nonpoint source (NPS) pollution continues to be the largest source of pollution within the USA (EPA, 2012a). NPS pollution is a broad category that includes many diffuse sources of aquatic contaminants carried by rainfall or snowmelt runoff (EPA, 2012b), or any source of water pollution which is not meeting the legal definition of a point source within the Clean Water Act. Many sources exist for NPS pollutants including sediments and nutrients are the most common NPS pollutants, though, pollution from pesticides, pathogens, salts, oil, grease, toxic chemicals, and heavy metals are also widespread (EPA, 2012a). According to EPA 2012a, urban area runoff is a significant contributor to the pollutant found in estuaries. This is also agreed by the result of Dowd, Press, and Huertos (2008) which identified agricultural activities and highly impervious urban areas as major sources of NPS pollutants. NPS pollution resulting from urban areas is exasperated by the extensive expanses of impervious surfaces that hamper the absorption of water (Esen & Uslu, 2008). One such water body that is susceptible to pollution due to development is Big Creek Lake. LULC is an important factor impacting NPS for its watershed because many other things such as nutrient, risk assessment, pollution level depend on this. The objective of this study is to analyze the change of land use from 2004 to 2019.

The area of Big Creek Lake is 3,600 acres which is a tributary-storage reservoir in Mobile County located in southwest Alabama. Although the lake itself is only 3,600 acres, the watershed draining into it covers approximately 65,920 acres or 103 square miles (MAWSS, 2011; Journey & Gill, 2001). It works as the primary drinking water resource for the City of Mobile and it is also used for recreation. Though it is a forested watershed, in the last few decades there has been growth of urbanized and developed areas. This development combined with other factors could result in an increase of nonpoint source pollution within the watershed. Such a rapid and uncontrolled urban growth in the watershed could result in a diminishing of water quality in the watershed. Since this watershed serves as

the primary drinking water resource, it is essential that a better understanding of how the degradation of the watershed will impact human life.

This study used Landsat images obtained from the USGS data hub (<https://earthexplorer.usgs.gov/>) and images were chosen based on the observation of minimum cloud cover to have the lowest atmospheric and seasonal effects. Each LULC product was primarily based upon the classification of one date of Landsat data using ERDAS Imagine for image processing and analysis. Classification was performed using a hybrid unsupervised/supervised approach. Initially, a given Landsat data set was subjected to unsupervised classification using ISODATA clustering with 20 total clusters, convergence set to 0.995 (on scale of 0 to 1), 100 iterations, and cluster means initialization along the principal axis. The resulting classification was then recoded into water, forest, urban, agriculture and grassland. The change detection method was applied to show how land cover changes to another land cover within these years. LULC change detection products were generated using standard GIS overlay analysis techniques. Change detection approach involved comparison of two dates of LULC classifications.

Overall, all land use types experienced changes, where forest and grassland were found to have decreased, while urban was significantly increased. Particularly, during the time period of 2004 to 2019, an area of 7473 acres of forest decreased. In contrast, other land use types showed a considerable change, where the expansion of urban area was most prominent. Urban area increased from 3698 acres to 5610 acres during the period of 15 years (2004-2019). Water decreased a bit of 141 acres of 15 years of time period likely due to varying precipitation levels. Overall, the result depicted that from 2004 to 2019, land-use activities have accompanied the expansion of the urban areas more than other land use types. Forest was the largest land-use type which experienced the conversion process during 2004-2019, which was converted to urban (261 acres), agriculture (305 acres), and grassland (5160 acres).

Similarly, grassland and agriculture area were further observed to convert into other land use areas during the same period.

## References

- Dowd, B. M., Press, D., and Huertos, M. L. (2008). Agricultural nonpoint source water pollution policy: the case of California's central coast. *Agriculture, Ecosystems and Environment*, 128: 151-161.
- EPA. (2012a). Nonpoint source pollution: The nation's largest water quality problem. [<http://water.epa.gov/polwaste/nps/outreach/point1.cfm>]. Last accessed 24 October 2019.
- EPA. (2012b) What is nonpoint source pollution? [<http://water.epa.gov/polwaste/nps/whatis.cfm>]. Last accessed 24 October 2019.
- Esen, E., & Uslu, O. (2008). Assessment of the effects of agricultural practices on non-point source pollution for a coastal watershed: a case study Nif watershed, Turkey. *Ocean & Coastal Management*, 51: 601-611.
- Journey, C. A., & Gill, A. C. (2001). Assessment of water-quality conditions in the J.B. Converse Lake watershed, Mobile County, Alabama, 1990-98. U.S. Geological Survey Water-Resources Investigations Report 01-4225.
- MAWSS. (2010). ALDOT, MAWSS Settle Highway 98 Lawsuit. [[http://www.mawss.com/pdf/aldotmawssettle\\_advisory.pdf](http://www.mawss.com/pdf/aldotmawssettle_advisory.pdf)]. Last accessed 24 October 2019.
- USGS. (2017). Using the USGS Landsat 8 Product | Landsat Missions. <<https://landsat.usgs.gov/using-usgs-landsat-8-product>> (Accessed on 12 December 2017).

## Affiliations

Department of Geosciences, Auburn University

# “Connecting the Corridors”- Rethinking Parkerson Mill Creek, AU Campus

Riffat Farjana

Parkerson Mill Creek, upholding the historical value of Auburn, Alabama, creates a complex paradox of functional activities and future potentiality. As an interconnected part of people’s lives, PMC offers layers of connecting corridors not only for green spaces, pollinators, wildlife habitats but also for a connected whole for headwaters. The multidimensional possibilities of the future development of PMC can combine the historical, cultural, economic, natural, and constructive layers to reshape people’s lives, which has faded away throughout time. Human-made migration barriers have created a significant impact on the complex ecosystem of the urban fabric. Most parts of the creek are culverted, and only the position of water inlets tells us where it used to be. The ecology has changed and adapted tremendously due to the significant man-made changes during past decades. Nonetheless, *E.coli* has caused the primary degeneration of the quality of water of PMC over time.

The historical Comer Hall, which is the agriculture building of Auburn University, adjacent to Parkerson Mill Creek, is still a distinction between old and new. The culverted part of Parkerson Mill Creek is now being used as the transitional space for the passer-by. People used to come here and go by instead of knowing the historical value of this space. The mesic and hydric condition of the site gives a clue to the viewers to think a bit deeper about the area, how the space used to be, and how it evolved in the recent past.

## Analysis and Findings

To comprehend how Parkerson Mill Creek at Roosevelt Avenue used to be, series of historical Aerial photographs, GIS analysis helped to understand the land use of Auburn that has changed over time. The research was done on the physical traffic flow, pedestrian flow, smell, placement of historical trees, movement of water during a rainy day and the fluctuation of visible surface water level, level of public gathering and future possibilities and potentialities about the site in front of RBD where the Parkerson Mill Creek had been culverted.

The site analysis, drawings, mapping, and research was the substructure to develop “concept design” for this site. For Parkerson Mill Creek, my finding of lack of transitional space drove me to create conceptual sketches to connect different important watersheds and headwaters, pedestrian connections with different green spaces of Auburn University, and the city of Auburn, an increase of pervious surfaces and simplify the movement of people with functionality. Here in Parkerson Mill Creek’s design, I discovered that daylighting the creek would be the best solution. Moreover, designing a public gathering space alongside the creek would add another dimension in creating a transitional space for a greater ecosystem, which was the main gap in the analysis phase of the project. Thus, I created a strong linear North-South connection to connect two important historical building (Langdgon Hall & Comer Hall) with Mell street ( which connects the remanence of a different era of campus landscape design of Auburn University) along with East-West pedestrian connection by making the Roosevelt Avenue full pedestrian (by promoting pervious materials like Mell street in front RBD) and miller avenue to connect the Pine hill Cemetery which follows the Town creek. This is how I tried to make a connection to Parkerson Mill Creek with the Town Creek in the big picture.

## Planting Plants

As a diagrammatic planting plan, I have tried to keep the existing trees as much as possible and have been attempting to choose trees that could complement the existing pallet of trees. Water oak, willow oak, sweetgum, Black locust, green ash, Hackberry, black oak, Japanese elm, pin oak, post oak, River birch, southern magnolia, bald cypress and last but not the least loblolly pine are some existing trees that are found in and around the site. The selection of trees for the design was based on three major categories. First, keeping the existing trees and its features and add tress to complement them. Secondly, trees with changing fall colors and blooms. And thirdly, shrubs that have a wildlife value along with the quality of tolerating the standing water alongside the water features.

I wanted to amplify the cluster of historical loblolly pine (approximately 80’ tall). The elevated walkways will cut through them to experience the texture and monumentality of the tree in a different elevation. Longleaf pine and Virginia pine are the substitute option for loblolly pine. Another essential feature of the site is the cluster of water oak trees. To make these features more prominent, pin oak, southern red oak, Shumard oak, and sawtooth oak had been selected as the substitute of water oak with changing fall color. For the understory, I selected the species which could go well in the shade and partial shade area. I chose Oakleaf hydrangea and azalea, which could grow well under the cluster of pine and oak. Both the azalea and hydrangea have white bloom twice a year. However, Sweetspire had also been chosen for its white bloom with fall color.

Additionally, different types of berry trees had been chosen to amplify biodiversity. Beautyberry, Highbush blueberry, black chokeberry, American Elderberry are berries that had been selected for the design. The fruits are edible for humans and wildlife at the same time. Nonetheless, for the area where the creek has been daylighted along with the other areas where the place could hold water has been designed with small shrubs like Purple Coneflower, black-eyed Susan, summersweet clethra, lowbush blueberry, and Northern bayberry. Those trees can survive on standing water. However, ferns like lady fern, marginal wood fern and ostrich fern have been selected as the ground cover in some places adjacent to the water features.

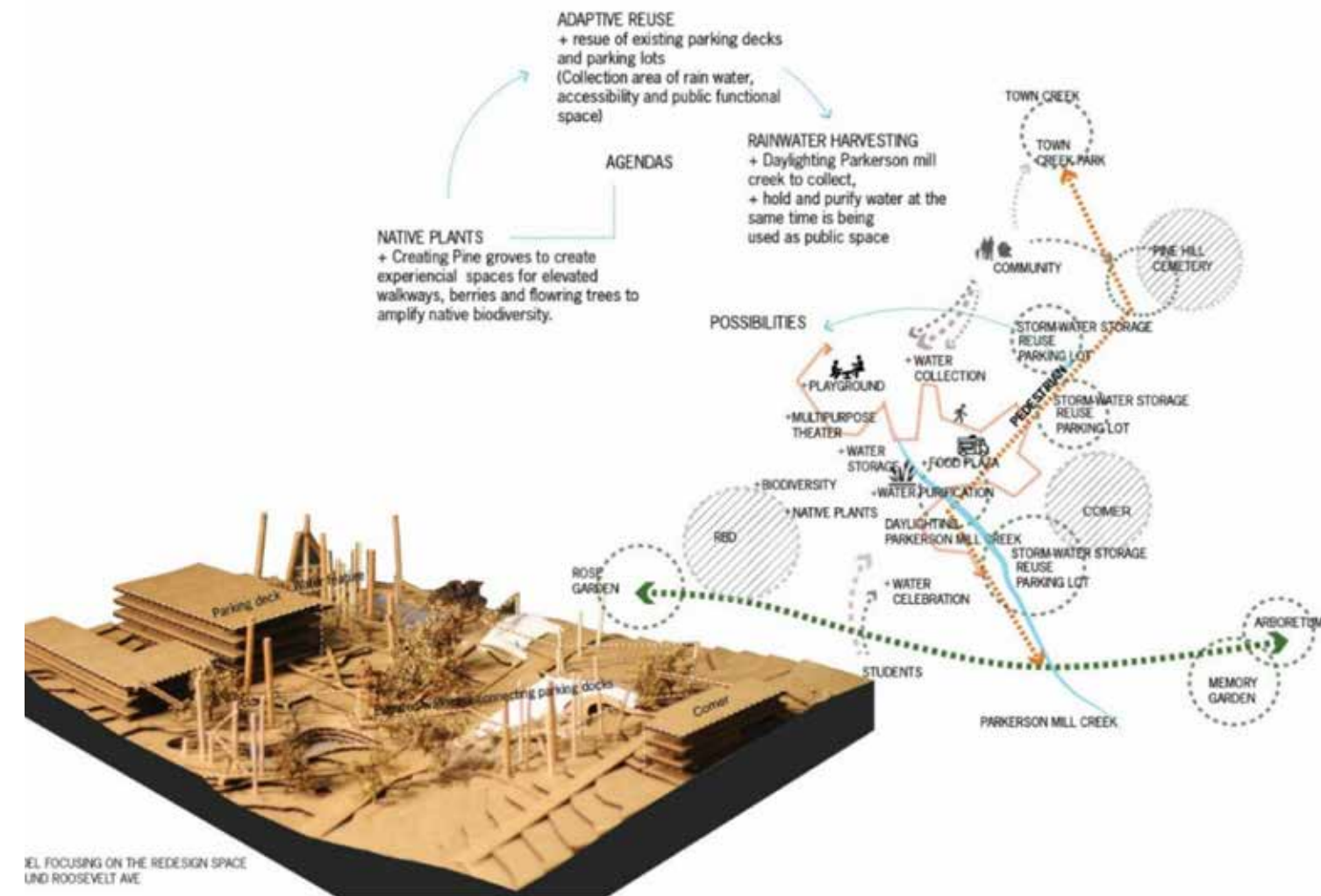


Figure 1. Design proposal for Roosevelt Avenue.

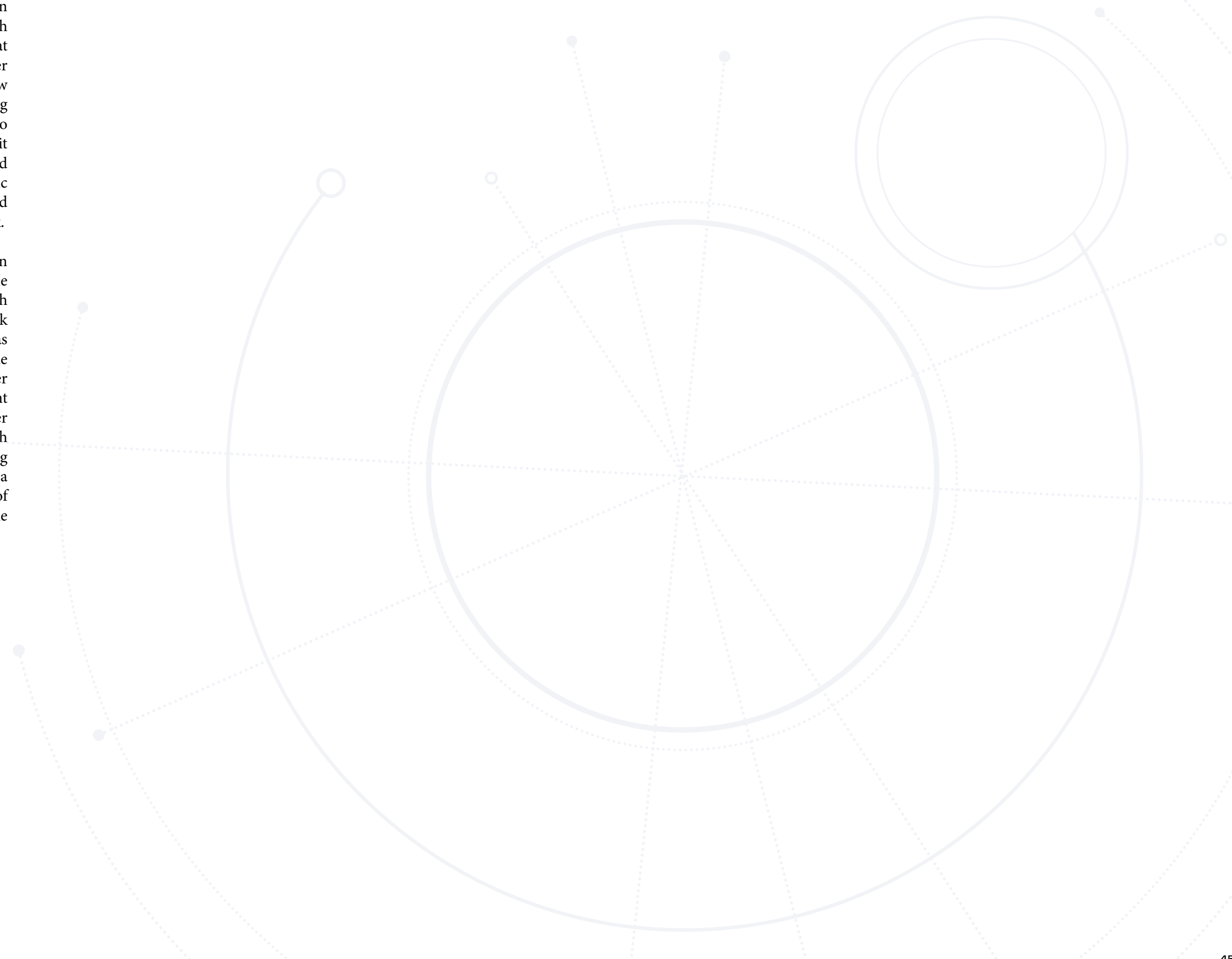
## Materials

Reused and recycled materials had been prioritized in this project to promote sustainability. The roof of each building had designed to collect the rainwater, and that passed through the channel and poured into the water feature below that had been designed with high and low bush berries and with shrubs and could hold standing water. The terraces like water features are designed to work as a waterfall when it rains, and other times it could be used as sitting areas with colorful shrubs and berry trees for the students and visitors. Corten rustic steel had been chosen as the water channel. The elevated walkways were designed with a sustainable boardwalk.

In capsulation, designing a creek has always been challenging, since people must be speculative about the continuous changing movement of groundwater, with surface runoff. Creating a new theoretical framework for Parkerson Mill Creek at Roosevelt Avenue has allowed me to address some issues of connectivity while taking a stand to design with the ephemerality of water movement and landscape. However, the movement of people and functionality has created another dimension of complexity in the overall situation which needed to be addressed. Daylighting PMC and creating the possible green connections in urban fabric is a small try to reconnect the biodiversity with the help of landscape design that could change and evolve while also defending the history of PMC.

## Affiliations

School of Architecture, Planning and Landscape  
Architecture, Auburn University



# Field and Laboratory Investigations of Groundwater Arsenic Sequestration in Biogenic Pyrite at an Industrial Site in Florida

Alicia Fischer and Ming-Kuo Lee

Arsenic (As) contamination of groundwater is one of the most pervasive health hazards worldwide. Over 100 million individuals who rely on groundwater suffer from arsenic contamination (Pi et al., 2017; World Health Organization, 2019). Arsenic is the twentieth most common element in the Earth's crust, with water-rock interactions (e.g., weathering, oxidation, and bacterial-mediated reduction) releasing the metalloid into many water bodies, including aquifers (Gong et al., 2002). More recently, however, anthropogenic arsenic from arsenical herbicides and pesticides has become three times more prevalent than naturally occurring arsenic (Woolson, 1983). This increase in groundwater As contamination is extremely concerning, considering high exposure to the toxic metalloid causes arsenicosis (arsenic poisoning), which induces skin lesions, diabetes, peripheral neuropathy, cardiovascular disease, cancers of the skin, bladder, and lungs, and a higher risk of preterm and stillborn births (World Health Organization, 2019). Moreover, communities in developing regions in Bangladesh, China, and India report the highest cases of arsenicosis due to a lack of resources needed to reduce arsenic concentrations to safe levels (World Health Organization, 2019). To combat this pervasive arsenic crisis, this study has developed a cost-effective technique using sulfate-reducing bacteria (SRB) to form As-sequestering pyrite (arsenian pyrite) (Saunders et al., 1996), testing its effectiveness at an industrial site in Florida over nine months.

Previous studies have investigated the removal of groundwater arsenic using SRB bioremediation with limited success (e.g., Pi et al., 2017). To improve upon these past methods, this study has devised a new injection mixture and scheme to sequester As for nine months: The injectate consisted of 5 kg of ferrous sulfate, ~27 kg (60 lbs) of molasses, and ~1 kg (2 lbs) of fertilizer per 3,785.4 L (1,000 gallons) of water, which was injected into eleven wells located hydrologically upgradient of the plume to allow the injectate to travel

downgradient for full-scale remediation. The mixture provided the necessary amounts of iron, sulfate, and organic carbon to stimulate SRB reduction and engender the precipitation of pyrite at the industrial site. From June 2018 to March 2019, groundwater samples and precipitated solids were collected weekly for the first four weeks, monthly for the first three months, and quarterly for the remaining months. X-ray diffraction (XRD) and X-ray fluorescence (XRF) analyses, electron microprobe (EMP) measurements, scanning electron microscope (SEM) imaging, and geochemical calculations of arsenic speciation and mineral saturation were used to determine whether As had been safely sequestered in arsenian pyrite.

The analyses demonstrated the rapid reduction of arsenic and precipitation of arsenian pyrite after the injection (Fig. 1). The SRB bioremediation technique reduced As concentrations to near or below the site's clean-up standard of 0.05 mg/L in many wells across the site over the nine months (Fig. 1a). Specifically, As concentrations decreased in the monitoring wells from the pre-injection average of 0.17 mg/L to 0.08 mg/L, equating to a >80% removal rate (Fig. 1a). Imaging and quantitative results revealed that pyrite formed as euhedral crystals and spherical aggregates (framboids) 1-30  $\mu\text{m}$  in diameter after two weeks, with these precipitated pyrites sequestering 0.03-0.89 wt% As (Fig. 1b). As such, this study is one of the first to demonstrate long-term sequestration of groundwater As using SRB bioremediation. Considering these promising findings, the study is close to optimizing an affordable procedure for remediating As in both industry settings and developing communities.

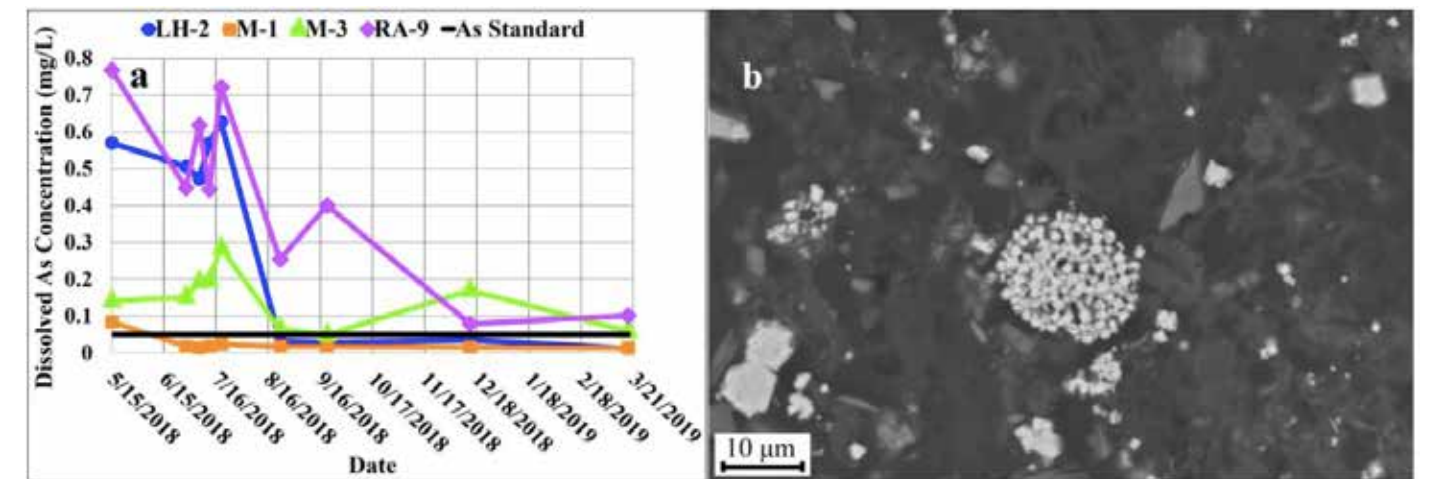


**Figure 1.** (a) Time series data of dissolved arsenic concentrations in four selected monitoring wells. (b) SEM backscatter image of a 15- $\mu\text{m}$  arsenian pyrite framboid at four thousand times magnification from injection well I-2 two weeks after injection.

## References

- Gong, Z., Lu, X., Ma, M., Watt, C., & Le, X.C. (2002). Arsenic speciation analysis. *Talanta*, 58 (1), 77–96. [https://doi.org/10.1016/S0039-9140\(02\)00258-8](https://doi.org/10.1016/S0039-9140(02)00258-8)
- Pi, K., Wang, Y., Xie, X., Ma, T., Liu, Y., Su, C., Zhu, Y., & Wang, Z. (2017). Remediation of arsenic-contaminated groundwater by in-situ stimulating biogenic precipitation of iron sulfides. *Water Research*, 109, 337–346. <https://doi.org/10.1016/j.watres.2016.10.056>
- Saunders, J., Cook, R., Thomas, R., & Crowe, D. (1996). Coprecipitation of trace metals in biogenic pyrite: implications for enhanced intrinsic bioremediation, in: Bottrell, S.H. (Ed.), *Proceedings of the Fourth International Symposium of the Geochemistry of the Earth's Surface: short papers*. University of Leeds, Ilkley, United Kingdom. pp. 470–474.
- Woolson, E.A. (1983). Emissions, cycling and effects of arsenic in soil ecosystems, in: Fowler, B.A. (Ed.), *Biological and Environmental Effects of Arsenic. Topics in Environmental Health*, Elsevier, New York, pp. 51–139.
- World Health Organization. (2019). Exposure to arsenic: A major public health concern (2019 revision). <https://apps.who.int/iris/bitstream/handle/10665/329482/WHO-CED-PHE-EPE-19.4.1-eng.pdf?ua=1>

## Affiliations

Department of Geosciences, Auburn University

# Binary Versus Ternary Metal Oxide Synthesis Pathways: A Study on Copper Oxide Formation Catalyzed by Group 13 Metals

Noah Gibson, Alexandria Bredar, and Byron Farnum

The study of metal oxide nanocrystals has garnered great interest given their applications in photovoltaic devices, catalysis, batteries, sensing, and solar fuels. Indeed, one of the largest bottlenecks in renewable fuels is the development of cheaper, yet catalytically efficient materials for mass production. The introduction of defects, morphology of particles, and nanoparticle size are all influential in the functionality of these materials in devices. As such, a variety of synthetic approaches have been developed to effectively tune these components. A recent modification of the hot-injection approach has been shown to be a less time intensive, effective, and an environmentally friendly method for binary metal oxide formation (Ito et al., 2014; Jansons & Hutchison, 2016). However, its use in ternary metal oxide synthesis has been largely underexplored due to the difficulties of tuning the reactivities of multiple metals. Herein, we show that this method can be utilized to effectively synthesize spinel  $AFe_2O_4$  ( $A = Mn, Co, Ni, Cu$ ) and that late transition metals (Cu, Ni) represent a significant hurdle for these materials (Jansons et al., 2017). We use copper as the representative example due to its poor reactivity, which can be partially rectified using trivalent group 13 metals.

Briefly, the nanoparticles were synthesized by complexing the metal starting materials to oleic acid. Termed metal oleate, this precursor is then continuously injected at a set rate into oleyl alcohol at an elevated temperature which undergoes a metal-catalyzed esterification (Cooper et al., 2018). This step is critical as it forms the crucial metal-oxygen bond and contributes to the differences in reactivity between metals. To characterize the reactivity Fourier transform infrared spectroscopy (FTIR) and UV-vis spectroscopy were employed on the reaction oils. To analyze the solids, powder x-ray diffraction (pXRD), energy dispersive x-ray spectroscopy (EDS), scanning electron microscopy (SEM), and tunneling electron microscopy (TEM) were used to

characterize size, crystal structure, and stoichiometry.

The synthesis of spinel  $MnFe_2O_4$ ,  $CoFe_2O_4$ , and  $NiFe_2O_4$  was successful and confirmed via pXRD and EDS. Elemental analysis revealed an A:Fe ratio of  $0.46 \pm 0.08$ ,  $0.47 \pm 0.17$ , and  $0.34 \pm 0.02$  respectively. The diffractogram revealed inverse and normal spinel structures, with TEM revealing monodisperse particles 10 to 15 nm in size. No binary or ternary oxide product was obtained for the copper-based reactions. Interestingly, the Ni deficiency and absence of Cu product pointed to an inherent problem with later transition metal precursors. We attempted to synthesize simpler binary NiO and  $Cu_2O$  using a similar method with little success. We theorized that this was due to poor metal-catalyzed esterification which prevents the proper formation of reactive monomer units for reliable nanoparticle nucleation.

In an effort to support this argument we introduced trace amounts of group 13 metals (aluminum, gallium, indium) which have known Lewis acid properties and can aid in the esterification process and influence copper reactivity and  $Cu_2O$  formation. Gallium was found to be the most effective catalyst. Figure 1a shows the FTIR spectra with varied amounts of Ga concentration. The reactivity can be qualitatively monitored via the formation of ester at  $1760\text{ cm}^{-1}$  and consumption of metal oleate at  $1650\text{ cm}^{-1}$ .<sup>1,2</sup> Pairing this with the decrease in Cu absorbance in the UV-vis spectra (Figure 1b) indicates that increasing Ga concentrations greatly improves the Cu esterification process, effectively forming more Cu monomer units for nanoparticle formation. We confirmed the identity of  $Cu_2O$  via pXRD. The diffractogram is shown in Figure 1c and shows a cubic structure typical for  $Cu_2O$ . No gallium side product was observed in any case. Finally, SEM was used to characterize particle size (Figure 1d). The images revealed monodispersed particles with a tunable size range of  $1\text{ }\mu\text{m}$  to 100 nm based on the

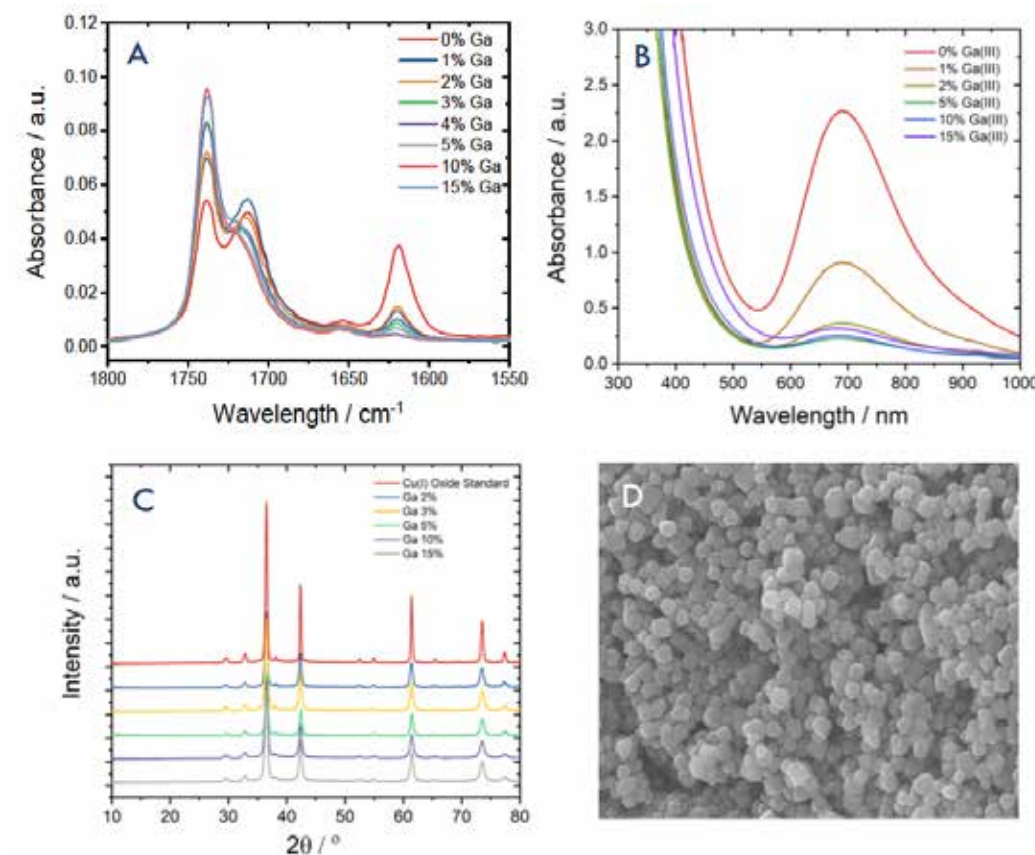


**Figure 1.** (a) FTIR spectra of the post-reaction oils containing 0% to 15% catalytic amounts of gallium to monitor ester formation. (b) UV-vis absorption spectra of the reaction oils in a 1 mm pathlength cuvette to monitor unreacted copper precursor post-injection for reactions containing varied gallium concentrations. (c) pXRD diffractograms for the catalyzed formation of  $Cu_2O$ . (d) SEM images of the particles obtained from an injection containing 5% catalytic amount of gallium.

concentration of catalyst. Aluminum was also explored as a catalyst with little success. Indium showed similar results to Ga, however it showed a propensity to form unwanted  $In_2O_3$  at higher concentrations.

In conclusion, we have showed that a continuous injection methodology can produce more complex ternary metal oxide nanocrystals with tunable size and good stoichiometry. This has great potential as new materials are investigated with applications in renewable energies. Tuning metal reaction rates is a key step in synthesizing more complex and functionalized materials which can also help prevent unwanted side reactions. In this regard, we have shown that including trace amounts of group 13 metals can effectively aid in the discrepancy of metal reactivity. Still, more research is needed to better reconcile the thermodynamic and kinetic barriers associated with multi-metal systems or

nanoparticles with more complex crystal structures to fully access the tunability and economic advantages of this synthesis.

## References

- Cooper, S. R., Plummer, L. K., Cosby, A. G., Lenox, P., Jander, A., Dhagat, P., & Hutchison, J. E. (2018). Insights into the magnetic properties of sub-10 nm iron oxide nanocrystals through the use of a continuous growth synthesis. *Chemistry of Materials*, 30 (17), 6053–6062.
- Ito, D., Yokoyama, S., Zaikova, T., Masuko, K., & Hutchison, J. E. (2014). Synthesis of ligand-stabilized metal oxide nanocrystals and epitaxial core/shell nanocrystals via a lower-temperature esterification process. *ACS Nano*, 8 (1), 64–75.

Jansons, A. W., & Hutchison, J. E. (2016). Continuous growth of metal oxide nanocrystals: Enhanced control of nanocrystal size and radial dopant distribution. *ACS Nano*, 10 (7), 6942–6951.

Jansons, A. W., Koskela, K. M., Crockett, B. M., & Hutchison, J. E. (2017). Transition metal-doped metal oxide nanocrystals: Efficient substitutional doping through a continuous growth process. *Chemistry of Materials*, 29 (19), 8167–8176.

### Affiliations

Department of Chemistry & Biochemistry,  
Auburn University

# Effect of Load Magnitude on Muscle Activation During Unilateral Suitcase Dumbbell Carries

Peyton Gober, Nicole Bordelon, and Gretchen Oliver

The lumbopelvic-hip complex (LPHC) and scapular stabilizing muscles are proximal connections in the kinetic chain, whereby energy is transferred from the lower to the upper extremity during dynamic sport tasks (Kibler et al., 2006). Stability of these regions is necessary for maximizing proximal force generation and transfer through segments of the kinetic chain. Therefore, instability of the LPHC (Kibler et al., 2006) and scapular stabilizing muscles (Kibler, 1998) can result in inefficient transfer of energy and upper extremity compensation to maintain performance. Over time, this undue stress placed on the upper extremity can lead to increased risk of overuse injury (Kibler, 1998). Therefore, strength and conditioning professionals should program exercises targeting improvements in proximal LPHC and scapular stability to decrease risk of upper extremity injury. Weighted carries are often used to improve isometric stability in preparation for more multi-directional and task specific exercises (McGill et al., 2013). Unilateral carries can be especially advantageous to improve stability due to the uneven load distribution that further enhances contralateral muscle activation (McGill et al., 2013). However, the effect of load magnitude on magnitude of LPHC and scapular muscle activation should be understood during programming. Therefore, the purpose of this study was to investigate if load magnitude affects the degree of muscle activation during unilateral dumbbell suitcase carries.

Eighteen ( $22.5 \pm 2.5$  yrs,  $174.9 \pm 8.7$  cm,  $71.8 \pm 27.8$  kg) injury-free and resistance trained individuals completed 3 trials of 3 load conditions relative to body weight including: light (30%), moderate (35%) and heavy (45%). A single dumbbell was carried across a 12m distance in a suitcase position on the dominant side. Electromyography was used to analyze muscle activation of the following: dominant upper and lower trapezius, latissimus dorsi, and serratus anterior as well as bilateral gluteus medius and external obliques. Manual muscle tests were performed on each muscle to determine maximal voluntary isometric contractions (MVIC)

for trial normalization. One investigator performed all manual muscle tests to increase consistency [ICCs (3,1) 0.86-0.99,  $p < 0.002$ ]. A 3 (load) x 8 (muscle) repeated measures ANOVA (RM-ANOVA) compared muscle activation (% MVIC) between load conditions.

RM-ANOVA revealed a significant load by muscle interaction effect [ $F(4.564, 77.582) = 2.454, p=0.045$ ]. Post hoc analysis revealed greater activation in heavy loads compared to light in the upper trapezius ( $p=0.001$ ), latissimus dorsi ( $p=0.005$ ), non-dominant external oblique ( $p=0.008$ ), and the non-dominant gluteus medius ( $p<0.001$ ). Greater activation was also present in the moderate loads compared to light loads in the upper trapezius ( $p=0.003$ ), non-dominant external oblique ( $p=0.003$ ) and non-dominant gluteus medius ( $p=0.001$ ) as seen in Figure 1.

In conclusion, LPHC and scapular muscle activation increased with load, but the changes were muscle specific. The increases in non-dominant (contralateral) external oblique and gluteus medius muscles is consistent with previous research and likely occurred from a greater demand on the LPHC to resist lateral flexion and maintain vertical alignment. Increases in upper trapezius and latissimus dorsi can be explained by maintaining an elevated scapula and adducted shoulder position, respectively. Therefore, unilateral weighted suitcase carries can be beneficial for targeting contralateral LPHC in addition to latissimus dorsi and upper trapezius musculature to improve proximal kinetic chain stability. However, future research should consider other carried positions and the longitudinal training effects on improved stability.

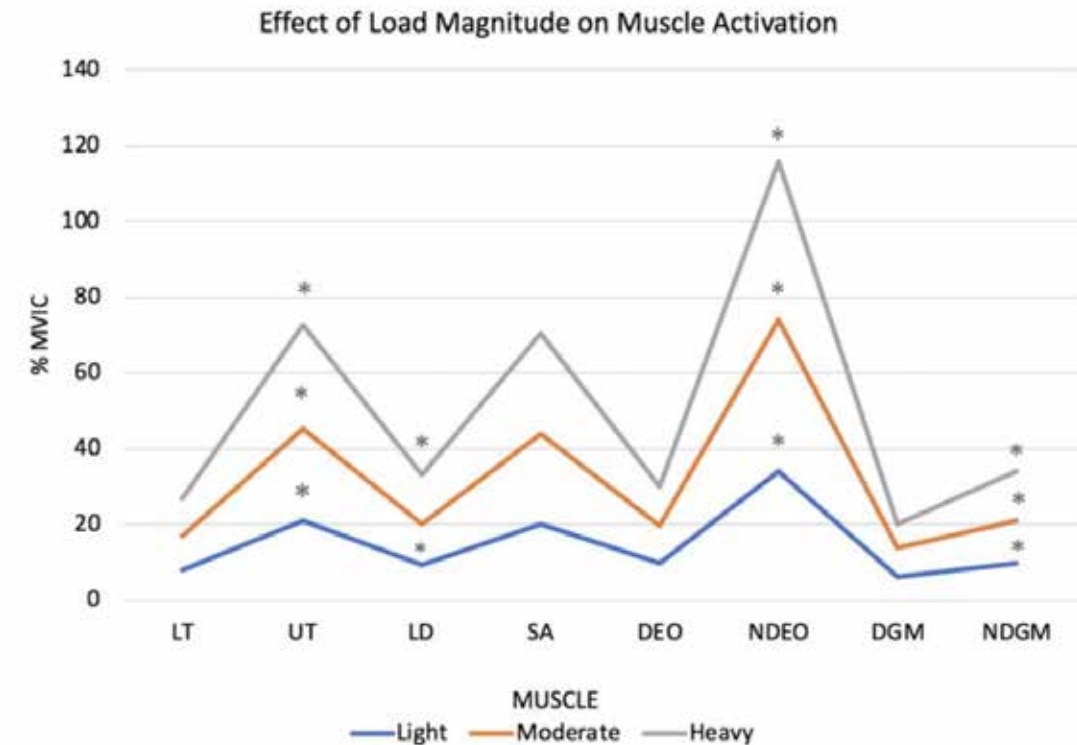


Figure 1. Effect of load magnitude on muscle activation.

Note: \* Indicates significant differences ( $p < 0.05$ ); LT = lower trapezius, UT = upper trapezius, LD = latissimus dorsi, SA = serratus anterior, DEO = external oblique, NDEO = non-dominant external oblique, DGM = dominant-gluteus medius, NDGM = non-dominant gluteus medius.

## References

- Kibler, W. B. (1998). The role of the scapula in athletic shoulder function. *The American Journal of Sports Medicine*, 26(2).
- Kibler, W. B., Press, J., & Sciascia, A. (2006). The role of core stability in athletic function. *Sports Medicine*, 36(3), 189-198.
- McGill, S. M., Marshall, L., & Andersen J. (2013). Low back loads while walking and carrying: Comparing the load carried in one hand or in both hands. *Ergonomics*, 56(2), 293-302.

## Affiliations

School of Kinesiology, Auburn University

# Tiered Collaboration: Addressing the Impact of High Poverty School Culture on Novice Teachers

*Bertha Guilford and Mashika Tempero*

Retaining teachers, in general, has been a nationwide problem for school systems. High poverty schools, in particular, face this challenge of hiring and retaining quality teachers. Research reveals that many high poverty schools, especially those in rural areas, have a hard time hiring highly qualified teachers (Dessoff, 2010). Throughout all of the United States, Alabama is among those states ranking at the highest level of poverty (U.S. Census Bureau, 2017). Alabama is suffering the consequences of a teacher shortage in critical areas: STEM, foreign language, special education, and rural areas. Researchers note more than half of teachers voluntarily leave the profession, leading to a major loss of taxpayer dollars amounting to about \$20,000 per teacher (in large urban districts), with a national price tag of about \$8.5 billion dollars per year (Phi Delta Kappan, 2017). Without adapting recruiting practices to this new generation, Alabama will continue to experience shortages for years to come and will also lose the most highly qualified teaching force possible (Phi Delta Kappan, 2017).

As a result, many high poverty schools hire novice teachers, teachers with zero to three years of work experience, who may or may not be prepared to handle the extraneous demands that are present (Joiner & Edwards, 2008). Consequently, many novice teachers often cannot educate students to the capacity needed to prepare them for the real world due to their having to adjust to the culture and flow of the school, while having to fulfill their traditional instructional duties. In addition, these novice teachers often do not get the support they need, which ultimately pushes them to move to other schools or change careers (Joiner & Edward, 2008). Recent research confirms that up to half of all new teachers leave within the first five years in the profession, with almost 30% leaving within the first three years (Kelly, 2004; Maciejewski, 2007; Ingersoll & Smith, 2004).

The research states that teachers choosing to depart from the school due to job dissatisfaction link their decision to inadequate administrative support, isolated working

conditions, poor student discipline, low salaries, and a lack of collective teacher influence over school-wide decisions (Alliance for Excellent Education, 2014).

To address the demand for hiring and retaining teachers in high poverty schools across the state of Alabama a modified conceptual model for a teacher residency program should be adopted. New teacher residency programs have become an increasingly popular method for district and school leaders to retain teachers. The residency model is a partnership with school districts and universities that provides a yearlong apprenticeship in classroom with a mentor. The resident or mentee will be able to put theory to practice in the classroom while receiving feedback from his or her mentee. According to the 2017-2018 Network Partner's report, eighty-six percent of teachers who received training through the residency model are teaching in the same school after three years (NCTR, 2017). Retention rates show a positive correlation to the implementation of the teacher residency programs (Guha, Hyler, & Darling-Hammond, 2016). In future studies, we plan to examine the school administrators have on the teacher residents' experience as a first-year teacher.



Figure 1. Proposed modified conceptual model.

## References

- Alliance for Excellent Education. (2004). Tapping the potential: Retaining and developing high-quality new teachers. Retrieved from <http://all4ed.org/reports-factsheets/tapping-the-potential-retaining-and-developing-high-quality-new-teachers>
- Dessoff, A. (2010). Persuading teachers to go rural: District administrators craft incentives to attract and retain teachers. *District Administration*, 46(6), 58-60. Retrieved from: <http://www.districtadministration.com/article/persuading-teachers-go-rural>
- Guha, R., Hyler, M.E., & Darling-Hammond, L. (2016). *The teacher residency*. Palo Alto, CA: Learning Policy Institute.
- Joiner, S. & Edwards, J. (2008). Novice teachers: Where are they going and why don't they stay? *Journal of Cross-Disciplinary Perspectives in Education*, 1(1), 36 – 43.
- Kelley, L. M. (2004). Why induction matters. *Journal of Teacher Education*, 55(5), 438- 448.
- Maciejewski, J. (2007). Supporting new teachers: Are induction programs worth the cost? *District Administration*, 43(9), 48-52.
- Phi Delta Kappan (2017) Teacher shortages: why, where, what to do. "Sticky schools: How to find and keep teachers in the classroom". p. 19
- Smith, T. M. & Ingersoll, R. M. (2004). What are the effects of induction and mentoring on beginning teacher turnover? *American Educational Research Journal*, 41(3), 681- 714.
- The National Center for New Teacher Residency. Retrieved from <https://nctrresidencies.org/>
- U.S. Census Bureau (2017). Income and Poverty in the United States: 2017. Retrieved from <https://www.census.gov/library/publications/2018/demo/p60-263.html>

# Development of a Novel Rotating Volumetric Velocimetry Technique for Rotor Flows

*Abhishek Gururaj, Mahyar Moaven, Zu Puayen Tan, Brian Thurow, and Vrishank Raghav*

Understanding the aerodynamics over rotors is important to design better performing helicopters, wind turbines, and unmanned aerial vehicles etc. Various qualitative as well as quantitative flow measurement techniques like hot-wire anemometry, tuft visualization, smoke flow visualization, and particle image velocimetry (PIV) etc. have been used to characterize the flow over rotors. In the studies that employ PIV for studying the flow, the method of phase-averaging has been widely employed. Phase-averaging is a technique in which an external signal is used to trigger the light source and the camera at a particular phase repeatedly, and then the images are averaged together. However, past studies have noted that phase-averaging does not capture the cycle-to-cycle variations well. This necessitates time-resolved measurement to be performed to study the flow over rotors. In all the PIV studies, the measurement has been made from the lab-fixed frame of reference (i.e. the images of a body in the rotating frame is captured from a fixed frame). This difference in frame of reference between the imaging system and the wing induces limitations to perform time-resolved measurements. Hence, to overcome the limitations caused by the conventional PIV techniques, the measurement should be made in the rotating frame itself.

In this summary, the development of a novel methodology to study the flow over a rotor in the rotating frame of reference will be discussed. The schematic of this methodology is shown in Figure 1. A mirror at an inclination of 45° is mounted at the hub of the rotor and is simultaneously rotated with it. A plenoptic camera is used instead of a standard camera due to its ability to capture the three-dimensional flow information, and is co-axially mounted with the mirror. Also, a volumetric field illumination is considered instead of a planar field illumination. As the wing rotates, the flow evolving over it is reflected onto the mirror. Hence, the flow field evolving over the wing is captured by the camera through the mirror. The combination of a rotating

mirror, a plenoptic camera and volumetric illumination allows the user to perform time-resolved and three-dimensional flow measurement over a wide range of azimuth angles. To study the flow over a rotating wing using this methodology, a water tank experimental test rig was designed and developed. Experiments were conducted on a rectangular flat plate wing mounted at a pitch angle of 45°. The wing was rotated at 1 RPM, which corresponded to a chord-based Reynolds number of 1200.

$$\left( Re_c = \frac{\Omega R_{tip} c}{\nu} \right)$$

Flow field analysis over the rotating wing showed the evolution of a leading-edge vortex as shown in Figure 1. It can be observed that a vortex has started to form at  $\psi = 1^\circ$ . As the azimuth angle increases, this vortex grows in size. However, after a certain angle, the vortex does not convect downstream with the same velocity across the wing span. It can be observed that the vortex near the tip moves slower compared to vortex towards the root ( $\psi = 8^\circ$ ). Further increase in azimuth angle increases this non-uniformity. Finally, at  $\psi = 10^\circ$ , it can be observed that the vortex has started losing its coherent structure near the wing tip while the coherent structure is maintained towards the root. This flow field analysis proves the feasibility of the rotating volumetric velocimetry methodology to study the time-resolved and three-dimensional flow field over a rotating wing. In the future, the methodology will be further validated for various other parameters like different pitch angles, Reynolds numbers, wing sizes etc.

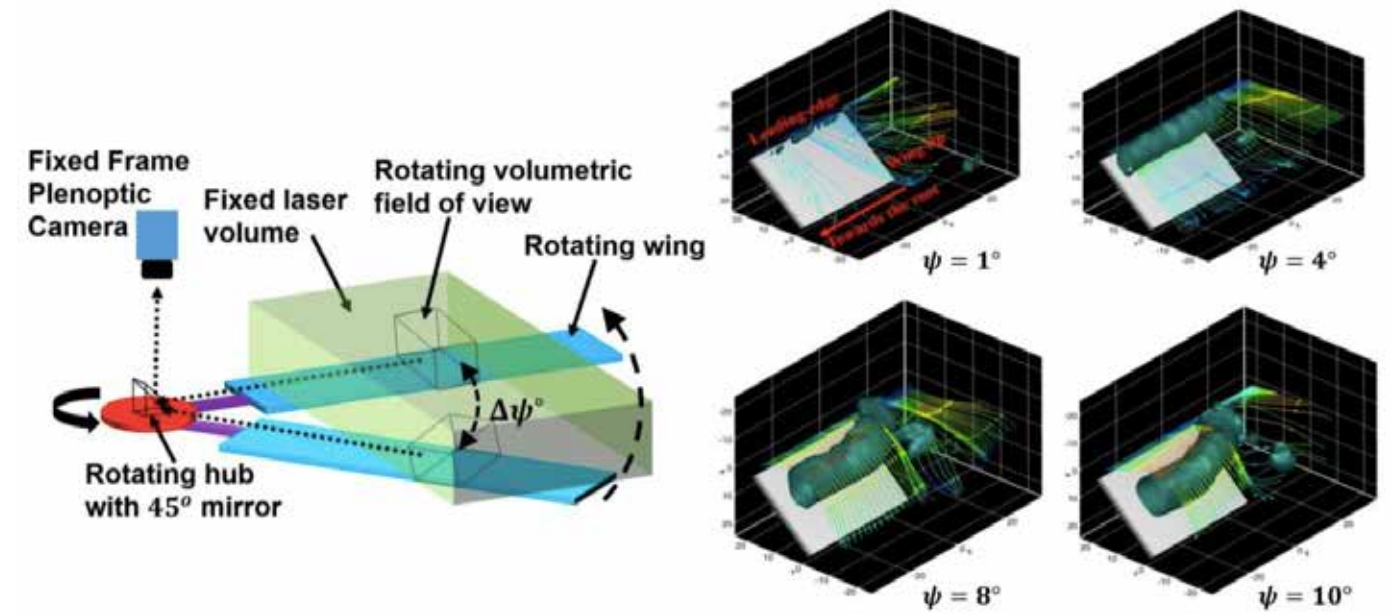


**Figure 1.** Schematic of the rotating volumetric velocimetry methodology (left); Images showing the iso-surfaces of q-criterion for various azimuth angles (right).

## Affiliations

Department of Aerospace Engineering,  
Auburn University

# Investigation of the Antibacterial Activity Against Foodborne Pathogens and Chemical Composition of Extracts and Partitions of *Psidium guajava*

Audrey Hall<sup>1</sup>, Emefa Monu<sup>2</sup>, and Angela Calderón<sup>3</sup>

Foodborne illness is a common, costly, yet preventable public health issue. The CDC estimates that each year around 1 in 6 (or 48 million) people in the United States gets sick of foodborne illnesses. Of the total number, 128,000 are hospitalized and 3,000 died (Scallan et al., 2011). The number of foodborne disease outbreaks continues to rise each year; thus, finding ways to prevent foodborne illness is of great importance. *Escherichia coli*, *Salmonella enterica*, and *Staphylococcus aureus* are among the most common pathogens that contribute to this public health issue. Many plant species from around the world have been studied for their natural antibacterial activity. *Psidium guajava*, commonly called guava, is a plant that has been traditionally used in folk medicine for the prevention and treatment of diarrhea and stomach-aches (Gutierrez et al., 2008). The aim of the specific research project is to identify, isolate, and fully characterize the chemical constituents responsible for antibacterial activity of *P. guajava* extract and partitions against foodborne pathogens and spoilage organisms.

The *Psidium guajava* L. (Myrtaceae) leaves collected from Ghana, West Africa, were dissolved in 70% ethanol, dried, and powdered. The ethanolic extract was shown to decrease the levels of all three pathogens (*E. coli*, *S. enterica*, and *S. aureus*) below the detection limit after 24 hours, suggesting that *P. guajava* is a source of antibacterial agents against *E. coli*, *S. enterica*, and *S. aureus*. The ethanolic extract was then dissolved in water and sequentially extracted with n-hexane and dichloromethane to remove the hydrophobic compounds. The aqueous phase was then extracted with ethyl acetate to remove the polar compounds. Each of the four separate partitions were concentrated under reduced pressure and dried into a powder form. The antibacterial activity of each partition was evaluated by determining the minimum inhibitory concentration

(MIC) against *E. coli*, *S. enterica*, and *S. aureus*. The MIC was determined by growing the pathogens in nutrient broth at their optimum growth temperature for 24 hours in the presence of varying concentrations of the partitions. Antibacterial assays displayed the MIC's against *E. coli* for the dichloromethane, aqueous, and ethyl acetate partitions are 1%, 0.75%, and 0.5%, respectively. In comparison, the MIC of the crude ethanolic extract was 1%. Because the ethyl acetate partition has the lowest MIC, it is considered the most active partition against *E. coli*. The same method will be utilized to determine the MIC for the remaining two pathogens. The most active partition will be further investigated using Liquid Chromatography Mass Spectrometry (LC-MS), a technique typically used for chemical fingerprinting of plant extracts. The chemical fingerprinting of active *P. guajava* partitions will be used to replicate compounds found in existing literature and to potentially identify new compounds. The resulting LC-MS data will be analyzed using a chemometrics software called Mass Professional Profiler (MPP) that performs statistical analysis on the sample and correlates with the biological activity to develop a biochemometrics approach. Biochemometrics correlates the chemical profile of the compounds with their bioactivity and is very effective in providing a comprehensive representation of which compounds are responsible for the activity in the extract (Britton et al., 2017). Structure elucidation will then be performed using Mass Spectrometry (MS) and Nuclear Magnetic Resonance (NMR).

The antibacterial constituents of *P. guajava* leaves that act against *E. coli*, *S. enterica*, and *S. aureus* can then be used to formulate a substance that is applicable to fruits and vegetables after harvesting that will prevent the growth of foodborne pathogens, thereby reducing the consumer's chance of acquiring foodborne illnesses.

With the rising number of foodborne illness cases each year, the global impact of my research project has great potential.

## References

Britton, E. R., Kellogg, J. J., Kvalheim O. M., & Cech, N.B. (2017). Biochemometrics to identify synergists and additives from botanical medicine: A case study with *Hydrastis Canadensis* (Goldenseal). *Journal of Natural Products*. DOI: 10.1021/acs.jnatprod.7b00654

Gutierrez, R., Mitchell, S., & Solis, R. (2008). *Psidium guajava*: A review of its traditional uses, phytochemistry and pharmacology. *Journal of Ethnopharmacology*, 117 (2008) 1-27.

Scallan, E., Hoekstra, R. M., Angulo, F. J., et al. (2011). Foodborne illness acquired in the United States—Major pathogens. *Emerging Infectious Diseases*, 17(1):7-15. doi:10.3201/eid1701.p11101

## Affiliations

<sup>1</sup> Department of Chemical Engineering, Auburn University

<sup>2</sup> Department of Poultry Science, Auburn University

<sup>3</sup> Department of Drug Discovery and Development, Auburn University

# The Effect of Trunk Kinematics on Net Normalized Shoulder Kinetics in Baseball Pitching

Michael Hankes, Kevin Giordano, and Gretchen Oliver

Baseball pitchers often vary the position of their trunk during a pitch as a means to alter arm slot in attempt to increase performance and deceive the hitter. It is known that increased shoulder kinetics, forces acting through or causing rotation about the joint, are correlated with increased rates of injury (Fleisig et al., 1995), but it is unknown how trunk positioning affects shoulder kinetics. Because energy must be funneled from the trunk through the shoulder and out the arm during a pitch, it could be theorized that altered trunk position could play a factor in determining kinetics at the shoulder. Given the adverse effects of increased shoulder kinetics on shoulder injuries (Fleisig et al., 1995), we aimed to examine the correlation between trunk positioning and shoulder torque during baseball pitching.

Seventeen youth male baseball pitchers (15.4±1.1 years; 181.75±4.5 cm; 74.4±8.3 kg) each threw 3 fastball pitches, which were averaged for analysis. An electromagnetic tracking system collected kinematic data. Using anthropometric norms, top-down inverse dynamics were used to calculate our kinetic variable, net shoulder torque, and normalized to the participants' body mass. For analysis, we broke the pitch apart into phases between the following events: (FC) front foot contact, defined as when the front foot hits the ground; (MER) maximum external rotation, when the humerus is rotated to orient farthest posterior to the pitcher; (BR) ball release, when the ball leaves the pitchers hand. Specifically, we analyzed the effect of average trunk kinematics during each phase prior to ball release, on maximum shoulder net torque.

Linear regression analysis revealed greater trunk rotation to the throwing arm side, during the phase from FC to MER, correlates with an increase in maximum shoulder net torque during a baseball pitch (Figure 1). Altering trunk rotation during the pitch may be detrimental to the transfer of energy through

the kinetic chain, resulting in compensation at the shoulder joint to maintain performance, potentially leading to injuries. Trunk rotation to the pitching arm side may alter the length-tension relationship of the active support structures crossing the anterior shoulder responsible for transferring elastic energy, such as the pectoral and subscapularis muscles. To maintain performance, greater energy must be generated across the shoulder joint, potentially resulting in greater stress upon passive structures such as the glenoid labrum and shoulder capsule, possibly leading to instability or injury. This study aids coaches and clinicians in identifying increased trunk rotation to the pitching arm side as a potentially injurious aspect of pitching mechanics.

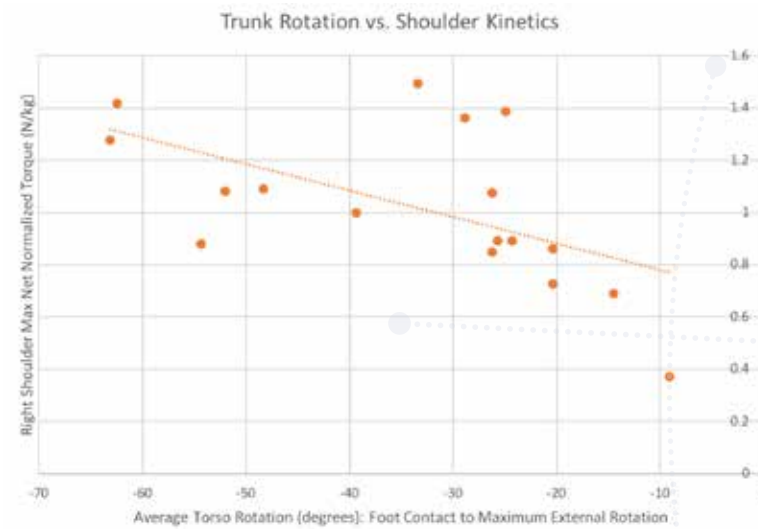


**Figure 1.** The correlation between trunk rotation and shoulder kinetics are shown. Positive trunk rotation indicates rotation to the left.

## References

Fleisig, G. S., Andrews, J. R., Dillman, C. J., & Escamilla, R. F. (1995). Kinetics of baseball pitching with implications about injury mechanisms. *American Journal of Sports Medicine*, 23(2), 233–239. <https://doi.org/10.1016/j.ijadhadh.2016.05.002>

## Affiliations

School of Kinesiology, Auburn University

# Racial Disparities in Sleep Among College Students

William Illiano<sup>1</sup> and Thomas E. Fuller-Rowell<sup>2</sup>

Sleep has shown to be vastly important in the maintenance of physical and mental health. The effects of insufficient or low-quality sleep are well-documented to be associated with negative health outcomes including endocrine dysfunction (Spiegel et al., 1999), worse mental health (Milojevich et al., 2016), and dysregulation of glucose (Morselli et al., 2010). Recently, it has been identified that Black/African Americans (AAs) tend to receive less and lower quality sleep than Whites/European Americans (EAs). Thus, sleep may be an important factor in the larger racial disparities that are observed in American public health. However, much of the literature relies on self-report measures of sleep, and, of the studies that employ objective measures of sleep, few have been conducted within a college sample. To better understand this topic, the present research seeks to (1) evaluate the extent of racial disparities in objective measures of sleep within a college sample and (2) evaluate the role of socioeconomic factors in the race-sleep relationship.

To address these topics, 263 first- and second-year undergraduate students completed a laboratory visit during which participants answered questions about general life experiences, health behaviors, socioeconomic background, and sleep. Following the visit, participants wore an Actiwatch 2 (Philips Respironics) actigraph for eight consecutive nights from which measures of sleep duration, sleep efficiency, and waking after sleep onset (WASO) were derived. Twenty-two participants were excluded due to missing data, leaving a final analytic sample of 241 (19.21±1.01 yrs.; 53% female; 52% AA, 48% EA).

To address the first objective, t-tests were performed on sleep outcome variables. Statistically significant racial differences were observed in sleep duration ( $p < .001$ ) and sleep efficiency ( $p < .001$ ) but not in WASO ( $p = .294$ ). The average nighttime sleep duration was 6 hours and 3 minutes for AAs and 6 hours and 38 minutes for EAs. The average sleep efficiency (calculated as the percentage sleep time divided by

total time in bed) was 77% for AAs and 81% for EAs. To address our second objective, a series of linear regression models were estimated to examine race differences in sleep duration and sleep efficiency, and the degree to which they are attenuated after adjusting for four measures of socioeconomic status: parent education, household income to needs ratio, neighborhood deprivation, and financial strain (each examined separately and all together in the final model). All models also adjusted for age, sex, and napping minutes. Results are displayed in Table 1.

In general, the socioeconomic factors did not significantly account for the racial disparity in objective sleep measures. In all models, race remained a significant predictor of sleep outcomes and the magnitude of the race disparities remained similar, suggesting that, in this sample, the observed race differences in sleep are distinct from the socioeconomic factors considered. It may be possible that the experience of attending college mitigates the extent to which socioeconomic factors affect sleep due to many students sharing a similar environment and stressors (e.g., academics). Also noteworthy was that napping was a significant factor in explaining the observed racial differences, accounting for approximately a quarter of the race difference in both sleep outcomes. This is because AAs tended to nap significantly more than EAs in our sample ( $p < .001$ ) and because napping is associated with shorter periods of nighttime sleep. Short periods of nighttime sleep can lead to daytime tiredness which can lead to naps, and more napping can lead to lower levels of nighttime tiredness which can result in less nighttime sleep. The reasons for this difference in napping behavior and its implications are a future topic of investigation. Further research with this dataset will consider different and more complex models, potentially considering additional control variables and different stressors (e.g., discrimination) in order to better elucidate what other factors may be giving rise to the observed race differences in sleep outcomes.

Table 1. Linear regression models for sleep duration and sleep efficiency.

Variables	Model 1		Model 2		Model 3		Model 4		Model 5	
	B	SE	B	SE	B	SE	B	SE	B	SE
<b>Sleep Duration</b>										
Race	-27.6***	6.35	-25.4***	6.60	-27.3***	6.84	-25.0***	6.43	-26.5***	7.10
Gender	18.6**	6.25	17.7**	6.28	17.8**	6.26	17.5**	6.24	17.5**	6.30
Age	-3.97	3.08	-3.99	3.05	-4.25	3.09	-3.89	3.08	-3.79	3.07
Napping	-.685***	.121	-.706***	.121	-.681***	.122	-.675***	.121	-.698***	.122
Parent Education	.605	1.54							.194	1.74
Income:Needs			.76	1.09					.379	1.26
Area Deprivation					-.026	.163			-.129	.182
Financial Strain							-5.84	3.57	-5.96	3.92
<b>Sleep Efficiency</b>										
Race	-2.90***	.814	-3.11***	.864	-2.90**	.871	-2.85**	.825	-3.40***	.929
Gender	2.78**	.801	2.76**	.821	2.65**	.798	2.65**	.801	2.84**	.824
Age	-.390	.395	-.341	.399	-.422	.393	-.428	.395	-.287	.402
Napping	-.039*	.015	-.040*	.016	-.038*	.015	-.038*	.016	-.037*	.016
Parent Education	.179	.198							.357	.227
Income:Needs			-.138	.143					-.193	.165
Area Deprivation					-.008	-.024			-.004	.024
Financial Strain							.211	.458	.230	.513

Note. Sleep duration is coded by total minutes and sleep efficiency by percentage. Race is coded so that White/EA = 0, Black/AA = 1, Gender is coded Male = 0, Female = 1. \* $p < .05$ . \*\* $p < .01$ . \*\*\* $p < .001$ .

## References

Milojevich, H. M., & Lukowski, A. F. (2016). Sleep and mental health in undergraduate students with generally healthy sleep habits. *PloS One*, 11(6).

Morselli, L., Leproult, R., Balbo, M., & Spiegel, K. (2010). Role of sleep duration in the regulation of glucose metabolism and appetite. *Best Practice & Research Clinical Endocrinology & Metabolism*, 24(5), 687-702.

Spiegel, K., Leproult, R., & Van Cauter, E. (1999). Impact of sleep debt on metabolic and endocrine function. *The Lancet*, 354(9188), 1435-1439.

## Affiliations

<sup>1</sup> Biomedical Sciences Program, Auburn University

<sup>2</sup> Department of Human Development and Family Studies, Auburn University

# Off Campus Students' Participation Gap Linked to Difficulties with Transportation and Parking

Jhayla Isom<sup>1</sup> and Sara Driskell<sup>2</sup>

Students who live off campus may enjoy many benefits, such as increased independence, but they may also struggle with student engagement on campus, especially if they find it difficult to get back to campus after classes. Auburn University is home to many on-campus events, student groups, and academic and social resources, such as concerts, talks, the Student Center, RBD Library, and more. However, these events and resources may be underutilized by off-campus students after classes. This research investigated the extent that parking services and transportation options affected off-campus students' involvement on campus.

The Psychology Department's participant pool was used to collect the 498 undergraduate students surveyed for this study ( $M_{\text{age}}=19.24$ ,  $SD=1.49$ ). Of these, there were 48.6% Freshmen, 17.3% Sophomores, 12.1% Juniors, 8.2% Seniors, and 13.8% did not answer. Additionally, 69.5% identified as women, 19.5% identified as men, and 11.1% did not select an answer. Participants were 76.6% White American, 4.3% Black/African American, 3.6% Asian American, 0.9% Latinx American, 3.6% Biracial or other, and 11.1% did not answer. Participants were divided by housing status, with 44.5% living on-campus and 55.5% living off-campus.

We surveyed participants' ease of getting to campus after school hours, avoidance going to social and academic events after school hours specifically because of the difficulty getting to campus, attendance at events on campus for personal enjoyment rather than class, average number of hours spent on campus outside of classes for off-campus students, and their demographics, including whether they live on or off campus. In addition, we asked what they most wanted to change about Auburn, what they thought Auburn's biggest construction goals should be, and their attitudes toward parking and transportation services for Auburn in particular.

We found that off-campus students ( $M=3.36$ ,  $SD=1.11$ ) reported significantly more difficulty getting to campus

after hours compared to on-campus students ( $M=5.74$ ,  $SD=0.97$ ),  $F(1,492) = 660.11$ ,  $p < .001$ ,  $\eta^2 = .57$ . Moreover, we found that off-campus students ( $M = 3.47$ ,  $SD = 1.17$ ) reported significantly more avoidance of social and academic events on campus due to their difficulty getting to them when compared to on-campus students ( $M = 4.11$ ,  $SD = 1.04$ ),  $F(1,492) = 45.18$ ,  $p < .001$ ,  $\eta^2 = .08$  (see Figure 1). We also found that off-campus students ( $M = 3.22$ ,  $SD = 1.09$ ) reported being significantly less likely to attend events on campus for their personal enjoyment when not required by a class, compared to their on-campus counterparts ( $M = 2.98$ ,  $SD = 1.02$ ),  $F(1,496) = 5.718$ ,  $p = .017$ ,  $\eta^2 = .011$ . When off-campus students were asked about how much time they spend on campus outside of class time, the average was only 2.46 ( $SD=2.54$ ), aligning with 2-3 hours per day on the provided scale.

We also found that 22.1% of participants wrote in a transportation-related response when asked about what they would change about Auburn. Moreover, 68% of participants chose adding more parking as what they thought should be one of Auburn's biggest construction goals, the highest-select option. When asked about their top three issues regarding transportation services, participants most commonly selected the wait times for the security shuttles (41.5%), not having enough buses per transit line (30.8%), not having enough security shuttles (24.6%), and that there were not enough transit lines (21.6%).

Overall, we found that compared to students living on campus, those living off campus felt they had a significantly harder time getting to campus. This difficulty resulted in them avoiding events and on campus resources, especially when those events or campus resources were not needed for classes. These findings can be used to provide insight on how to close the participation gap between on and off campus students and help all students get the most out of their time at Auburn. Student event and resource accessibility could be key to increasing student engagement and

improving academic outcomes, especially early in students' college careers. This may be particularly true for freshmen who live off campus, given that dorms are not guaranteed to all incoming students. Therefore, it is important that university leaders address student transportation concerns to try to mitigate these gaps in student engagement.

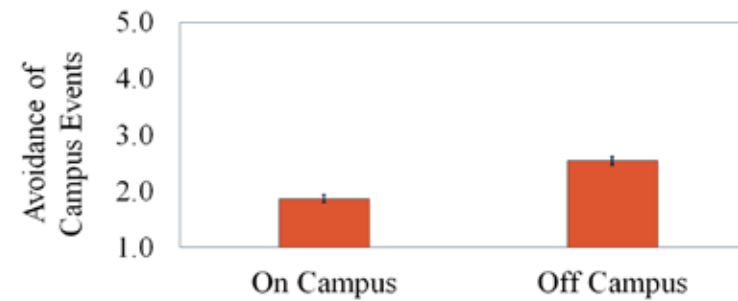


**Figure 1.** Students' reported level of avoidance of on-campus social and academic events held after hours due to difficulty related to getting to and from campus. Error bars are standard errors.

## Affiliations

<sup>1</sup> College of Sciences and Mathematics, Auburn University

<sup>2</sup> Department of Psychology, Auburn University

# Novel SIRT3 Agonist Alter Lipid Accumulation in Lipid Mediated Hepatic Steatosis

Victoria Jiminez, Sieun Yoo, Ian Steinke, Jared Senfeld, Nila Ghanei, Taylor Schaedig, Manoj Govindarajulu, Forrest Smith, and Rajesh Amin

The most severe form of non-alcoholic fatty liver disease (NAFLD) emerging around the world today is non-alcoholic steatohepatitis (NASH). NASH is a progressive fibrotic disease, in which cirrhosis and liver-related death result in death in up to 20% of people affected over a 10 year time span. Obesity, diabetes, and hyperlipidemia are conditions highly associated with NAFLD and NASH. The prevalence of NAFLD is 80-90% in obese adults, 30-50% in diabetic patients, and up to 90% in hyperlipidemic patients. To mitigate the development of NAFLD and prevent its progression towards NASH there is a critical need for novel therapies. The most significant factor leading to this progression is mitochondrial dysfunction associated with insulin resistance and ensuing hepatic lipid accumulation.

SIRT3, a mitochondrial protein, has recently been discovered to be altered in function and reduced in expression in heart and liver models of obesity and diabetes. By deacetylation, SIRT3 regulates many mitochondrial proteins associated with metabolic homeostasis, oxidative stress, and cell survival. Currently, no clinical agonists for SIRT3 exist for mitochondrial dysfunction associated with metabolic disorders. Our current investigations towards developing novel SIRT3 agonists have helped identify select amino acids in the active binding site of SIRT3 resulting in opening up the active site for the required cofactor NAD<sup>+</sup> binding. Our modeling predicts that this activation stimulates the protein to improve lipid mediated steatosis in the liver.

The current hypothesis predicts that the activation of SIRT3 promotes protection against fatty acid induced hepatic steatosis. Novel SIRT3 agonists were computationally developed using Site ID module of Sybyl X-1.3 for potential allosteric binding sites. Hepatic steatosis was developed using BSA-conjugated oleic acid and palmitic acid. SIRT3 activity for compounds was based upon a fluorescence based assay. We applied increasing concentrations (10 nm-500µM) of our SIRT3

activators or inhibitors to measure levels of fluorescence. Lipid accumulation and lipid vesicle size was measured using an Oil Red O stain. Lipid levels and droplet size was measured by Bio Tek Cytation imaging software in HepG2 (Figure 1). In addition, mitochondria were isolated and mitochondrial membrane potential was measured using tetramethylrhodamine ethyl ester (TMRE) and thus measuring mitochondrial energy regulation. An MTT Assay was utilized to measure mitochondrial viability (cell viability) using a tetrazolium salt conversion to formazan salt. Finally, a western analysis was conducted using acetylated lysine antibody cell signaling (#9441) to measure acetylated lysine in mitochondrial fractions. pAMPK was measured using pAMPK-α2 for Thr-172 (#2535) and standardized by T-AMPK-α2 (2757). These gave measurements of direct SIRT3 effector expression levels.

The pan-SIRT agonist *Honokiol*, a plant extract from the bark of a magnolia tree, shows interaction with Asn229 and Pro155 amino acids in the catalytic site and our lead compound **AU-42** (5148442) displays the same binding pose as seen in *Honokiol*, but also interacts with *ILE154* to which we predict enhances the interaction with the cofactor NAD<sup>+</sup>, thus improving SIRT3 activity and possesses the best docking score among all the ligands. We have also observed that *Honokiol* reduced lipid accumulation in our fatty acid steatotic model 20%, whereas our lead compounds reduced lipid accumulation by 30-45%. In addition, we observed lipid vesicle diameters in hepatocytes were reduced by approximately 20% by *Honokiol* and 40-50% by our lead compounds.

In conclusion, we have observed that our lead compound AU-42 induces an increase in SIRT3 activity, mitochondrial deacetylation, decreased lipid accumulation and increased pAMPK levels. We predicted that our lead compound displays a higher

EC50 than optimally desirable and we are developing further derivatives of AU-42 to lower the EC50. Results from preliminary animal work in diabetic and SIRT3 knockout mice have helped delineate the role of selective amino acids that are compromised from diabetes and can be altered by activation of alternative amino acids in the conformational site. To improve mitochondrial bioavailability, we will add a peptide signal for mitochondrial delivery of our compound. Most significantly, this data is preliminary and further analysis of downstream effects of SIRT3 in the mitochondria must be explored, such as Acetyl-CoA Carboxylase and SOD with and without fatty acid treatment. However, we have screened more than 30,000 compounds from various *in silico* databases using Surflex Dock module in Sybyl X-1.3. Our work is ongoing and further *in vivo* testing is needed.

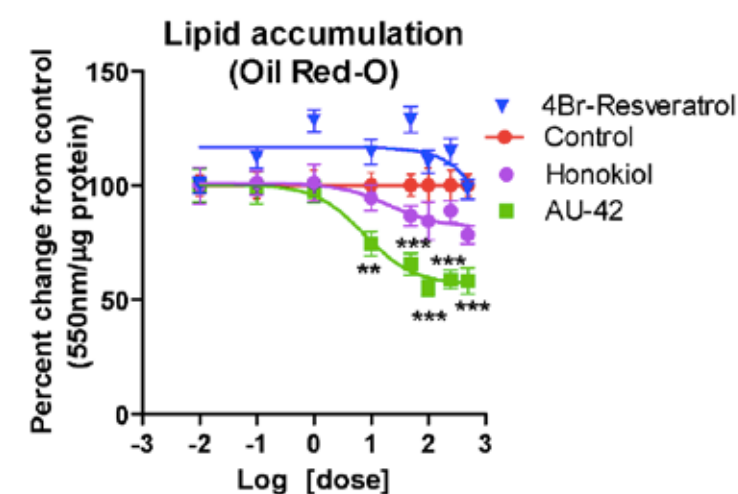


**Figure 1.** SIRT3 activation reduces lipid accumulation in HepG2 cells. Lipid accumulation was measured by Oil Red O staining as measured by using a BioTek Cytation imaging software from cells in panel A. Statistical analysis of data was accomplished using Prism software and where n= 3 independent experiments and values are presented as percent change from control. \*\*, P< 0.001, \*\*\*, P< 0.0001.

## Affiliations

Department of Drug Discovery and Development, Auburn University

# Inventory and Characterization of Gulf Coast Salt Marsh Soil Resources

Brooke Johnson and Joey Shaw

This project was jointly conducted by the Auburn University Soil Characterization Laboratory and the USDA Natural Resources Conservation Service – Coastal Zone Soil Survey to classify, characterize, interpret, and improve our understanding of tidal marsh soils. Coastal marsh environments are essential habitats for economically important shellfish, improving water quality, and storing carbon. As development and sea-level rise pose increasing threats to coastal marsh ecosystems, an improved understanding of tidal marsh soils and more accurate soil inventories will facilitate marsh preservation and restoration.

Eleven pedons (soils) from Mississippi (4) and Alabama (7) Gulf Coast marshes were investigated. The soils were classified using field descriptions and laboratory analyses including electric conductivity, incubation pH, soil organic carbon (SOC), loss on ignition (LOI), total sulfur, particle size distribution, and exchangeable bases. Regression analyses indicated that LOI-SOC described 85% of SOC (dry combustion) data variability. Contrary to expectations, the LOI-SOC under-estimated SOC dry combustion content. Previous research indicated increasing clay content results in higher error from LOI estimates due to weight loss from hydrated clay minerals. When the LOI percent error was related to clay content, no relationship was found. However, the average LOI percent error was slightly lower for soils with relatively low clay content (< 22%).

Soils classified as Terric Sulfasaprists, Histic Sulfaquents (2), Typic Sulfaquents (5), Typic Fluvaquents, Typic Sulfasaprists, and Typic Fluviwassents (Figure 1). Sulfur and organic soil material content were identified as determining factors in the classification of these Gulf Coast salt marsh soils. The classification of samples collected will be used to facilitate the development of soil surveys and provide a greater understanding of tidal marsh ecosystems in the Mississippi and Alabama Gulf Coast. An understanding of the soils that compose the tidal marsh environment will allow for preservation and targeted restoration of key habitats and facilitate the

development of accurate soil mapping. Soil inventories can identify erosion and pollutant risk, habitats suitable for restoration and preservation of various species (e.g. Eelgrass, oysters, clams, scallops, diamondback terrapin), and areas unsuitable for dredging. Soil information can also be used to evaluate water quality and risks associated with coastal development.

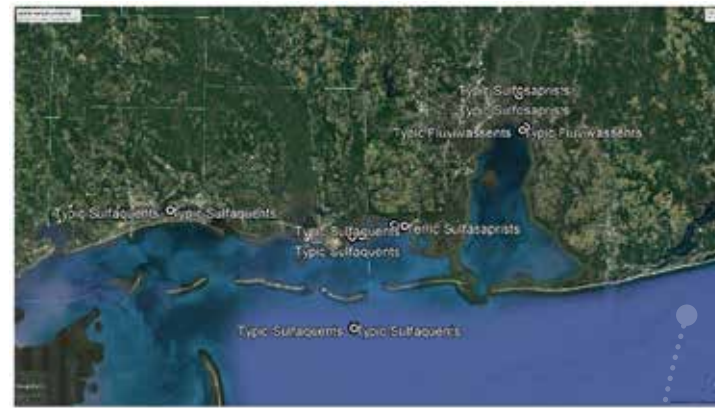


Figure 1. Map of soils sampled, analyzed, and classified.

## References

Veres, D. (2002). A comparative study between loss on ignition and total carbon analysis on minerogenic sediments. *Studia Universitatis Babeş-Bolyai, Geologia*, XLVII, 1, 171-182.

## Affiliations

Department of Crop, Soil and Environmental Sciences,  
Auburn University

# Studying the Relevance of Stomatal Characteristics on Drought Tolerance in Peanut

Seth Johnston<sup>1</sup> and Alvaro Sanz-Saez<sup>2</sup>

Approximately 65% of peanuts in the U.S. are produced without irrigation due to their tolerance to short-term drought. However, the American Peanut Council has identified drought damage as the most serious challenge facing peanut sustainability in the U.S. Improved resistance to abiotic stress is crucial for the long-term viability of U.S. peanut production. A general model for crop production under limited water environments can be defined as:  $Y = T \times TE \times HI$ , where Y is yield, T is the total water transpired by plants, TE transpiration efficiency, and HI is the harvest index. Therefore, increased transpiration efficiency leads to higher yield under drought conditions. Our theory is that differences in stomatal conductance and photosynthetic rates, each influencing overall transpiration efficiency and carbon assimilation rate, are related to smaller and less dense stomata on more drought tolerant peanut cultivars. Our objectives were: (1) to develop a method to obtain clear stomatal images, and then (2) use this method to test the relationship between stomatal density and size with photosynthetic parameters of peanuts in well-watered and drought conditions.

To evaluate this, two main research stages were conducted. First, a procedure was refined to take clear stomatal prints from peanut leaflets. The process developed is summarized as follows: (1) harvest leaf from the field and preserve in a Ziplock bag in a cooler; (2) spread Gorilla Super Glue on a leaflet, (3) quickly wipe off the excess glue with acetylene paper, (4) press the leaf firmly onto a microscope slide and wait 15 seconds, (5) then roll the leaf away from the slide. The slide can then be stored at room temperature for long periods of time and imaged later using a light microscope equipped with a camera digital camera. An image achieved in this manner is shown in Figure 1.

The second objective was pursued by assessing six peanut cultivars selected for their drought tolerance or sensitiveness using the method above, as well as assessing additional plant characteristics. These peanuts were grown in a greenhouse during summer, and at 60 days a water stress treatment started on half

of the plants. Midday photosynthesis and transpiration measurements were taken four times throughout the drought period for each plant. Leaf samples were taken on each plant coordinating to the time of the photosynthesis measurements. These samples stomata were captured using the developed printing. StomataCounter (stomata.uvm.edu) software was used to count the number of stomata within each leaf sample area, and ImageJ 1.52 was utilized to measure the length and width of the sampled stomata to calculate average stomatal area. To determine the statistical effect on stomatal density and size of leaf side, water treatment, and cultivars, a 3 Way ANOVA was performed in SAS. A correlation test was performed using PROC CORR in SAS to assess relationships between stomata characteristics and each cultivar's photosynthetic parameters.

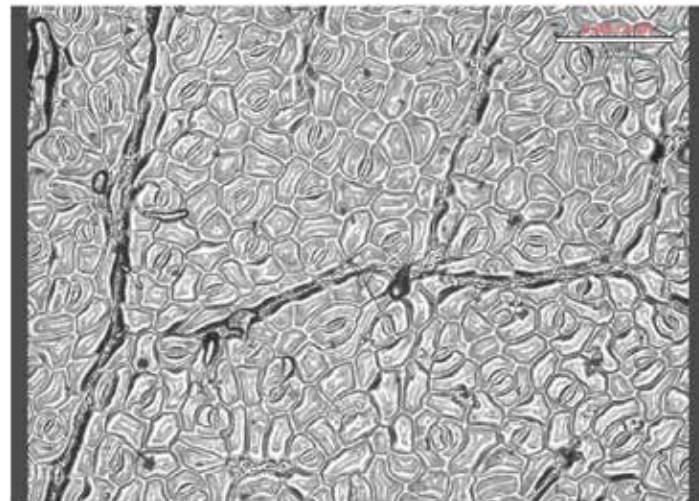


Figure 1. Stomata on adaxial leaflet surface.

A significantly higher ( $p < 0.05$ ) stomatal concentration was observed on the adaxial (upper) side of the tested peanut leaflets in comparison with the abaxial (lower side). On the adaxial surfaces, drought treatment generally increased stomatal density while it had no effect on the stomatal density on the abaxial surfaces. A significantly higher number of stomata was seen on both the adaxial and abaxial sides of the leaf in drought

conditions as compared to the same cultivars in the well-watered treatments. These results are against of our previous hypothesis and more research needs to be done to understand this behavior. No significant relationship was found between stomata area and photosynthesis, or stomatal area and conductance. There was variation in response ranging between slightly significant to no significance in the relationship between photosynthetic parameters (midday photosynthesis and stomatal conductance) and abaxial and adaxial stomatal density.

These results could underline the fact that other stomatal characteristics such as vapor pressure differential responsiveness or hormone sensitivity may be more important than physical stomatal characteristics in determining drought resistant cultivars (Vadez et al., 2014). Future research could be conducted on the accuracy of the testing procedure to ensure leaf drying does not affect stomatal size or density. VPD relationships between cultivars could also be assessed on cultivars to correlate vapor pressure differential responsiveness with other cultivar characteristics. The developed printing procedure and stomatal relationships could be used to build on characterizing and understanding the mechanisms of drought tolerance within peanut. Greater comprehension of these mechanisms could result in more effective cultivar development and overall food security for our future.

## References

Vadez, V., Kholova, J., Medina, S., Kakkera, A., & Anderberg, H. (2014). Transpiration efficiency: New insights into an old story. *Journal of Experimental Botany*, 65(21), 6141–6153. doi: 10.1093/jxb/eru040

## Affiliations

<sup>1</sup> Department of Biosystems Engineering, Auburn University

<sup>2</sup> Department of Crop, Soil and Environmental Sciences, Auburn University

# Theoretical Studies on Non-Enzymatic Dipeptide Hydrolysis Reactions and Their Applicability to Other Therapeutics

Katherine Lawson and Andrew Adamczyk

Studies on peptide degradation mechanisms are of interest because of the high demand for protein-based therapeutics and the development of biopolymer drug delivery systems in the pharmaceutical industry. Due to the size constraints of experimental systems, molecular models are used to determine critical thermochemical and kinetic parameters of the reactions. One reaction of particular interest is non-catalytic hydrolysis, a degradation mechanism that uses water to cleave peptide chains at the central amide bond. This reaction was modelled at a neutral pH, using quantum chemistry and statistical thermodynamics. The 20 dipeptides used in the training set were split into two reactive classes—ionized and non-ionized—to generalize our model further. Ultimately, our model computed the following quantities (Enthalpy of Reaction ( $\Delta H_R$ ), Entropy ( $\Delta S$ ), Gibbs Free Energy of Reaction ( $\Delta G_R$ ), Activation Energy (EA), and the Arrhenius pre-exponential factor ( $\log(A)$ ) for each dipeptide. Additionally, our model matched the experimental trends that dipeptide hydrolysis is both an exothermic and spontaneous reaction. From this validation of our model, we can generalize vital reaction properties as a function of the dipeptide reactive class, and subsequently expand these learnings to other systems (Lawson & Adamczyk, 2019).

The reactive center conservation and Arrhenius parameters were analyzed to generalize the reaction system and expand learnings to other peptide classes. The central amide bond, i.e. the covalent linkage between the two amino acids, was conserved as a function of the separate reactive classes. Within each reactive class, post-sensitivity analysis confirmed reactive center conservation was within the bounds of statistically insignificant error and identified potential outliers. Examination of Arrhenius parameters, as depicted in Figure 1, indicated that the kinetic rates of both reactive classes were primarily functions of their activation barriers, where the reactions with larger activation barriers contained functionalities identified by previous studies as less prone to chemical degradation. Specifically, peptide stability is decreased when residues incapable of hydrogen bonding are present in the amino terminus and aspartate residues are more prone towards cyclization when in the N-terminus position of a polypeptide chain (Subramaniam et al., 2001; Donald et al., 2011).

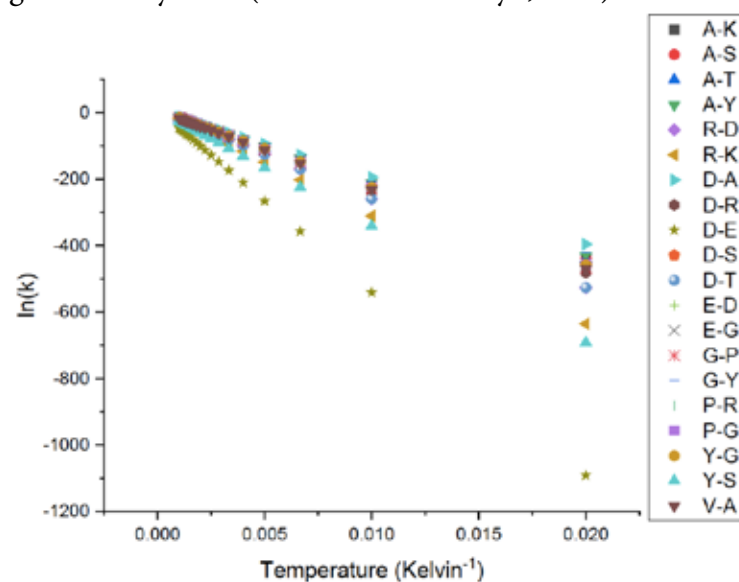


Figure 1. Arrhenius plot of dipeptide hydrolysis at a neutral pH computed in the forward direction.

Further generalization of the non-ionized reactive class was achieved through the use of an Evans-Polanyi correlation. The Evans-Polanyi correlation is a common model which generalizes a linear relationship between the activation barrier ( $E_a$ ) and the enthalpy of the reaction ( $\Delta H_{RXN}$ ) (Roy et al., 2008). From this correlation, thermochemical parameters of reactions within a specified reactive class can be estimated. The computed Evans-Polanyi correlation for the non-ionized reactive class was found to be statistically significant at a 90% confidence level.

The learnings we derived from this study can also be applied to other amide systems for hydrolysis studies. Review of other amide hydrolysis studies found our non-ionized reactive center geometry bounds to be within 0.4Å pre-sensitivity analysis, and 0.1Å after sensitivity analysis (Lopez et al., 2008). Additionally, experimental pre-exponential factors for amide hydrolysis within a neutral system were found to be within the range of pre-exponential factors computed in our study.

In summary, a theoretical investigation on the hydrolysis of both ionized and non-ionized dipeptides in both the solvated phase was completed. Rate coefficients and Arrhenius parameters for dipeptide hydrolysis were calculated for 20 reactions using quantum chemistry and statistical thermodynamics. The overall reaction of dipeptide hydrolysis was found to be exothermic and spontaneous for all dipeptides. Future studies will expand the generated library of dipeptide structures, thermochemical and kinetic parameters from solely at a neutral pH to acid and basic pH's. Computation of the specified parameters will then be used to generate a robust microkinetic model of dipeptide hydrolysis reactions as a function of reactive class.

## References

- Lawson, K. E., & Adamczyk, A. J. (2019, Fall). Towards pharmaceutical protein stabilization: Insights from theoretical studies on peptide hydrolysis reactions, AICHE Annual Meeting, Orlando, FL. USA
- Subramaniam, V., et al. (2001). *The Journal of Biological Chemistry*, 276(24): 21506.
- Donald, J. E., et al. (2011). *Proteins*, 79(3): 898-915.
- Roy, S., et al. (2008). *Physical Review E*, 77(5): 056707.
- Lopez, X., et al. (2003). *The Journal of Physical Chemistry A*, 107(13): 2304-2315.

## Affiliations

Department of Chemical Engineering,  
Auburn University

# Medicare Part D Prescription Payments by Prescriber Specialty Types in 2017

Chao Li, Shahariar Fahim, Salisa Westrick, and Jingjing Qian

Total Medicare benefit payments were \$702 billion in 2017 and the Part D prescription drug benefits spending represent 14% (Cubanski & Newman, 2017). However, Medicare Part D prescription expenditures across prescriber specialties varied by different medical specialty's preferences or prescribing patterns (De Lott et al., 2016). Better understanding of the prescribers' preference and patterns can help form strategies to reduce Part D expenditures. The objective of this study was to describe Medicare Part D prescription payments by prescriber specialty type for better understanding prescription utilization and needs among Medicare population.

To address our objective, we conducted a cross-sectional analysis using the most recently available 2017 Medicare Part D Prescriber Public Use and Summary data files. Total Medicare Part D Payments and number of Part D prescriptions were aggregated by specialist groups. Monthly supply was calculated by aggregating the daily supply of drugs for each provider within a specialist group, then being divided by 30 to obtain the total number of monthly supplies per provider. Payments per monthly supply of drugs were calculated by dividing the total payments by aggregated monthly supply of drugs for each individual prescriber. After that, medians for the total number of monthly supplies per provider and the total payments per monthly drug supply were obtained within each specialist group, respectively. The proportion of generic claims in each prescriber specialty was calculated by all generic medication claims divided by the total medication claims.

We found internal medicine, family practice, and nurse practitioner represented the highest total number of Part D prescribers and were the top 3 healthcare provider groups who received the highest total Medicare Part D payments (\$31 billion, \$26 billion, and \$15 billion, respectively). The top 3 specialties with highest median payment per monthly supply of drugs were hematology/oncology, medical oncology, and infectious disease (\$1.01 thousand, \$0.96 thousand, and \$0.69 thousand,

respectively). Part D prescriber specialty types in pulmonary disease, endocrinology, and ophthalmology had the lowest proportion of generic claims among all specialty groups (41%, 45%, and 53%, respectively).

In conclusion, internal medicine, family practice, and nurse practitioner were the top 3 medical groups with the highest total Medicare Part D payments, which may need more closely monitoring of their high-volume Part D prescriptions. Prescribers specialized in oncology and infectious disease had the highest payment per monthly supply of medications, which needs more attentions on their high-dollar Part D prescriptions. Medicare Part D payment to low proportion of generic claims such as pulmonary disease, endocrinology, and ophthalmology could be reduced by increasing generic drug utilization.

## References

Cubanski, J., & Neuman, T. (2017, July). The facts on Medicare spending and financing. *Henry J. Kaiser Family Foundation*. <https://www.kff.org/medicare/issue-brief/the-facts-on-medicare-spending-and-financing/>. Accessed June 18, 2018.

De Lott, L. B., Burke, J. F., Kerber, K. A., Skolarus, L. E., & Callaghan, B. C. (2016). Medicare Part D payments for neurologist-prescribed drugs. *Neurology*, 86(16):1491-1498. doi:10.1212/WNL.0000000000002589

## Affiliations

Department of Health Outcomes Research and Policy, Auburn University

Table 1. Total Medicare Part D Payments by Specialty Type in 2017

Specialty	Total drug payment, \$, millions	No. providers	Median month's supply/provider ^	Median payment/month of drug, * \$	Proportion of claims, generic
Internal medicine	31,433	130,302	703	47	0.82
Family practice	25,875	110,990	3,073	39	0.83
Nurse practitioner	15,454	153,964	302	50	0.83
Hematology/oncology	9,327	8,526	805	1,006	0.79
Neurology	8,187	13,885	1,360	168	0.84
Physician assistant	6,654	92,495	127	49	0.85
Cardiology	5,848	20,265	4,790	41	0.80
Pulmonary disease	4,908	9,463	1,115	239	0.41
Gastroenterology	4,868	13,596	842	229	0.74
Rheumatology	4,780	4,713	2,930	262	0.79
Endocrinology	4,490	5,931	3,548	158	0.45
Psychiatry	4,002	25,413	829	65	0.91
Ophthalmology	3,064	19,790	1,051	81	0.53
Nephrology	2,992	8,632	2,098	109	0.78
Infectious disease	2,880	5,383	336	691	0.65
Medical oncology	2,753	3,158	580	955	0.79
General practice	1,760	9,923	852	37	0.84
Specialty surgery	748	69,867	50	41	0.94

^ Month's supply was calculated by aggregating the day's supply of drugs for each provider within a specialist group, then dividing by 30 to obtain the total number of monthly supplies per provider.

\* Payment per monthly supply of drugs was calculated by dividing the total payments by day's supply, multiplying by 30 for each drug, and then aggregating for each individual provider.

# Do Bark Beetle Associated Fungi Contribute to Loblolly Pine Decline and Mortality?

John K. Mensah<sup>1</sup>, Mary Sword Sayer<sup>2</sup>, Ryan Nadel<sup>1</sup>, George Matusick<sup>1</sup>, Zhaofei Fan<sup>1</sup>, and Lori Eckhardt<sup>1</sup>

*Pinus taeda* L (loblolly pine) is the predominant tree crop in forest plantations across the southeastern United States. However, the tree crop suffers from attack by several root pathogens that culminate in growth declines and/or mortalities. Bark beetle vectored fungus *Leptographium terebrantis* is commonly isolated from roots of *P. taeda* undergoing growth decline. Over the past decades, the root pathogen has been implicated as one of the agents that contribute to *P. taeda* decline and mortality. We examined the potential of *L. terebrantis* to cause growth decline symptoms and the threshold of the fungus inoculum density needed to cause decline.

The study was undertaken in a 13-year-old open-pollinated *P. taeda* plantation in Eufaula, Alabama, using artificial inoculations of pathogen colonized toothpicks at different inoculum densities. We found that *L. terebrantis* is not only associated with dying *P. taeda* trees but causes decline symptoms and mortality. One *L. terebrantis* colonized toothpick per 1.2 cm over the bark is the threshold of inoculum density required to produce decline symptoms after 19 months of infestation. The pathogen caused 20% mortality among the high inoculum treatment trees. However, at low and medium inoculum densities, the trees tolerated the pathogen by forming a complete ring of new sapwood devoid of pathogen infestation to sustain physiological and metabolic activities (Figure 1). This suggests that management practices that reduce bark beetle infestation in *P. taeda* plantations should be encouraged to minimize the pathogen inoculum density.



**Figure 1.** Cross-Section of *P. taeda* Tree Showing New Growth Around Dark Brown Occlusions Caused by *L. terebrantis* at Medium Inoculum Density

## Affiliations

<sup>1</sup> School of Forestry and Wildlife Sciences, Auburn University

<sup>2</sup> U.S. Forest Service

# The Effect of a pH-Dependent Arginine Switch on Protein-Based Cofactor Formation in Catalase-Peroxidase (KatG)

Laura Minton<sup>1</sup>, Hui Xu<sup>2</sup>, Jessica Krewall<sup>2</sup>, and Douglas Goodwin<sup>2</sup>

Tuberculosis (Tb) is an infectious disease caused by *Mycobacterium tuberculosis*, an intracellular bacterial pathogen that infects cells in the human lungs. Tb remains a public health crisis, as there were 10 million new cases of Tb in 2018 according to the World Health Organization. The leading cause of death from a single infectious agent is Tb. There were 1.5 million Tb-related deaths in 2018 (Ghebreyesus, 2019).

Humans and other eukaryotes commonly produce reactive oxygen and nitrogen species as a critical component of immune responses against pathogenic infections. Central among these species is hydrogen peroxide (H<sub>2</sub>O<sub>2</sub>). H<sub>2</sub>O<sub>2</sub> is not particularly harmful in an unreacted state, but H<sub>2</sub>O<sub>2</sub> is a necessary prerequisite for the production of highly damaging species, such as hypochlorous acid or hydroxyl radicals. However, some pathogens such as *M. tuberculosis* and the pathogenic *Escherichia coli* strain O157:H7 have a multitude of enzymes which allow them to elude the powerful effects of this host immune response. KatG, an enzyme vital to the ability of several pathogens to survive in host cells, can catalyze both of biology's major H<sub>2</sub>O<sub>2</sub> degradation reactions, those being catalase and peroxidase. KatG also activates the pro-drug isoniazid (INH) which disrupts the ability of *M. tuberculosis* to make its protective mycolic acid coat. Unfortunately, mutations to the katG gene have resulted in INH-resistant strains.

Within the active-site structure of KatG, an arginine-switch (R-switch), a methionine-tyrosine-tryptophan (MYW) cofactor, and heme all assist in conducting the enzyme's optimal H<sub>2</sub>O<sub>2</sub> degrading ability. The R-switch is particularly interesting, because the position of the switch changes based upon pH. Catalase activity is contingent upon the formation of the MYW cofactor and the pH-dependent conformation of this R-switch. The Goodwin lab used site-directed mutagenesis to generate an arginine-switch variant of KatG, where the arginine has been replaced by an asparagine (R418N KatG).

The R418N variant can be studied in apo (aR418N), reconstituted (rR418N), or holo-as-isolated (hR418N) forms, each of which is named for the timing of heme introduction. The aR418N proteins are expressed in *E. coli* cells and are then purified to only include the KatG protein. Heme is never added and remains absent, so no catalase activity is expected. The rR418N proteins are expressed in *E. coli* cells and are then purified to only include the KatG protein; however, the heme is added during purification but after expression, so the heme has not been exposed to the H<sub>2</sub>O<sub>2</sub> that is naturally generated within the cell. The hR418N proteins are prepared so that heme is introduced during expression in the *E. coli* cells. Heme contacts H<sub>2</sub>O<sub>2</sub> in the cells. Then, KatG is purified. Comparison of these forms of the R418N variant provides information on the formation of the protein-based cofactor, a necessary facet for understanding KatG's ability to evade host immune responses through its catalase mechanism.

Stopped-flow (SF) experiments were utilized to investigate the enzyme intermediates produced by the R418N variant. SF is a rapid mixing instrument which provides multiaxial data collection including wavelength, absorbance, and time. The difference between hR418N and rR418N is that the MYW cofactor forms during protein preparation expression of hR418N while the MYW cofactor forms during the SF experiment for rR418N. rR418N was not exposed to H<sub>2</sub>O<sub>2</sub> in a great quantity until the SF experiment, so initial formations of compounds are able to be experimentally tracked.

INH activation by wild-type and R418N KatG to form the IN-NAD adduct was measured using UV-Vis spectroscopy. UV-Vis spectroscopy is a method that measures the absorbance of light due to the presence of specific compounds, such as the IN-NAD adduct which absorbs at 326 nm. Interestingly, our findings

showed a lag in INH activation to IN-NAD for both holo forms (hWTKatG, hR418N). The same was not observed in either rWTKatG or rR418N KatG, suggesting that the MYW cofactor delays INH activation. This research is relevant not only within the biochemistry discipline, but Tb remains a concern for public health. With my research, I sought to address lingering questions and improve the knowledge base concerning the mechanisms behind INH activation as well as frequent INH-resistant *katG* gene mutations. Further research should continue investigating how INH activation is affected by the presence or absence of the R-switch. Additional experiments should also seek to study the mechanism by which INH activation is affected, either in the presence or absence of the MYW cofactor. Understanding the roles of different amino acids and cofactors will aid towards the goal of KatG characterization, which will holistically assist in enhancing INH efficiency for global use against Tb.

## References

Ghebreyesus, T. A. (2019). *Global tuberculosis report*. Geneva: World Health Organization.

## Affiliations

<sup>1</sup> Biomedical Sciences Program, Auburn University

<sup>2</sup> Department of Chemistry and Biochemistry, Auburn University

# Petrographic and Geochemical Analyses to Elucidate the Genesis of Au-Ag Deposits on Florida Mountain Epithermal Deposit, Silver City District, Idaho

Lucas Monroe, Laura Bilenker, Willis Hames, Raeann Garcia, and Will Ebbert

Florida Mountain (FM) is classified as an epithermal deposit, which are important global sources of gold (Au) and silver (Ag). FM is one of a trio of similar deposits in the Silver City District of southwestern Idaho. Epithermal deposits are targets for modern mining because they form close to the surface of the Earth and host high ore (Au, Ag) grades (Simmons et al., 2005). Metals like Au and Ag are concentrated at these sites as a result of fluid flow driven by the heat of a nearby magma body (Fig. 1). Three sub-categories of epithermal deposits exist based on the minerals and metals they host, which vary due to their proximity to the magma; they are called low-, intermediate-, and high-sulfidation. FM has a rich mining history as a low-sulfidation epithermal deposit and produced about 257,000 oz. of Au and 18 million oz. of Ag over 51 years (Integra Resources, 2019). Despite extensive mining at FM until the 1990's, current exploration shows great potential for future success. Studies have been completed on similar deposits in the region, but few have focused on FM (Integra Resources, 2019). Furthermore, those studies only analyzed samples on or near the surface within the richest locations; this constraint left many questions unanswered about the origin of FM. A partnership with the FM exploration company, Integra Resources, has provided access to a new, extensive inventory of drilled rock cores, which sample the entirety of the deposit and allow us to fill important knowledge gaps regarding local metal enrichment and the regional geologic history.

In summer 2019, I traveled to FM to make field observations and perform detailed sampling from drill core extracted during exploration. Core samples were taken from all of the rock units seen at FM and at various depths to ensure full representation of the deposit.

During this time, two geologic maps of a neighboring deposit (DeLamar Mountain) were produced for use in exploration of the area. These maps included units that are also present at FM.

This study aims to answer the following research questions (RQ): 1) When did the FM Au-Ag deposit form and was mineralization related to the Yellowstone hotspot, which currently sits below Yellowstone National Park? 2) What is the source of the Au and Ag? 3) What indicators exist to help with ongoing exploration? 4) How are FM and its neighboring deposits (e.g., DeLamar Mountain) related? The answers to these questions will allow us to develop a genetic model for FM and evaluate current models for all low-sulfidation epithermal deposits. Furthermore, assessing the link between mineralization and the Yellowstone hotspot will reinforce or revise components of the broader geologic history of the western United States. The results of this study will also have a direct and immediate contribution to exploration at FM and help refine future techniques for finding low-sulfidation epithermal deposits.

Optical and geochemical analyses will be used to characterize the composition and appearance of the minerals at FM, which will provide insight into its formation including the behavior of Au and Ag in the system. Measurements of argon will determine the age of the deposit to investigate the role of the Yellowstone hotspot and assess the possibility of multiple ore (Ag, Au) deposition events. So far, microscopic analyses of the appearance and composition of minerals have begun in addition to preliminary age dating in the Auburn Noble Isotope Mass Analysis Lab. These first argon isotope analyses address RQ #1 and show a range of ages that

is consistent with the birth of the Yellowstone hotspot (about 16 million years). Additional age analyses will constrain the number and timing of individual events within the deposit. Microscopic observations and compositional analyses of minerals within the samples are ongoing with the aim to identify exploration indicators (RQs #3) and evaluate FM's relationship with neighboring deposits (RQ#4). Analyses of sulfur within minerals throughout FM will be performed this fall to track the source (magmatic or meteoric) of the fluids that transported the Au and Ag (RQ #2).

This detailed geochemical study will elucidate the genesis of FM and advance our understanding, not only of FM, but all low-sulfidation epithermal deposits. Since the success of the Au and Ag industry is key to the success of technological advancement, this research has important implications for the technology that runs our daily lives.

## References

Integra Resources. (2019). Florida Mountain Project. Project History. [integrareources.com/project/florida-mountain-project/project-history](https://integrareources.com/project/florida-mountain-project/project-history).

Hedenquist, J. W., & Lowenstern, J. B. (1994). The role of magmas in the formation of hydrothermal ore deposits. *Nature*, 370, 519-527.

Simmons, S. F., White, N. C., & John, D. A. (2005). Geological characteristics of epithermal precious and base metal deposits. *Economic Geology 100th Anniversary Volume*, 485-522.

## Affiliations

Department of Geosciences, Auburn University

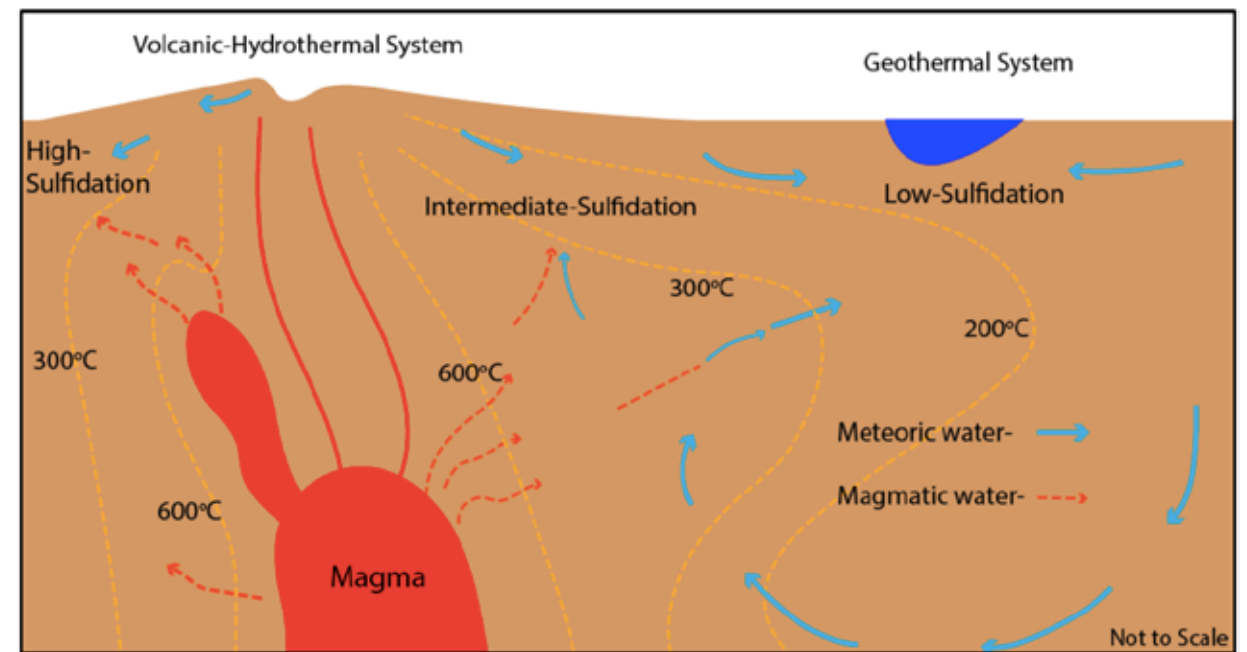


**Figure 1.** Sketch of the Environment Where Epithermal Ore Deposits Form Within the Uppermost Portion of Earth's Crust. Three types of epithermal deposits are depicted here; the high-, intermediate-, and low- sulfidation classes differ in composition due to their proximity to a deeper magma body (red area). The yellow dashed lines represent areas of equal temperature (redrawn from Hedenquist & Lowernstern, 1994).

# The P2Y2 Nucleotide Receptor Mediates Tissue Factor Expression in Human Monocytes

Qianman Peng<sup>1</sup> and Jianzhong Shen<sup>2</sup>

Thrombosis, the abnormality of blood coagulation, is the lethal stage of a number of major pathological conditions, such as atherosclerosis, stroke, DIC and pulmonary embolism. Platelet activation and aggregation is the final stage of thrombosis, which is developed from a hyper-coagulable status due to tissue factor (TF) exposure to blood. An abundance of active TF in atherosclerotic lesions plays a key role in atherothrombosis by triggering a hyper-coagulable blood status (Steffel et al., 2006; Mackman, 2008). Recently we reported that in human coronary artery endothelial cells, activation of the P2Y2 receptor induces up-regulation of tissue factor (TF), the key initiator of the coagulation cascade (Ding et al., 2011; Liu et al., 2016). This finding demonstrated that P2Y2 receptor might be a new drug target for the prevention and/or treatment of thrombotic vascular diseases. However, it has been shown by others that monocyte TF is more important than endothelial TF in terms of provoking pro-thrombotic conditions. Also, it is unknown whether monocyte P2Y2 receptor mediates TF expression as much as it did in endothelial cells. Thus, we aimed to study whether human monocytes express P2Y2 receptor and its role in control of TF expression.

*In vitro* study, RT-PCR and receptor activity assays revealed that among the eight P2Y nucleotide receptors (n=3), the P2Y2 subtype was selectively and functionally expressed in human monocytic THP-1 cells. Consistent with this, stimulation of the THP-1 cells by ATP or UTP at micromolar concentration dramatically increased TF protein expression measured by Western blotting (n=3), which was abolished by AR-C118925XX, a selective P2Y2 receptor antagonist, suggesting a key role for P2Y2 receptor. In addition, UTP or ATP treatment induced a rapid accumulation of TF mRNA (n=3), which was maximal at 2h and preceded with an increased TF pre-mRNA (n=3), indicating enhanced TF gene transcription. However, we also observed a significant increase in TF mRNA stability after UTP and ATP treatment. Furthermore, activation of the

monocyte P2Y2 receptor by a low dose of UTP or ATP (1 $\mu$ M) significantly activated (n=3) the MAPK pathways including ERK1/2, JNK, and p38, along with their downstream transcription factors including c-Jun, c-Fos and ATF-2 (n=3), whereas blocking the ERK1/2, JNK or p38 pathways respectively, all significantly suppressed P2Y2 receptor-mediated TF expression.

These findings demonstrate for the first time that the P2Y2 receptor mediates TF expression in human monocytes through new mechanisms involving ERK1/2, JNK and p38, and that both transcriptional and posttranscriptional mechanisms contribute to a pro-thrombotic status in monocytes through the P2Y2-TF axis (Fig.1), highlighting monocyte P2Y2 receptor may be a new drug target for the prevention and/or treatment of relevant thrombotic diseases. However, further study *in vivo* is needed to determine the significance of these findings in our future research.

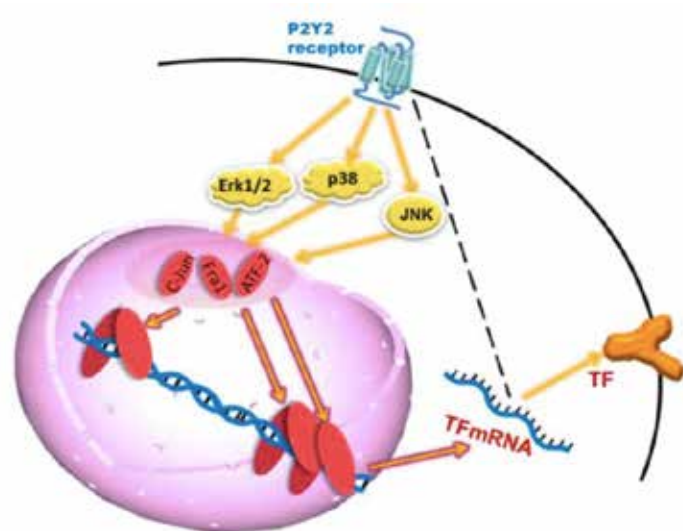


**Figure 1.** A systematic diagram shows the mechanism underlying P2Y2R-controlled cell signaling, AP-1 activation, and TF gene transcription in THP-1 cells.

## References

- Ding, L., Ma, W., Littmann, T., Camp, R., & Shen, J. (2011). The P2Y 2 nucleotide receptor mediates tissue factor expression in human coronary artery endothelial cells. *Journal of Biological Chemistry*, 286(30), 27027–27038.
- Liu, Y., Zhang, L., Wang, C., Roy, S., & Shen, J. (2016). Purinergic P2Y2 receptor control of tissue factor transcription in human coronary artery endothelial cells. *Journal of Biological Chemistry*, 291(4), 1553–1563.
- Mackman, N. (2008). Triggers, targets and treatments for thrombosis. *Nature*, 451(7181), 914–918.
- Steffel, J., Lüscher, T. F., & Tanner, F. C. (2006). Tissue factor in cardiovascular diseases: Molecular mechanisms and clinical implications. *Circulation*, 113(5), 722–731.

## Affiliations

<sup>1</sup> Pharmacology Program, Harrison School of Pharmacy, Auburn University

<sup>2</sup> Department of Drug Discovery and Development, Auburn University

# Anthropometric Factors in Softball Hitting Performance

Johann Phan<sup>1</sup>, Kenzie Friesen<sup>2</sup>, and Gretchen Oliver<sup>2</sup>

Baseball is considered one of America's pastimes, and as such, is one of the most popular sports today in America among youth. Despite the popularity of the sport, there are limited data available when examining hitting mechanics, especially in conjunction with anthropometric measurements of the hitters. Hitting is a major component to team success in baseball; therefore, research dedicated to understanding performance parameters that improve hitting performance is valuable to the development of the sport. Research has found arm length has been an important anthropometric factor in elite players of other sports, particularly those that require extensive use of the upper extremity (Bourgois et al., 2000; Garcia-Gil et al., 2018; Nikzad et al., 2018; Tsolakis & Vagenas, 2010; Mohamed et al., 2009). Given how the upper extremity is an important link within the kinetic chain in hitting, the objective of this study was to find the effect of arm length and other physical traits on baseball hitting performance.

To conduct the study, nine youth baseball players (11.2 ± 1.3 years, 149.8 ± 9.6 cm, 51.1 ± 14.1 kg) volunteered to participate. Prior to the examination, the participants and their parents/guardians signed consent documents. Each participant was then measured for bilateral hip and shoulder isometric strength and range of motion using a dynamometer and inclinometer, respectively. Hip measures were conducted with the participant sitting on an athletic trainers table, with their hips and knees both flexed to 90 degrees. Shoulder measures were completed with the participant lying supine on an athletic trainers table, with their shoulder abducted 90 degrees and their elbow flexed 90 degrees. Participants were then hooked up to an electromagnetic motion capture system synced with motion analysis software, which was used to record weight, height and arm length for all participants. Yakkertek, a ball tracking device, was used to measure batted ball distance, launch angle and exit speed for all trials (see Figure 1). Each participant warmed up for as long as needed, then completed ten swings from a front tossed pitch. Of the ten swings, the four trials with the closest launch angle to the average launch angle for the ten trials were used

for data analysis.

Pearson's correlations ( $p < 0.05$ ) revealed a significant relationship between player mass and batted ball distance (Figure 2), as well as player height and exit speed (Figure 3). Therefore, these findings would suggest overall height and mass have a greater impact on hitting performance than arm length, strength and range of motion measures.

These results suggest that arm length nor isometric strength has a significant effect on batted ball performance in youth. These findings could indicate the overall importance of total body kinetic chain sequencing versus absolute brute strength in hitting performance. Additionally, it should be noted that these findings may also be due to the inconsistency of isometric strength and lean muscle mass in youth athletes. Future research should be conducted to examine the relationship between anthropometric factors and hitting performance among a larger age range of athletes accounting for those with bigger body characteristics and more hitting expertise.



**Figure 1.** Yakkertek Device Used to Measure Batted Ball Characteristics

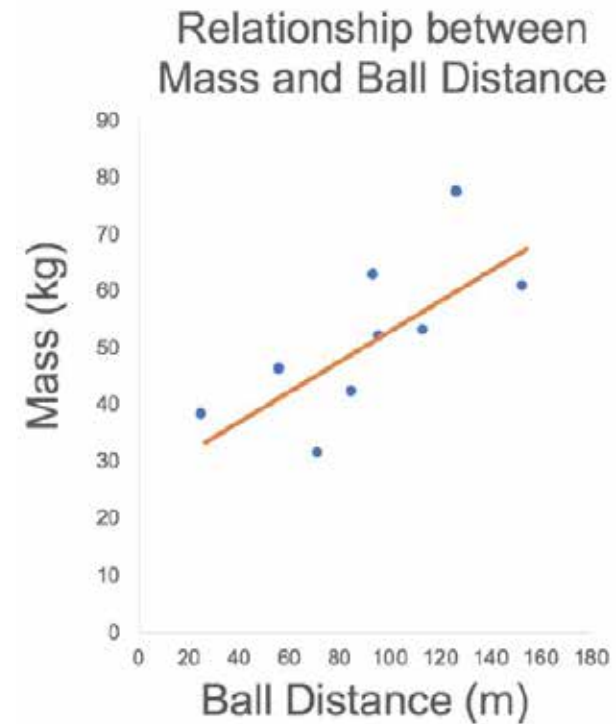


**Figure 2.** Relationship Between Mass and Ball Distance

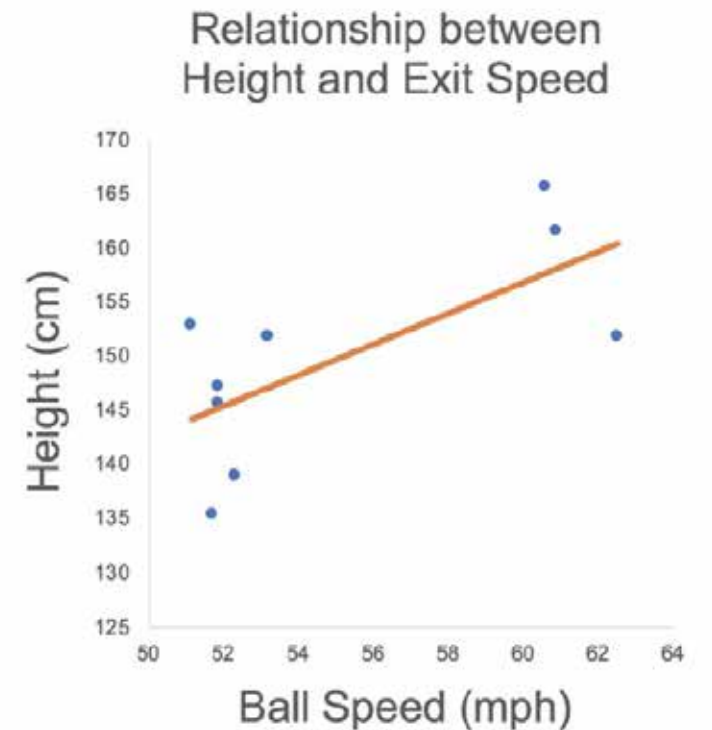


**Figure 3.** Relationship Between Height and Exit Speed

## References

- Bourgois, J., Claessens, A. L., et al. (2000). Anthropometric characteristics of elite male junior rowers. *British Journal of Sports Medicine*, 34(3), 213-216.
- Garcia-Gil, M., Torres-Unda, J., Esain, I., Duñabeitia, I., Gil, S. M., Gil, J., & Irazusta, J. (2018). Anthropometric parameters, age, and agility as performance predictors in elite female basketball players. *The Journal of Strength & Conditioning Research*, 32(6), 1723-1730.
- Mohamed, H., Vaeyens, R., Matthys, S., Multael, M., Lefevre, J., Lenoir, M., & Philippaerts, R. (2009). Anthropometric and performance measures for the development of a talent detection and identification model in youth handball. *Journal of Sports Sciences*, 27(3), 257-266.
- Nikzad, N., Karasch, R. A., Anantasagar, T., Vinod, V., Disch, J. G., & Papadakis, Z. (2018). Anthropometric and performance statistics comparisons in baseball pitchers: A longitudinal study. *Medicine & Science in Sports & Exercise*, 50(5S), 798.
- Tsolakis, C., & Vagenas, G. (2010). Anthropometric, physiological and performance characteristics of elite and sub-elite fencers. *Journal of Human Kinetics*, 23(1), 89-95.

## Affiliations

<sup>1</sup> Department of Chemical Engineering, Auburn University

<sup>2</sup> School of Kinesiology, Auburn University

# Gentamicin-Loaded 3D-Printed Metal Implants for Post-Surgical Infections

Ishwor Poudel<sup>1</sup>, Manjusha Annaji<sup>1</sup>, Robert D. Arnold<sup>1</sup>, Amal Kaddoumi<sup>1</sup>, Nima Shamsaei<sup>2</sup>, Seungjong Lee<sup>2</sup>, Jonathan Pegues<sup>2</sup>, Kayla Corriveau<sup>3</sup>, and Jayachandra R. Babu<sup>1</sup>

Post-surgical infection (PSI) is an impending issue with any surgical procedures related to bone injuries. The protective barrier and body defense are compromised with surgical trauma, thus leaving the local site prone to infections, resulting in severe complications. Such incidences put an economic burden on patients with increased medication, revision surgery, extended hospital stays, increased expenditure, and patient mortality (McGaffey et al., 2019). 316 L Stainless Steel (SS) has been found corrosion-resistant, biocompatible, and superior in quality for the fabrication of bio-implants (Navarro et al., 2008; Kato et al., 2013) for surgical rehabilitation. The mechanical and biological adhesion of implants is another primary concern for implant installation. Recent work on microstructure modification by laser surface melting has shown a huge improvement in surface roughness and bioactivity (Majumdar et al., 2018). The polymeric porous coatings and biomaterials have also been utilized on implants to enhance long-term fixation and osteointegration (Geetha et al., 2009). Based on these newer findings, we aimed to fabricate novel 3D Printed 316L SS implants, load the implants with an anti-infective agent using a polymeric coat to achieve controlled release, and evaluate the antimicrobial efficacy of the implants to treat PSIs.

3D-printed metal implants were fabricated using layer by layer approach of additive manufacturing using Renishaw AM 250 printer. The printer utilizes a selective laser melting technique based on the principle of laser-bed powder fusion to devise an implant prototype using 316 L SS powder. The standard design of the implants was optimized as a square block of 20mm\*20mm\*3mm. The overall process was processed under argon gas to prevent oxidation, and the final implants reproduced roughness of the desirable range. Line roughness of metal surface was determined using the average arithmetic mean roughness value (Ra) and the maximum height of profile (Rz).

With an intent to achieve controlled release, a biodegradable polymer PLGA (Poly Lactic-co-glycolic acid) was employed. Gentamicin was selected as the active molecule to prevent bacterial growth on the surgical site as well as on implant surface. Gentamicin was solubilized in an organic solvent along with PLGA, followed by deposition on implant surface by using airbrush spray coating technique. The surface roughness and thickness of the coat were determined using the Keyence VHX-6000 microscope. The *in vitro* release profile of the drug was investigated in Phosphate-buffered Saline (pH 7.4) as release media for six weeks to determine the nature of drug elution from the implant surface. The aliquots were analyzed using ninhydrin colorimetric assay using UV-spectrophotometer. The drug loading and thickness of polymer layer was optimized. The content uniformity of gentamicin was within 95-105%. The thickness of the top layer was observed to be 552.49±17.49 μ. Resomer RG 503 (PLGA 50:50, molecular weight, 24-38k ester terminated) showed biphasic release profile of gentamicin with initial burst release of 21.62%±1.11 (n=3) in six hours, and 96.69%± 5.74 (n=3) of cumulative release by five weeks. Through this study, a controlled release pattern of gentamicin eluting 316 L SS implants was achieved for a month utilizing PLGA as a polymer of choice. We further plan to investigate the effectiveness of gentamicin delivery from the metallic implants to inhibit the growth of the biofilm by the zone of inhibition technique (Agar well diffusion method) with respect to the concentration of gentamicin in the implant surface.

In summary, 3D printing technology was successfully employed to design bio-implant prototypes of uniform thickness, size and roughness, which were sprayed with gentamicin loaded PLGA coatings to prevent infections

at the surgical site after the implant installation. The antimicrobial efficacy is yet to be established and is currently under progress. Once the gentamicin effectiveness is established, it will direct us towards a novel approach to utilize personalized, drug-loaded, 3D-printed implants for local administration with customized modulation of drug release. We plan to perform *in vivo* implantation of these metal implants in large animals like cattle and horses.

This study is financially supported by an Auburn University Presidential Awards for Interdisciplinary Research (AU-PAIR) grant.

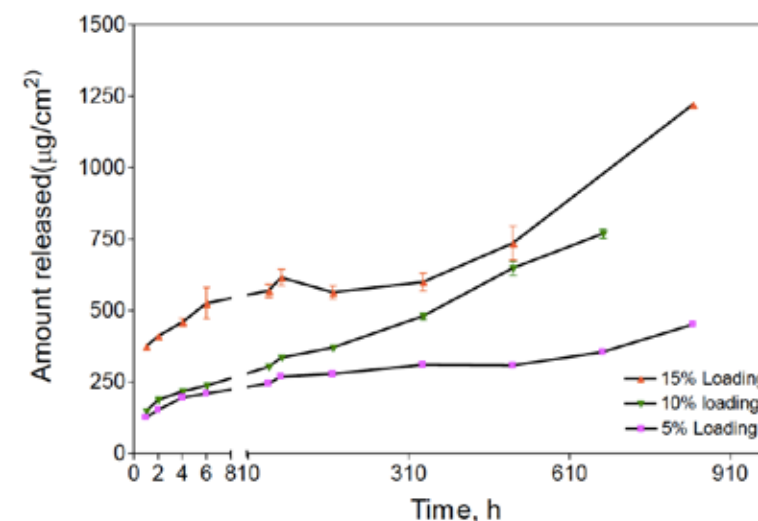


Figure 1. Release Profile of Gentamicin Loaded Steel Implants with Different Drug Loading

## References

- Geetha, M., Singh, A. K., Asokamani, R., Gogia, A. K. (2009, May 1). Ti based biomaterials, the ultimate choice for orthopaedic implants—A review. *Progress in Materials Science*, 54(3):397-425.
- Kato, K., Yamamoto, A., Ochiai, S., Wada, M., Daigo, Y., Kita, K., & Omori, K. (2013, July 1). Cytocompatibility and mechanical properties of novel porous 316 L stainless steel. *Materials Science and Engineering: C*, 33(5):2736-43.
- Majumdar, J. D., Kumar, A., Pityana, S., & Manna, I. (2018, September 1). Laser surface melting of AISI 316L stainless steel for bio-implant application. *Proceedings of the National Academy of Sciences, India Section A: Physical Sciences*, 88(3):387-403.

McGaffey, M., zur Linden, A., Bachynski, N., Oblak, M., James, F., & Weese, J. S. (2019). Manual polishing of 3D printed metals produced by laser powder bed fusion reduces biofilm formation. *PloS One*, 14(2).

Navarro, M., Michiardi, A., Castano, O., & Planell, J. A. (2008, October 6). Biomaterials in orthopaedics. *Journal of the Royal Society Interface*, 5(27):1137-58.

## Affiliations

<sup>1</sup> Department of Drug Discovery and Development, Auburn University

<sup>2</sup> Department of Mechanical Engineering, Auburn University

<sup>3</sup> Department of Clinical Sciences, Auburn University

# Assessment of Angle of Repose as a Tool to Measure the Flowability of Different Particle Sizes of Ground Corn with and Without Added Soybean Oil

Marc R. Presume, Jorge L. Sandoval, Gerardo A. Abascal-Ponciano, Allan J. Calderon, Danny B. Patino, Kevin E. Ordonez, Luis P. Avila, Samuel F. Leiva, Josh J. Flees, Wilmer J. Pacheco, and Charles W. Starkey

Corn is the major grain used in animal feed diet worldwide because it is a significant source of energy and is highly digestible (Ravindran, 2011). This cereal is often mixed with vegetable oils, such as soybean oil (SBO) and fat, due to their energetic contribution. However, the mixture of corn and oil should be in adequate proportions for an optimal feed flow from storage to animal feeders (Groesbeck, 2003).

Flowability is known as the ability of grains and powders to flow during discharge from storage containments to animal feeders. It affects batching time, mixability and conveyance of the feed throughout the feeding system (Jadhav et al., 2017). Flowability of grains is often influenced by their particle size (PS) (Ganesan et al, 2008). According to Jadhav et al. (2017), poor flowability is a continual source of frustration for many commercial producers. It often reduces the rate of feed conveyance to feeders. Some common issues associated with poor feed flow include bridging, pipe formation, caking and equipment damage (Figure 1).

Ensuring a consistent feed flow is necessary for an adequate delivery of animal feed and an optimal body

weight of animals. A common method to assess the flowability of a material is to measure its angle of repose (AOR), which is the angle formed between the horizontal and the slope of a feed pile (Jadhav et al., 2017).

The objective of this study was to assess the effects of PS and SBO additions on AOR, and thus flowability of ground corn. A randomized complete block experiment with an 8 x 6 factorial treatment structure with 3 replicates per treatment was conducted. Corn was ground using a two pair roller mill at 8 different roller settings to produce samples with mean PS of 693, 882, 968, 1,750, 1,877, 2,826, 2,911, and 3,343  $\mu\text{m}$  (Figure 2). Then, SBO was added to corn sample of each PS to achieve 0, 2, 4, 6, 8, and 10% fat. A transparent box of 30 cm height x 6 cm width x 18 cm length was used to determine AOR, and 200 g of sample were poured into the box using a funnel with a 3.18-cm opening (Figure 3). Then, the right and the left angles of the pile were measured with a protractor to determine the AOR for each sample. Finally, AOR was compared to the table elaborated by Lumay et al. (2012) for flowability assessment (Figure 4).



Figure 1. Problems Associated with Poor Flowability of Grains and Powders



Figure 2. Particle Size of Ground Corn

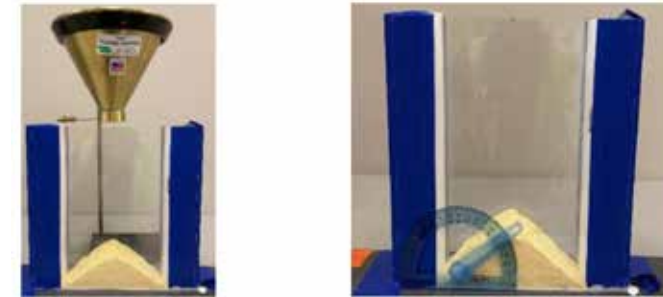


Figure 3. Transparent Box Used for Angle of Repose Measurement of Ground Corn

AOR, °	Flowability
25 to 30	Excellent
31 to 35	Good
36 to 40	Fair
41 to 45	Passable
46 to 55	Poor
56 to 65	Very poor
>66	Very, very poor

Figure 4. Relationship Between Angle of Repose and Flowability of Ground Corn (Adapted from Lumay et al., 2012)

Data were analyzed using GLIMMIX procedure of SAS (V.9.4) and means were separated using the PDIFF option at  $P \leq 0.05$ . Results showed interactions between corn PS and SBO additions ( $P < 0.0001$ ). For samples containing no added SBO, the AOR did not differ for any PS ( $P > 0.05$ ). In every case, increasing additions of SBO increased the AOR ( $P < 0.0001$ ). For corn with PS of 882, 968, 1,750, 1,877, 2,911, and 3,343  $\mu\text{m}$ , AOR was similar but was differed for PS of 693 and 2,862- $\mu\text{m}$  ( $P < 0.0001$ ). Increasing SBO additions increased AOR for every corn PS except for 3,343  $\mu\text{m}$  ( $P < 0.0001$ ). Ground corn presented excellent and good flow properties for all PS with 6 % or lower SBO concentrations. With 8% of SBO, flowability was fair and passable, while with 10% of SBO, ground corn presented fair, passable and poor flow properties. In conclusion, corn PS and SBO additions affected the AOR, thus flowability of ground corn.

## References

- Ganesan, V., Rosentrater, K. A., & Muthukumarappan, K. (2008). Flowability and handling characteristics of bulk solids and powders – A review with implications for DDGS. Retrieved from <https://www.sciencedirect.com/science/article/pii/S1537511008002791>
- Groesbeck, C N., Lawrence, K. R., Hastad, C. W., Goodband, R. D., Tokach, M. D., Nelssen, J. L., & Dritz, S. S. (2003). Particle size, mill type, and added fat influence flow ability of ground corn, *Kansas Agricultural Experiment Station Research Reports*, 0(10). <https://doi.org/10.4148/2378-5977.6842>

Jadhav, H. T., Ozoh, C., MARRIPUDI, S. T., CAO, X., & ROSENTRATER, K. A. (2017). Studies on ground corn flowability as affected by particle size and moisture content. Spokane, Washington July 16 - July 19, 2017. doi:10.13031/aim.201701175

Lumay, G., Boschini, F., Traina, K., Bontempi, S., Remy, J.-C., Cloots, R., & Vandewalle, N. (2012). Measuring the flowing properties of powders and grains. *Powder Technology*, 224, 19–27. doi:10.1016/j.powtec.2012.02.015

Ravindran, V. (2012). Poultry feed availability and nutrition in developing countries. Retrieved from <http://www.fao.org/3/a-al703e.pdf> [Google Scholar]

### **Affiliations**

Department of Poultry Science, Auburn University

# Determining the Effect of Chinese Privet (*Ligustrum sinense*) Invasion on the Occurrence of Ground-Dwelling Herpetofauna Species

Gabrielle Ripa, Christopher Anderson, and James Stiles

Chinese privet (*Ligustrum sinense*) is a highly invasive shrub species capable of altering the composition of native plant and animal communities (Hanula & Horn, 2011). As it is becoming increasingly common in the Southeastern United States, especially in bottomland hardwood forests and floodplains, it is important to examine its effect on native species (Wilcox & Beck, 2007). Because Chinese privet can form dense thickets, it has the potential to specifically impact on smaller, ground-dwelling herpetofauna (amphibians and reptiles) and their habitats by altering forest communities and their contribution to forest leaf litter. The bottomlands of the Southeast are home to many species of herpetofauna which may be impacted by Chinese privet; however, this effect has not been previously studied. The objective of this study was to determine, through animal surveys and habitat variables of soil moisture, temperature, and leaf litter mass, what effects Chinese privet has on litter-dwelling herpetofauna.

Between August 2019 to March 2020, herpetofauna, microhabitat, and vegetation data were collected monthly on a 3500-ha private property in Moundville, Alabama. There were 60 total study plots (314 m<sup>2</sup> each) on bottomland hardwood forest cover-type: 20 in dense privet (>50% privet cover), 20 in uninvaded forest (no privet), and 20 restoration sites where privet had been previously cut and burned. Twice during the study, (August-September and January – February), leaf litter was sampled within three 0.25 m<sup>2</sup> plots at random azimuths and distances from plot center. The leaf litter was later dry-weighed to calculate litter dry mass and moisture content. At each of the plots, time-area searches were conducted within the entire 314-m<sup>2</sup> area and reptile and amphibian individuals were identified to species-level. When an individual was found, soil moisture and temperature readings were taken using a soil moisture probe and temperature gun, respectively.

Environmental data were analyzed using ANOVA in R, while including a random-blocking variable for plot as these plots were resampled multiple times.

Results showed that where herpetofauna were detected, plots with privet had significantly lower average soil temperature (18.9 ±5.4 C) compared to plots with no privet (21.2 ±6.0 C) or restoration (22.4 ±6.0 C) plots. Preliminary leaf litter data (some leaf litter has not been dry-weighed and is forthcoming due to campus restrictions) showed plots with no privet had significantly higher dry-weight leaf litter mass (135.5 ±73.0 g m<sup>-2</sup>) compared to privet (59.6 ±32.3 g m<sup>-2</sup>) or restoration (57.1 ±49.0 g m<sup>-2</sup>) plots. From the time-area searches, the estimated total monthly density on restoration plots was 18.7 ±19.1 herps/ha, 14.8 ±14.2 herps/ha for privet plots, and 15.7 ±17.2 herps/ha for no privet plots. While the time-area searches yielded comparable numbers across forest types, the habitat variables and species composition varied somewhat between forest types. All forest types were dominated by amphibians but no-privet plots had the most marbled salamanders (*Ambystoma opacum*), which are typically less common than most other species detected. Additionally, because restoration plots were cut and burned as part of the treatment to eradicate the Chinese privet, these plots had brush piles and were more open which may have favored the higher occurrence of reptiles. Upon completion of leaf litter sampling, an occupancy analysis will be conducted to quantify the relationship between herpetofauna and leaf litter dry mass and other variables. A summary of these results is provided in Table 1.

**Table 1.** Mean (±SD) Leaf Litter Dry Mass, Temperature, and Ground-Dwelling Herpetofauna Density per Plot Type

	No Privet	Privet	Restoration
Leaf litter dry mass (g m <sup>-2</sup> )	135.5±73.0	59.6±32.3	57.1±49.0
Temperature (C)	21.1±6.0	18.9±5.4	22.4±6.0
Total monthly herpetofauna density (#/ha)	15.7±17.2	14.8±14.2	18.7±19.1
Amphibian monthly density (#/ha)	14.3±17.0	14.1±14.9	16.4±20.1
Reptile monthly density (#/ha)	1.4±1.9	0.7±1.3	2.3±1.8

The results at this point in the study show a clear difference in the microhabitat variables of leaf litter and temperature across the three plot types. Some differences related to reptile density and rarer species could be also detected. At the completion of this project, we hope to discern if there is a relationship between these different habitat variables due to privet and the occupancy of herpetofaunal species and groups.

## References

- Hanula, J. L., & Horn, S. (2011). Removing an invasive shrub (Chinese privet) increases native bee diversity and abundance in riparian forests of the southeastern United States. *Insect Conservation and Diversity*, 4:275-283.
- Wilcox, J., & Beck, C. W. (2007). Effects of *Ligustrum sinense* Lour. (Chinese privet) on abundance and diversity of songbirds and native plants in a southeastern nature preserve. *Southeastern Naturalist*, 6:535-550.

## Affiliations

School of Forestry and Wildlife Sciences,  
Auburn University

# High Chlorophyll Dietary Intervention in a High Red Meat Diet Caused No Significant Changes in Serum and Fecal Zonulin

Aaron Riviere and Andrew Frugé

Zonulin is a reversible regulator of the intestinal permeability in the intestinal tract. This naturally produced protein dysregulates the tight junctions between cells, allowing a gap for nutrients, microbes, and other molecules to flow in and out of the tract (Fasano, 2011). There are many nutrients and microbes that have been associated with changes in serum and fecal zonulin levels including gliadin, fiber, vitamin K, *Bacteroides*, *E. Coli*, and *Blautia* (Mokkala et al., 2016). Zonulin has also been associated with multiple cytokines including CRP, IL-6, and TNF $\alpha$  (Mörkl et al., 2018; , Arrieta et al., 2008). The goal of this study was to analyze changes in serum and fecal zonulin throughout a high green leafy vegetable dietary intervention. The dietary intervention was designed for the Meat and Three Greens (M3G) randomized control crossover trial to test for risk reduction of colorectal cancer through the described dietary intervention (Frugé et al., 2019). This intervention was not designed for improving zonulin levels, but the addition of green leafy vegetables provides multiple nutrients that may cause changes in zonulin secretion as well as potential to influence the gut microbiome. The population used was a twenty-participant subset from the M3G study, averaging 50 years old, obese, and consuming a high red meat and low green vegetable intake. Five males and five females each from the immediate and control groups were chosen using randomized software for use in the zonulin analyses. Serum and fecal samples were collected at the beginning and every four weeks during the twelve-week study. The serum and fecal samples were analyzed with a competitive ELISA to find relative zonulin levels (Immunodiagnostik AG). The serum and fecal zonulin levels were compared to dietary intakes, anthropometric measures, serum biomarkers, oxidative DNA damage (8-hydroxy-2'-deoxyguanosine), and fecal microbiome samples.

Two significant changes occurred in serum and fecal zonulin levels during the study; an increase in fecal

zonulin in the immediate group during the intervention period ( $p=0.002$ ) and a decrease in serum zonulin in the delayed group during the control period ( $p=0.040$ ). The only significant correlation found with zonulin levels and the cytokines analyzed was between lipopolysaccharide binding protein (LBP) and serum zonulin ( $p=0.015$ ). The dietary intake did not produce any significant correlations with serum or fecal zonulin. The gut microbiome is still being analyzed so no correlations have been assessed.

The results of this study contradict many previous findings. Zonulin was not shown to be significantly impacted by the multiple dietary factors analyzed or correlated with the cytokines assessed. There is a great need to understand the dietary factors that attribute to zonulin levels as well as the correlation between zonulin and inflammatory cytokines. The correlation between LBP and serum zonulin supports the understanding of the zonulin's role in gut permeability and the increased infection possibility with an increase in gut permeability. Many diseases have been associated with zonulin and gut permeability including IBS, metabolic diseases, food allergies, and Celiac Disease (König et al., 2016). Further research is needed to understand the dietary and microbiome factors that influence zonulin secretion. Understanding zonulin could have therapeutic effects in the reduction of symptoms and decreasing risks for the many diseases associated with zonulin.

## References

Arrieta, M. C., et al. (2008). Reducing small intestinal permeability attenuates colitis in the IL10 gene-deficient mouse. *Gut*, 58(1): pp. 41-48.

Fasano, A. (2011). Zonulin and its regulation of intestinal barrier function: The biological door to inflammation, autoimmunity, and cancer. *Physiological Reviews*, 91(1): pp. 151-175.

Frugé, A. D., et al. (2019). Primary outcomes of a randomized controlled crossover trial to explore the effects of a high chlorophyll dietary intervention to reduce colon cancer risk in adults: The meat and three greens (M3G) feasibility trial. *Nutrients*, 11(10): pp. 2349.

König, J., et al. (2016). Human intestinal barrier function in health and disease. *Clinical and translational gastroenterology*, 7(10): pp. e196-e196.

Mokkala, K., et al. (2016). Gut microbiota richness and composition and dietary intake of overweight pregnant women are related to serum zonulin concentration, a marker for intestinal permeability. *The Journal of Nutrition*, 146(9): pp. 1694-1700.

Mörkl, S., et al. (2018). Gut microbiota, dietary intakes and intestinal permeability reflected by serum zonulin in women. *European Journal of Nutrition*, 57(8): pp. 2985-2997.

## Affiliations

Department of Nutrition, Dietetics, and Hospitality Management, Auburn University

# Pore Network Modelling of Reactive Permeability Evolution

Mollie Sabo and Lauren Beckingham

Atmospheric carbon dioxide emissions contribute to global warming and continue to increase, making the demand for CO<sub>2</sub> emissions reduction more necessary. There are various approaches to reduce excess emissions such as geologic sequestration where my research is focused. Geologic sequestration is the action of injecting CO<sub>2</sub> in deep saline aquifers for long-term storage (Benson and Cole, 2008). As CO<sub>2</sub> is injected into the ground, it dissolves into the formation of brine, lowering pH and promoting mineral dissolution or precipitation reactions within the pores and pore throats (Khather et al., 2017). These reactions may alter the porosity and permeability of the formation in complex ways that are not well understood. In order to increase understanding of this relationship, we developed a pore network model in MATLAB that is comprised of pores and pore throats similar to those in a given sandstone specimen. The model simulates chemical reactions within the pores and pore throats with varying locations and extents of the reactions (Raeini et al., 2017). Each scenario includes 1000 pore network model simulations for a defined set of reaction extents (15-35% of radii).

One reaction scenario considers the effect of coupled mineral dissolution and precipitation reactions occurring simultaneously in different locations of the network. Here, we simulate dissolution in the pores and pore throats at the inlet of the network and precipitation at the outlet of the network. To understand the whole scope of this scenario, we execute the opposite scenario where precipitation occurs at the inlet of the network while dissolution occurs at the outlet of the network. In general, dissolution increases porosity and permeability and precipitation decreases porosity and permeability. Porosity is controlled by the pore sizes while permeability is controlled by the pore throat sizes (Bensinger and Beckingham, 2019). Simulation results from both scenarios show that the porosity stays the same. This is because the simulated amount of dissolution and precipitation are the same which balances out the overall change in the size of the pores. Therefore, it is concluded the location of the reactions

does not affect the overall porosity. On the other hand, simulation results show that permeability decreases. Permeability is limited by the smallest pore throat size and thus even though some pore throats increase in size, the permeability decreases as precipitation occurs and reduces the smallest pore throat size. While permeability decreases due to reactions occurring, the location of the reaction does not affect the permeability.

Another scenario we conducted involved randomly distributing dissolution and precipitation reactions throughout the pores and pore throats in the network. In this simulation, the porosity increases with the increasing extent of the reaction and is controlled by the increasing dissolution occurring within the pores and pore throats. In contrast, the permeability stays the same due to the varying reactions of dissolution and precipitation occurring simultaneously throughout the network.

Regarding future work, we will develop simulations considering reactions occurring preferentially in small or large pores and pore-throats where previous work has suggested pore size may promote or inhibit dissolution and precipitation reactions. Here, we will simulate dissolution in large pores and pore throats and precipitation in smaller pores and pore throats. We will also execute the opposite scenario by simulating precipitation in the relatively larger pores and pore throats and dissolution occurs within the relatively smaller pores and pore throats. Through the understanding of these scenarios, we can develop a better understanding of the relationship between porosity and permeability in a way that will benefit those who want to design underground CO<sub>2</sub> storage systems and eliminate the excess emissions into the atmosphere.

## References

- Bensinger, J., & Beckingham, L. E. (2020). CO<sub>2</sub> storage in the Paluxy Formation at the Kemper County CO<sub>2</sub> storage complex: Pore network properties and simulated reactive permeability evolution. *International Journal of Greenhouse Gas Control*, 93, 102887., doi:10.1016/j.ijggc.2019.102887
- Benson, S. M., & Cole, D. R. (2008). CO<sub>2</sub> sequestration in deep sedimentary formations. *Elements*, 4, 325-331. doi:10.2113/gselements.4.5.325
- Khather, M., Saeedi, A., Rezaee, R., Noble, R. R. P., & Gray, D. (2017). Experimental investigation of changes in petrophysical properties during CO<sub>2</sub> injection into dolomite-rich rocks. *International Journal of Greenhouse Gas Control*, 59, 74-90. doi:10.1016/j.ijggc.2017.02.007
- Raeini, A. Q., Bijeljic, B., Blunt, M. J. (2017). Generalized network modeling: Network extraction as coarse-scale discretization of the void space of porous media. *Physical Review E*, 96, 013312. doi:10.1103/PhysRevE.96.013312

## Affiliations

Department of Civil Engineering, Auburn University

# Temperature Dependency of Magnetic Particle Characterization by Particle Tracking Velocimetry

Abhinav Sannidhi<sup>1</sup>, Thomas Hanley<sup>1</sup>, and Paul Todd<sup>2</sup>

Magnetic particles with different composition, size and magnetization are used in cell separation, cell labeling, cellular endocytosis, drug targeting, magnetic resonance imaging, hyperthermia, and *in vivo* diagnostics. By means of particle tracking velocimetry in darkfield illumination, we measured multiple characteristics of several thousand individual particles per sample. The Hyperflux™ velocimeter is utilized to provide quantitative video analysis of particles using high definition particle tracking velocimetry in an isodynamic magnetic field (Figure 1). Image analysis software converts the image data to the parameters of interest such as particle diameter and magnetophoretic mobility, which in turn provides scope to estimate intrinsic magnetic characteristics on a particle-by-particle basis, providing distributions of key properties and hence the scope for assessment of particle quality (Zhou et al., 2016; Zhou et al, 2017; Sannidhi et al., 2019).

Magnetophoretic mobility is defined as the ratio of terminal velocity attained by the particle in an isodynamic magnetic field to the magnetic pressure. The present study focuses on the temperature dependence of the magnetophoretic mobility measurements of micro-sized particles by particle tracking velocimetry. The magnetophoretic mobility of non-magnetic beads (5 μm in size) has been analyzed at different sample temperature conditions: hot, ambient and cold. The mobility of non-magnetic beads is almost zero, but the instrument reported a high mobility at hot and cold temperature conditions. We tested the hypothesis that the differences in the temperature of bead suspensions and glass channel cell resulted in Marangoni flow, or thermo-capillary convection, which is driven by an interfacial-tension gradient. To study the effect of the hot-sample temperature condition, we conducted three bead experiments: (1) sample and channel cell at room temperature, (2) sample at 98°C and channel

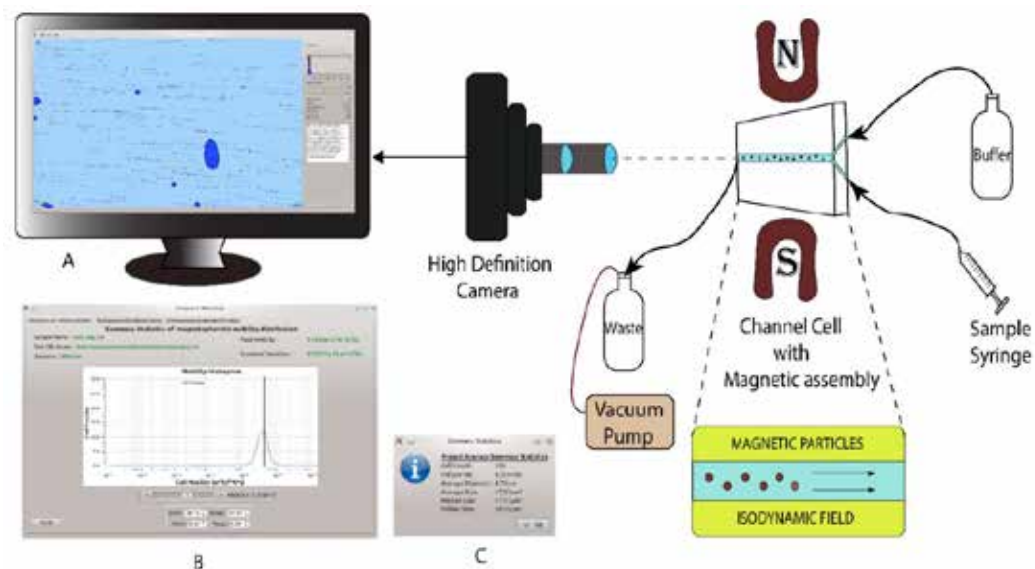


**Figure 1.** Mechanism of Hyperflux Velocimeter (A) the image of particle trajectories, (B) the magnetophoretic mobility histogram, (C) summary statistics of the sample (Adapted from Sannidhi et al., 2019)

cell at 50°C, (3) sample and channel cell at 50°C. Only under condition (2) did the non-magnetic beads show mobility. Thus, increased temperature per se does not induce motion; a temperature gradient is required. However, the observed particle velocity was not consistent with the predictions of thermo-capillary flow, so a contractile-flow hypothesis was tested. The incoming hot sample is rapidly cooled through the thin walls of the channel cell, and the water on the entry side of the cell is the hottest and contracting most rapidly, resulting in net fluid contractile motion toward the inlet. The observed particle velocity, about 100 μm/s was found consistent with the predicted rate of water cooling during contraction and the calculated heat-transfer rate. This resulted in the entire particle suspension movement, and therefore significant mobility is being recorded by the instrument.

In conclusion, this study indicates the importance of isothermal conditions for measuring magnetophoretic mobility by particle tracking velocimetry. The sample and channel cell must both be at ambient temperature or thermostated to a single temperature before injecting the sample into the channel cell to achieve optimal results which specify the particle quality accurately.

## References

- Sannidhi, A., Todd, P. W., & Hanley, T. R. (2019). Estimation of intrinsic magnetic properties of single particles by particle tracking velocimetry, *IEEE Magnetics Letters 1*. doi:10.1109/LMAG.2019.2950298.
- Zhou, C., Boland, E. D., Todd, P. W., & Hanley, T. R. (2016). Magnetic particle characterization—magnetophoretic mobility and particle size. *Cytometry Part A*, 89, 585–593. doi:10.1002/cyto.a.22866
- Zhou, C., Qian, Z., Choi, Y. S., David, A. E., Todd, P. W., & Hanley T. R. (2017). Application of magnetic carriers to two examples of quantitative cell analysis. *Journal of Magnetism and Magnetic Materials*, 427, 25–28. doi:10.1016/j.jmmm.2016.11.009

## Affiliations

- <sup>1</sup> Department of Chemical Engineering, Auburn University
- <sup>2</sup> Magnaquant, LLC, Louisville, Kentucky

# Assessment of Age and Region Differences in Health Beliefs and Dietary Habits Related to Colon Cancer Risk

Megan Schaberg, Kristen Smith, Michael Greene, and Andrew Frugé

In the United States (US), colon cancer (CC) is the third most common cancer (Siegel et al., 2020). Increased CC risk is associated with several factors including diets lacking in green leafy vegetables (GLV) and rich in red meat (RM) (Stein & Colditz, 2004). Furthermore, compliance with CC screening recommendations is associated with reduced risk for CC. (Shapiro et al., 2008). The recommended age to begin CC screenings is 45 with no known family history of CC, yet approximately half of the US population aged 50 and older do not follow the CC screening recommendations (Wolf et al., 2018; Shapiro et al., 2008). Additionally, CC is increasingly diagnosed in younger adults (Siegel et al., 2019). Awareness of CC risk factors and understanding the benefits of health-related behaviors can influence an individual to seek changes in order to reduce CC risk. The Dietary Habits and Colon Cancer Beliefs Survey (DHCCBS) was developed and validated using the Health Belief Model (HBM) to assess beliefs and attitudes related to diet and CC risk (Smith et al., 2019). The attitudes and health behaviors of US adults to modify behaviors to reduce CC risk are investigated herein.

Relationships within age groups and DHCCBS responses were explored and presented in Table 1. Perceived severity was significantly lower in younger adults (<35, n=487) compared to older adults (35-44, p=0.042; 45-54, p=0.003). Additionally, older participants (45-54, n=124) reported greater benefits to increasing GLV consumption to reduce CC risk than the younger age group (<35; p=0.006). Conversely, younger participants (<35) received more recommendations from friends and family members to increase GLV intake in order to reduce colon cancer risk (35-44, p=0.033; 45-54, p=0.002). The middle age group (35-44, n=227) in the Southern US consumed significantly more RM than corresponding individuals in the Northeast (South:  $\mu=0.73$ ,  $\sigma=0.75$ ; vs. Northeast:  $\mu=1.13$ ,  $\sigma=1.11$ ; p=0.021). Moreover, each age group

differed in GLV consumption between the South and West regions (South: <35,  $\mu=0.90$ ,  $\sigma=0.71$ , p=0.050; 35-44,  $\mu=1.15$ ,  $\sigma=1.31$ , p=0.005; 45-54  $\mu=0.85$ ,  $\sigma=0.76$ , p=0.044; vs. Northeast: <35,  $\mu=0.84$ ,  $\sigma=0.87$ , p=0.050; 35-44,  $\mu=0.68$ ,  $\sigma=0.50$ , p=0.005; 45-54  $\mu=0.90$ ,  $\sigma=0.53$ , p=0.044).

The DHCCBS survey results suggest the willingness to change health-related behaviors is associated with dietary habits and regional location. Younger participants do not recognize the severity of CC diagnosis compared to older participants, although the prevalence in this age group is increasing. These younger individuals are less likely to make the necessary changes to improve their health outcomes if they remain unaware of risk factors. Providing CC screenings for younger adults that also include behavioral risk reduction guidance may decrease CC morbidity and mortality. Furthermore, public health recommendations should be adjusted to provide feasible health behaviors and consider regional differences in dietary patterns. Dietary recommendations that address dietary habits and behavioral barriers, such as increasing GLV over reduction of RM to obtain benefits may be most beneficial.

	Total (n=838)	<35 (n=487)	35-44 (n=227)	45-54 (n=124)	
	Mean (SD)	Mean (SD)	Mean (SD)	Mean (SD)	between group p- value
<b>Susceptibility</b>					
Please rate your perceived risk for developing colon cancer in your lifetime:	2.12 (0.60)	2.08 (0.63)	2.18 (0.56)*	2.17 (0.58)	0.068
<b>Severity</b>					
Colon cancer can severely decrease my quality of life	4.67 (0.77)§	4.61 (0.85)I #	4.74 (0.67)*	4.77 (0.59)*	0.046
Colon cancer could lead to death	4.7 (0.70)§	4.65 (0.79)I	4.78 (0.57)*	4.78 (0.50)	0.028
<b>Perceived Benefits</b>					
If I eat less red meat I could decrease my risk of developing colon cancer	3.76 (0.97)	3.69 (0.952)	3.84 (0.96)	3.88 (1.03)	0.053
If I eat more green leafy vegetables I could decrease my risk of developing colon cancer	4.14 (0.85)§	4.09 (0.85)#	4.15 (0.85)	4.32 (0.81)*	0.024
<b>Perceived Barriers</b>					
I don't like the taste of other protein-rich foods	2.08 (1.00)	2.09 (0.98)	2.06 (1.08)	2.07 (0.94)	0.916
I don't like the taste of green leafy vegetables	1.95 (1.16)§	2.06 (1.19)I #	1.85 (1.16)*	1.71 (0.94)*	0.003
I can't imagine never eating red meat	3.25 (1.53)	3.26 (1.53)	3.3 (1.55)	3.14 (1.48)	0.628
<b>Cues to Action</b>					
A healthcare provider has recommended that I eat less red meat	1.64 (0.99)	1.63 (0.96)	1.62 (1.01)	1.72 (1.09)	0.627
A friend or family member has recommended that I eat less red meat	1.84 (1.18)	1.92 (1.22)I	1.72 (1.14)*	1.77 (1.10)	0.085
A healthcare provider has recommended that I eat more green leafy vegetables	2.69 (1.46)	2.71 (1.44)	2.68 (1.49)	2.61 (1.52)	0.798
A friend or family member has recommended that I eat more green leafy vegetables	2.78 (1.49)§	2.91 (1.46)I #	2.66 (1.52)*	2.44 (1.46)*	0.003
§ between group significance; *significance between >35 age group; I significance between 35-44 age group; # significance between 45-54 age group.					
Statistical Methods: differences in age groups and regions were assessed using one-way ANOVA with LSD corrections for multiple comparisons.					

## References

Shapiro, J. A., Seeff, L. C., Thompson, T. D., Nadel, M. R., Klabunde, C. N., & Vernon, S. W. (2008). Colorectal cancer test use from the 2005 National Health Interview Survey.

Siegel, R. L., Miller, K. D., & Jemal, A. (2019). Cancer statistics, 2019. *CA: A Cancer Journal for Clinicians*, 69(1), 7-34. doi:10.3322/caac.21551

Siegel, R. L., Miller, K. D., & Jemal, A. (2020). Cancer statistics, 2020. *CA: A Cancer Journal for Clinicians*, 70(1), 7-30. doi:10.3322/caac.21590

Smith, K. S., Raney, S. V., Greene, M. W., & Fruge, A. D. (2019). Development and validation of the Dietary Habits and Colon Cancer Beliefs Survey (DHCCBS): An instrument assessing health beliefs related to red meat and green leafy vegetable consumption. *Journal of Oncology*, 2326808. doi:10.1155/2019/2326808

Stein, C. J., & Colditz, G. A. (2004). Modifiable risk factors for cancer. *British Journal of Cancer*, 90(2), 299-303. doi:10.1038/sj.bjc.6601509

Wolf, A. M. D., Fontham, E. T. H., Church, T. R., Flowers, C. R., Guerra, C. E., LaMonte, S. J., Etzioni, R., McKenna, M. T., Oeffinger, K. C., Shih, Y-C. T., Walter, L. C., Andrews, K. S., Brawley, O. W., Brooks, D., Fedewa, S. A., Manassaram-Baptiste, D., Siegel, R. L., Wender, R. C., & Smith, R. A. (2018). Colorectal cancer screening for average-risk adults: 2018 guideline update from the American Cancer Society. *CA: A Cancer Journal for Clinicians*, 68(4), 250-281. doi:10.3322/caac.21457

## Affiliations

Department of Nutrition, Dietetics and Hospitality Management, Auburn University

# Engineering Lignin Transformation Mechanisms to Create Value-Added Products Using Atomistic Modeling

Jonathan Schuler<sup>1</sup>, Tanzina Azad<sup>1</sup>, Maria Auad<sup>1,2</sup>, Thomas Elder<sup>3</sup>, and Andrew Adamczyk<sup>1</sup>

Lignin is a component of biomass that makes up 20-35% of wood, the other major constituents being cellulose and hemicellulose (Kawamoto, 2017). The pyrolysis of lignin has been shown to produce valuable materials like phenol, benzene, xylene, and toluene, which can be used in the plastics industry or as renewable biofuels (Smock, 2012; Holliday, et al., 2007). Pyrolysis is the degradation of a substance at high temperature under a limited amount of oxygen (Kawamoto, 2017). While lignin, hemicellulose, and cellulose all have industrial potential, most research efforts have focused on only cellulose, because of its regular, fixed structure (Murillo, et al., 2017). Finding key reaction mechanisms for lignin decomposition could allow for substantial profit to be obtained from lignin byproducts from the pulp and paper industry that are currently not effectively utilized.

Lignin is made up of a combination of three different monomers: p-hydroxy-phenyl (P-unit), guaiacyl (G-unit), and syringyl (S-unit), aligned in a seemingly-random pattern (Kawamoto, 2017). Considering current understanding of lignin structure is far from complete, experimental studies for lignin pyrolysis are performed using computational chemistry on model lignin structures. This approach has the capability of predicting the useful electronic properties of lignin that ultimately helps study its reaction energetics and mechanisms. Typically, lignin pyrolysis has been modeled using dimer systems (Elder, 2007). This work broadens the scope to structures up to ten monomers in length (for both a G-unit and S-unit structure) in an attempt to address non-bonding energetics that would be observed in realistic lignin structures. The goal of this study was to use tools of computational chemistry to investigate the bond dissociation enthalpy of a 10-monomer model lignin structure made entirely of guaiacyl (G-unit) monolignols. Studying these energetics has the potential to provide new insight

for better understanding the key reactions in lignin pyrolysis.

To determine the bond dissociation energy of each  $\beta$ -O-4 ether linkage in the generated 10-monomer structure, a three-step method was followed. First, the reactant molecule and the two products formed by cleaving a bond were conformationally sampled to ensure that the input geometries were reasonable. Second, a more rigorous geometry optimization and energy calculation were performed using Density Functional Theory (DFT) calculations for both the reactant structure and product structures. Third, the bond dissociation enthalpy was calculated by subtracting the reactant's calculated energy from the sum of the products' calculated energies. Using this method, the bond dissociation energy of all nine ether linkages in two target structures (G-unit and S-unit) could be calculated.

The results from the G-unit study can be seen in Figure 1.

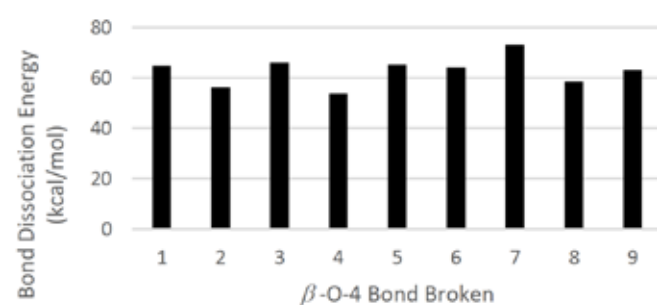


**Figure 1.** Position Dependence of Lignin Pyrolysis at 650 K.

For the G-unit structure, bond dissociation energies ranged from 54-73 kcal/mol, with an average value of 66.46 kcal/mol. This is quite close to the reported value for a G-unit dimer of 67.33 kcal/mol (Parthasarathi, et al., 2011). Interestingly, the structure appeared to have

different  $\beta$ -O-4 dissociation energies depending on the position of the bond in the molecule (for example, bond "1" above refers to the bond on one end of the chain, while bond "9" refers to the bond on the other end). This could indicate the importance of non-bonding interactions on  $\beta$ -O-4 dissociation enthalpy in lignin molecules. Additionally, thermodynamic properties were calculated for model structures which can help determine if a reaction is kinetically or thermodynamically governed at specified temperatures.

Results from this project are in the process of being submitted to a scholarly journal and have been presented at a national conference (Azad, et al., 2020; Azad, et al., 2019). Moving forward, a similar study is being performed to study the reaction energetics of the S-unit structure for comparison with the G-unit one. Additionally, results obtained from these studies can theoretically be used with a reaction network generation software to create plausible reaction pathways that can be utilized for the design of more selective reactors.

## References

Azad, T., Schuler, J., Auad, M., Elder, T., & Adamczyk, A. J. (2019). In *Engineering Lignin Transformation Mechanisms to Create Value-Added Products Using Atomistic Modeling*, 2019 AIChE Annual Meeting, AIChE: 2019.

Azad, T., Schuler, J. D., Auad, M. L., Elder, T., & Adamczyk, A. J. (2020). Model lignin oligomer pyrolysis: Coupled conformational and thermodynamic analysis of  $\beta$ -O-4' bond cleavage. *ACS Energy & Fuels* 2020, to be submitted.

Elder, T. (2007). Quantum Chemical determination of Young's modulus of lignin. Calculations on a  $\beta$ -O-4 model compound. *Biomacromolecules*, 8: 3619-3627.

Holliday, J et al. (2007). Top value added chemicals from biomass. *Pacific Northwest National Laboratory*, 2: 1-77.

Kawamoto, H. (2017). Lignin pyrolysis reactions. *Journal of Wood Science*, 63:117-132.

Murillo, J et al. (2017). Biomass pyrolysis kinetics: a review of molecular-scale modeling contributions. *Brazilian Journal of Chemical Engineering*, 34: 1-18.

Parthasarathi, R. et al. (2011). Theoretical study of the remarkably diverse linkages in lignin. *The Journal of Physical Chemical Letters* 2, 2660-2666.

Smock, D. (2012). Does lignin have legs as a future plastics feedstock? The Molding Blog. <http://www.themoldingblog.com/2012/05/03/does-lignin-have-a-future-as-a-plastics-feedstock/>

## Affiliations

<sup>1</sup> Department of Chemical Engineering, Auburn University

<sup>2</sup> Center for Polymer and Advanced Composites, Auburn, Alabama

<sup>3</sup> United States Department of Agriculture, Southern Research Station

# Performance Enhancement of Ditch Check Practices During Highway Construction

*Jaime Schussler<sup>1</sup>, Michael Perez<sup>1</sup>, Bora Cetin<sup>2</sup>, and Blake Whitman<sup>3</sup>*

Earthmoving activities associated with highway construction have increased erosion rates and risk of downstream pollution from sediment-laden stormwater runoff. To minimize downstream impacts, USEPA Construction General Permit requires all construction operators to develop a stormwater pollution prevention plan (SWPPP). Prior to this research, Iowa DOT had erosion and sediment control practice (E&SC) specifications and standard drawings that had not been evaluated for field performance. Opportunities existed to understand the performance of the E&SC practices, improve design and performance, and develop additional design guidance.

The research team outlined three objectives to meet this goal including: (1) compile E&SC practices to be used during DOT construction, (2) install and evaluate selected practices on active Iowa DOT construction sites, and (3) develop implementable improvements for DOT E&SC design guidance. A comprehensive literature and SWPPP review of E&SC practices was conducted. Based on this review, researchers coordinated with an Iowa DOT advisory committee to identify and modify E&SC practices of interest for field monitoring. Practices were evaluated for erosion reduction, sedimentation potential, and structural integrity. Based on practice success, design recommendations were made.

Two ditch check types, practices to interrupt flow and impound runoff in conveyance channels, were evaluated in this project: (1) silt fence and (2) wattle ditch checks. Monitoring was conducted on Highway U.S. 30 Expansion in Tama County, Iowa throughout the 2019 construction season (July- December). Data collection included daily rainfall, channel surveys, and weekly visual inspections. In addition to performance, stakeholder interviews and cost analysis was completed to determine the feasibility of adopting modified practices.

The Iowa DOT standard silt fence ditch check (S) specifies 4 ft (1.2 m) steel T-posts, spaced 4 ft (1.2 m) apart to be driven at least 28 in. (71 cm) into the ground.

Silt fence geotextile extends at 19 in. (48 cm) above the ground line and is tied to the posts through the top, middle, and bottom of the material. Material is sliced 12 in. (30.24 cm) into the ground. Modifications to this design included decreasing the t-post spacing to 3 ft (0.91 m), v-shape installation, dewatering weir, and wire reinforcement of the silt fence material. The modified design was evaluated with both a trenched (M1) and sliced (M2) method of keying the silt fence into the ground. In total, three installations of each method were evaluated. Installation methods included S, Standard with manufactured geotextile (SM), M1, and M2.

Weekly visual inspections were conducted to observe the structural integrity and failure modes and channel surveys were taken the day of installation and again after 11.82 in. (30 cm) of cumulative rain. The average sediment accumulation for S, SM, M1, M2 was 0.51 ft<sup>3</sup> (0.014 m<sup>3</sup>), 0.60 ft<sup>3</sup> (0.017 m<sup>3</sup>), 2.06 ft<sup>3</sup> (0.058 m<sup>3</sup>), and 1.29 ft<sup>3</sup> (0.037 m<sup>3</sup>), respectively. When compared to the standard design, the trenched and sliced modified installations improved sediment deposition by an average of 408% and 254%, respectively. The cost per ft<sup>3</sup> (m<sup>3</sup>) for S, SM, M1, and M2, was \$17.71 (\$625.42), \$90.23 (\$3,186.44), \$20.29 (\$716.53), \$32.08 (\$1,144.20), respectively. Despite the cost per volume of M1 being 1.1 times the cost of S, researchers recommended adopting M1 with the addition of an energy dissipater at the weir due to increased longevity observed in the weekly visual inspections.

Wattles were the second ditch check type evaluated in this study. Iowa DOT standard installation specifies a wattle placed perpendicular to flow direction in the channel, extending up the foreslope and backslope. Stakes are spaced every 2 ft (0.61 m) and driven through the wattle into the ground a minimum 12 in. (0.30 m). Modifications to the wattle ditch check included the addition an underlay pinned to the channel using a 6 in. (15.24 cm) sod pins and nondestructive tee-pee staking pattern every 2 ft (0.61 m). Five standard and three modified wood chip wattles were installed. The average

sediment capture of the standard installation was 0.12 ft<sup>3</sup> (0.0034 m<sup>3</sup>), whereas the modified installation was 1.51 ft<sup>3</sup> (0.043 m<sup>3</sup>), capturing 13.5 times more sediment. The cost per volume accumulation of the modified [\$113.07/ ft<sup>3</sup> (\$3,993/ m<sup>3</sup>)] was just 9% that of the standard [\$1,144.67/ ft<sup>3</sup> (\$40,423/ m<sup>3</sup>)]. Based on these findings researchers recommended the DOT adopting the modified design.

This project provided the research team a basis for ditch check improvements, field monitoring during active construction presented several unknown and immeasurable variables such as changing grade, thus altering flow patterns and drainage areas, vegetative growth, maintenance, and variability in storm events. Full-scale testing would allow practices to be subjected to known rainfalls, flows, drainage areas, slopes, sediment loads, and vegetative conditions. This would allow major components or groups of components contributing to practice success to be identified and adopted for design improvements.

## Affiliations

<sup>1</sup> Department of Civil Engineering, Auburn University

<sup>2</sup> Department of Civil Engineering, Michigan State University

<sup>3</sup> Middle Tennessee State University

# 3D Printing of Self-Healing Polymer Composites

*Vinita Shinde and Bryan Beckingham*

Polymers are materials made of many small molecules called monomers covalently linked together to form long chain molecules of high molecular weight. Goods and products made from polymers are present all around us: polyurethane foam cushions, polyethylene cups, cloths of synthetic fiber, acrylic paints and many more and thus, they have huge impact on our lives. However, high strength and stiffness equivalent to that of metal products is desirable for some applications in aerospace, automotive, marine, electronics industries while maintaining the lower density of polymer materials. This is where a key advantage of polymer composites comes into play. Polymer composites are multi-material systems where reinforcing additives are included within polymer matrices to achieve synergistic properties of both polymer and the reinforcing material. Thus, polymer composites are an increasingly popular choice for structural applications due their high modulus, light weight and excellent performance. In addition, additive manufacturing of polymer composites has recently shown dramatic increase in both attention and industrial applications. The expansion of interest is driven by its high degree of customization, ability to construct complex designs and due to decreasing costs of 3D printing materials and equipment.

Two popular choices of 3D printing techniques for polymer materials are: stereolithography (SLA) and fused deposition modeling (FDM). FDM utilizes a polymer filament or wire that is extruded through a hot nozzle in a layer-by-layer fashion to print an object from a 3D model and has found increasing application for rapid prototyping. SLA also builds an object layer-by-layer but does so by using photopolymerization. During SLA a beam of light is focused to a spot within a liquid resin bath where it causes a reaction that forms the solid polymer. By controlling the light position and resin chemistry, desired objects are printed from this liquid resin bath into the final solid object. SLA printing has high resolution and excellent surface finish. However, 3D printing of polymer materials remains somewhat limited due to limitations in mechanical properties and functionalities of fabricated parts. Also, many of the polymer material options for 3D printing are not intrinsically recyclable requiring disposal if they suffer

any damage. Moreover, during daily usage, polymer materials face mechanical stresses, atmospheric oxygen and moisture, etc., all of which can lead to damage in the materials. Thus, the lifetimes of composite materials are limited by fatigue or other material failure mechanisms due to this damage encountered during the processing or the application. In nature, biological systems overcome these issues by using self-healing as their strategy to heal the injuries. Thus, taking inspiration from nature, here, we aim to integrate self-healing properties with polymeric materials to extend lifetime of 3D printed composite materials. Based on the current research problem, our research objective is to develop new healing systems which can withstand the high shear stresses and elevated temperature during the 3D printing process while also restoring excellent healing response of the finished 3D printed objects.

The development of 3D printed self-healing composites pursues to resolve material damage issue by incorporating synthetic healing materials with the ability to self-repair, thus preventing catastrophic material failure and prolonging their operational lifetimes. The most common technique for achieving self-healing for practical applications involves incorporation of fluid filled microcapsules into the host polymer material. During the composite fracture, the microcapsules are broken, releasing the healing fluid which interacts with the polymer matrix to seal the fracture. The double walled microcapsules were synthesized using combined process of in-situ polymerization in oil in water emulsion with an interfacial microencapsulation containing healing fluid at the core. Once microcapsules were synthesized successfully, they were incorporated into bulk polymers or are coated on polymer filaments to produce 3D printed polymer objects via stereolithography (SLA) and fused deposition modeling (FDM) capable of self-healing. Healing efficiency achieved by these microcapsule-based self-healing systems is dependent on microcapsules size and morphology, chemistry of healing fluid and environmental conditions. Healing efficiency of microcapsule loaded 3D printed composites was investigated by single edge notch beam test. The healing efficiency of the samples showed a maximum recovery of 79% after 72 hours.

In summary, fluid-filled microcapsules are successfully synthesized and incorporated in polymer systems for 3D printing. Microcapsules survived harsh conditions of 3D printing processes, investigated by <sup>1</sup>H-NMR spectroscopy. Healing efficiency and mechanical properties of capsules loaded specimens was evaluated to investigate the recovery of fracture in composite materials after damage event and impact of capsules on mechanical properties of polymer matrix.

## Affiliations

Department of Chemical Engineering,  
Auburn University

# Study of the Vortex Interactions in the Near Wake of Coaxial Rotors in Hover

Lokesh Silwal and Vrishank Raghav

The near wake flowfield of the rotors have direct correlation with the rotor performance, vibration, noise, and structural problems. In addition, the comprehensive understanding of the flowfield is imperative for better prediction of the rotor performances under different operating conditions. Although the near wake of the single rotor has been studied comprehensively (Mula et al., 2013), the flowfield of the coaxial rotors across various design and operating conditions remains to be investigated. Thus, this study is focused on an experimental investigation of the near wake of a counter-rotating coaxial rotor system using a modular, thrust scaled experimental setup as shown in Figure 1.

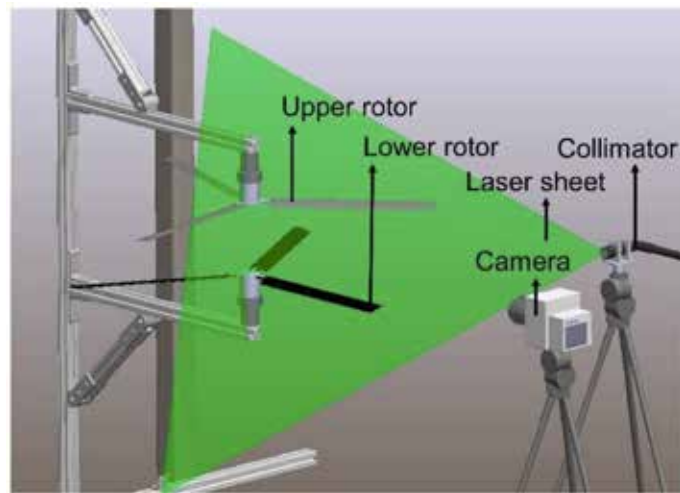


Figure 1. Experimental Setup

The primary objective of the current project was to study the instantaneous vortex interactions of the coaxial rotor system at different rotor spacings. For the current study, the spacing between the rotors was varied as 17.6%, 12% and 7% of the rotor diameter ( $D$ ). The rotors were operating at an RPM of 650 resulting in the tip Reynolds number of 64,000. The experiments were carried out in hover at thrust matched trim condition where each rotor was producing the non-dimensional thrust (thrust coefficient,  $C_T$ ) of 0.006. The near wake flowfield of the coaxial rotor was studied using high-speed particle image velocimetry (PIV). The PIV setup with the high-speed camera and the laser is shown in Figure 1.

The instantaneous vorticity field results obtained from the current study is shown in Figure 2. For larger rotor spacing of 0.176D and 0.12D (Figure 2 a and b), it was observed that there was high contraction of the upper rotor wake before impinging on the lower rotor plane resulting in larger center to center distance between the tip vortices of the upper and lower rotors. As a result, the inter-rotor tip vortex interactions were not observed. However, interactions between the lower rotor tip vortices were prevalent in the near wake and is referred to here as intra-rotor vortex interactions. It was also interesting to note that the interactions were only observed between lower rotor tip vortices and not for the upper rotor. This could be because the upper rotor tip vortices convect downwards at a higher velocity when compared to that of the lower rotor (Mortimer, et al., 2019). Consequently, the pitch of the tip vortices of the upper rotor is larger when compared to that of the lower rotor, reducing the chances of interactions.

For rotor spacing of 0.07D (Figure 2 c), it was observed that there were only inter rotor tip vortex interactions in the near wake. Since the upper rotor wake contraction ratio is low due to the smaller axial separation distance, the center to center distance between upper and lower rotor vortices is reduced resulting in a higher chance for vortex interactions. Thus, the current study shows that the spacing between the rotors have significant influence on the near wake dynamics of the coaxial rotor system. It can be concluded that at larger rotor spacings, the near wake of the coaxial rotor is dominated by the intra-rotor vortex interactions. When the spacing is reduced, inter-rotor vortex interactions becomes a prominent feature in the near wake.

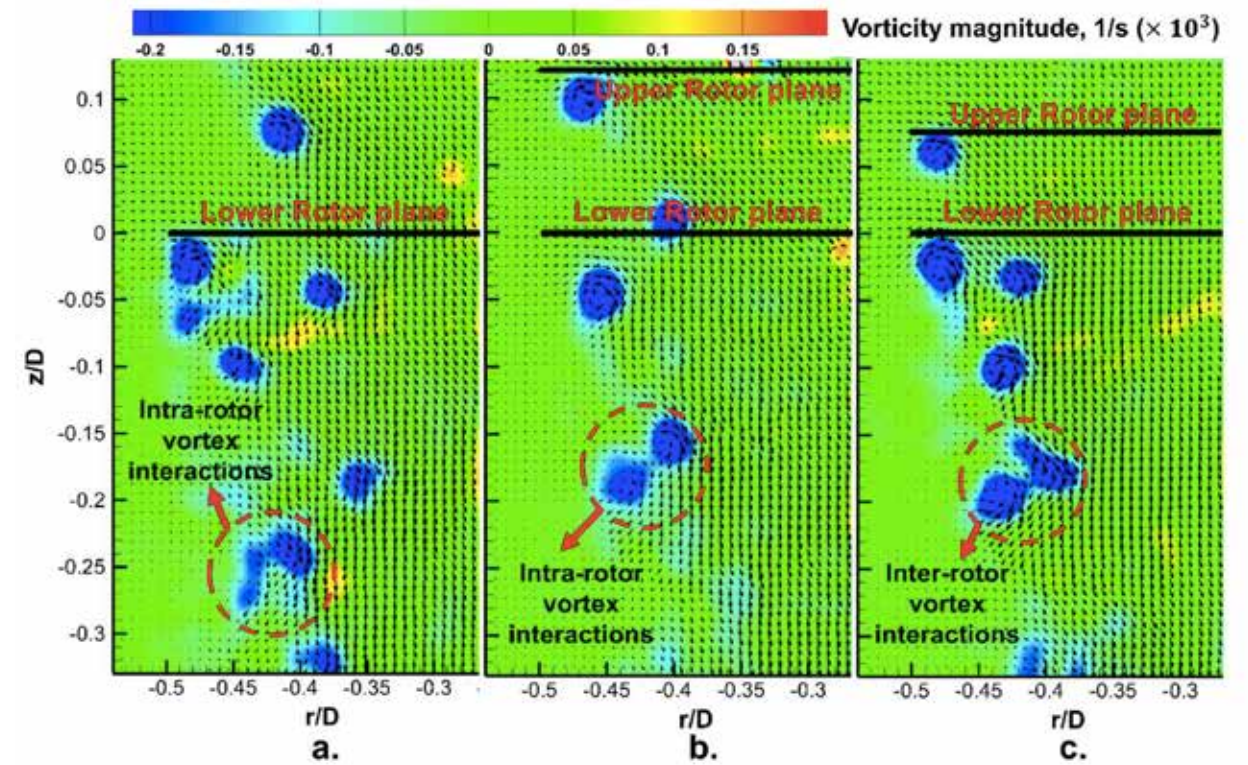


Figure 2. Instantaneous Vorticity Field for Coaxial Rotors Highlighting the Near Wake Vortex Interactions, a) 17.6% of rotor diameter, b) 12% of rotor diameter, c) 7% of rotor diameter

## References

- Mortimer, P., Sirohi, J., Platzer, S., & Rauleder, J. (2019). Coaxial rotor wake measurements in hover using phase-resolved and time-resolved PIV, *Annual Forum 75*, VFS.
- Mula, S. M., Stephenson, J. H., Tinney, C. E., & Sirohi, J. (2013). Dynamical characteristics of the tip vortex from a four-bladed rotor in hover, *Experiments in Fluids*, 54(10).

## Affiliations

Department of Aerospace Engineering,  
Auburn University

# Enhancing Heat Transfer in Microgravity Through Vapor Mobility in Phase-Change Cooling

*Karthekeyan Sridhar, Ryan Smith, and Sushil Bhavnani*

Negligible buoyancy forces in microgravity causes vapor bubbles to grow to very large diameters, leading to poor heat transfer and damage of electronic devices. Using an engineered surface modification, namely an asymmetric sawtooth ratchet, to create vapor mass mobility can alleviate this problem. This experimental, terrestrial study stems from a larger effort to dissipate increased heat fluxes through augmented pool boiling in spacecraft electronics as a precursor to a comprehensive study to be conducted on the International Space Station (ISS) under prolonged microgravity conditions. A prior NASA Zero-G flight (2012) demonstrated passive vapor mobility in microgravity conditions due to the sawtooth microstructure, but the effects of g-jitter could not be ruled out (Thiagarajan, 2015).

The primary objective of the terrestrial experiment at Auburn University is to observe vapor bubble dynamics in an experimental setup that mimics the hardware aboard the ISS to provide baseline data to the NASA implementation partner, Techshot Inc. Stainless steel (SS 316L) and titanium alloy (Ti-6Al-4V) test surfaces were fabricated using powder bed fusion, a metal additive manufacturing process. Engineered features, in the form of 250  $\mu\text{m}$  cavities, were placed on the shallow slopes of the asymmetric sawtooth surface to act as effective nucleation sites. Boiling experiments were conducted in the upward-facing and downward-facing orientations in the designed terrestrial setup. Apart from the surface orientation, parameters such as cavity density (1-mm or 2-mm apart), sawtooth structure (60°-30° or 75°-15°) were also studied. The downward-facing surface explored in this study is the bridge between the terrestrial and microgravity experiments, as buoyancy forces do not aid in detaching vapor bubbles from the surface.

Vapor mobility was observed in the downward-facing orientation for the asymmetric sawtooth microstructure. A thin liquid film was observed

between the microstructure and vapor bubbles, as they slid along the engineered surface. This observed film was non-uniform between the crest and trough of the sawtooth, providing insights into the dynamic nature of the induced motion. A baseline, flat test surface with no sawteeth showed stationary, growing vapor bubbles in the downward-facing orientation, validating the passive vapor mobility due to the asymmetric sawtooth in similar heat flux conditions as shown in Figure 1. Differences in vapor bubble mobility due to the sawtooth microstructure were observed with high-speed imaging, as the 75°-15° sawtooth structure rendered clear high-speed images compared to the 60°-30° structure in the downward-facing orientation. In the upward-facing orientation, test surfaces with cavities spaced 1-mm apart performed significantly better (~4.5 K lower wall temperature) than surfaces with 2-mm spaced cavities.

Validating the hypothesis of vapor mobility due to microstructured surfaces is essential to developing passive cooling solutions for electronic devices, to dissipate high heat fluxes in microgravity. The ability to cool a device without external pumps or complicated flow loops is especially critical in space applications, due to the limited amount of electrical power available. The upcoming ISS microgravity experiment (scheduled to launch in Fall 2020) is expected to provide further detail into vapor bubble dynamics from the microstructure.

## References

Thiagarajan, N., Bhavnani, S. H., & Narayanan, V. (2015). Self-propelled sliding bubble motion induced by surface microstructure in pool boiling of a dielectric fluid under microgravity.

## Affiliations

Department of Mechanical Engineering, Auburn University

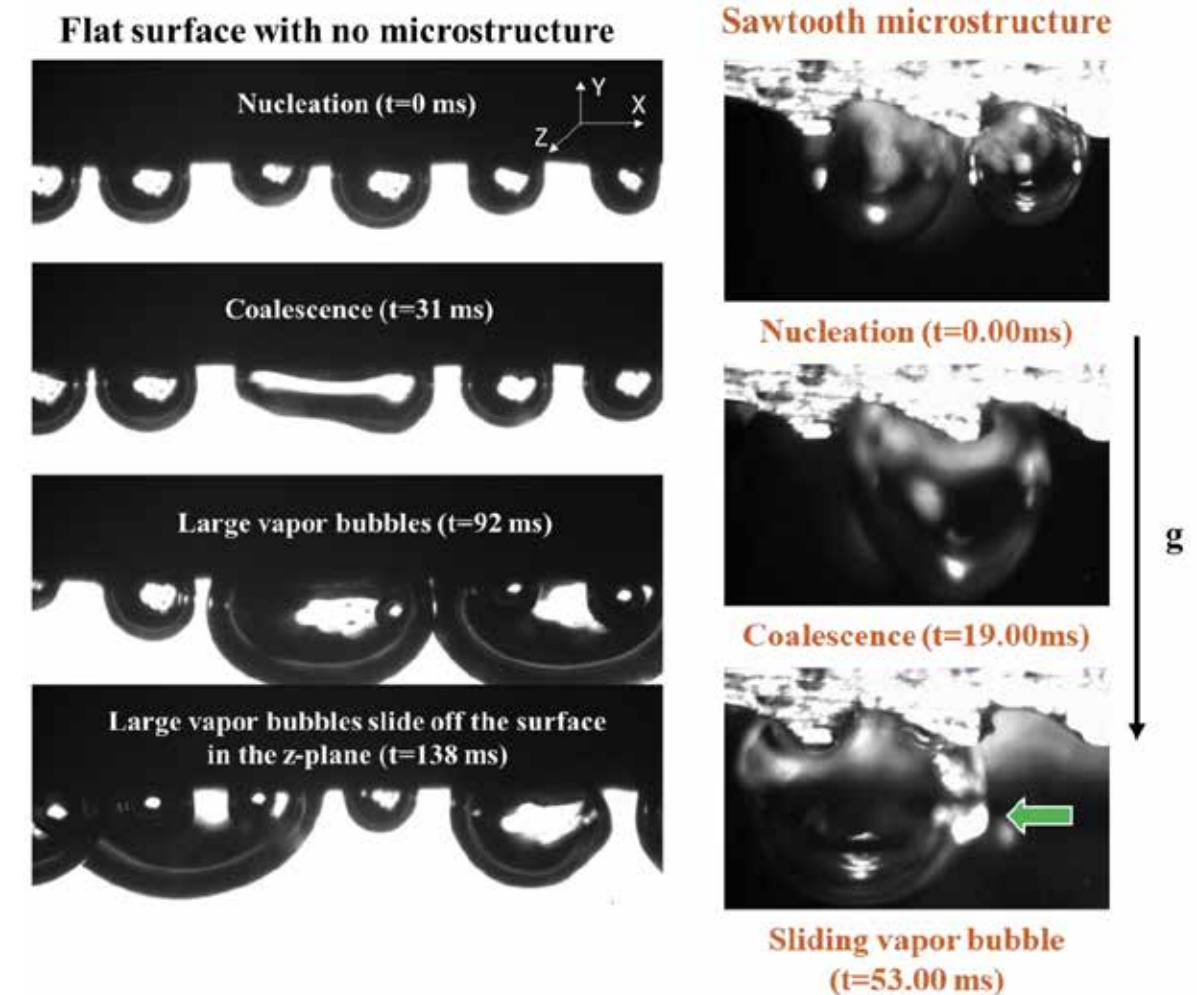


**Figure 1.** Comparison in vapor bubble dynamics between a flat and sawtooth-microstructured test surface in the downward-facing orientation is shown. Large vapor bubbles on the flat surface lead to a situation with poor heat transfer, while the sawtooth microstructure passively enables vapor bubble mobility.

# Development of MATLAB Trip/Slip Algorithms to Investigate the Effectiveness of Treadmill-Based Perturbation Training

Jacob Stotser<sup>1</sup> and Jaimie Roper<sup>2</sup>

Falls are the main cause of unintentional injury among older adults (Gudnadottir et al., 2018). Over a quarter of the population 65 or older suffers a fall each year, resulting in nearly a million hospitalizations and many more emergency treatments (Bergen et al., 2016). Perturbation training is growing in popularity for researchers and interventionists interested in lowering fall risk in aging and disabled populations. This type of training allows the researcher to measure an individual's ability to react to typical perturbations, such as trips and slips, in a safe environment at varying levels of user-specific intensity. Further, recent literature has indicated its effectiveness for improving dynamic balance control and decreasing fall incidence in at-risk groups (Chien & Hsu, 2018; Mansfield et al., 2015). Because of the widespread availability of treadmills in laboratory and clinical settings, treadmill-based perturbation training paradigms are of particular interest to researchers and clinicians. We aimed to develop unique treadmill-based perturbation software providing more realistic fall scenarios than existing options through greater control and customization.

MATLAB algorithms were developed to simulate both tripping and slipping perturbation patterns through a treadmill. These algorithms were then merged with a graphical user interface (GUI) featuring an intuitive layout and various safety features. An image of this GUI is shown in Figure 1. The “Trip/Slip” input box controls the initial direction of the perturbation with respect to the walking direction. In this software, a “trip” is characterized by an initial acceleration in the direction of walking, and a “slip” is characterized by an initial acceleration opposite the direction of walking. In addition to selecting between those two patterns, an optional “stutter-step” acceleration preceding the main perturbation can be added. Perturbation intensity can be adjusted by entering values for belt acceleration magnitude and acceleration time in the “Accel” and “Timestep” input boxes, respectively. The trip/slip can

be delivered through the right, left, or both treadmill belts using the “Trip Belt” input box. The perturbations can be triggered either immediately upon mouse-click or at varying points during a single-leg gait cycle using real-time force data provided by an instrumented treadmill. This software also features split-belt walking support, allowing for perturbations while the treadmill belts are moving at different speeds. Trip/slip trials can be imported to or exported from the GUI using a custom spreadsheet template. Multiple back-end safety checks were implemented to prevent potentially dangerous perturbations.

These algorithms were also integrated with existing Self-Selected-Walking software, allowing the user to walk at a continuously self-selected speed while experiencing perturbations; however, additional testing is required to ensure safety and repeatability of this feature. Continuing, this software will be used to examine the effects of dual-tasking paradigms on motor control adaptation during treadmill-based perturbation training. Ultimately, this software will be used to identify fall-risk and as a preventative training tool to decrease falls in the Auburn/Opelika aging community.



Figure 1. Treadmill User Interface

## References

- Bergen, G., Stevens, M. R., & Burns, E. R. (2016). Falls and fall injuries among adults aged  $\geq 65$  years — United States, 2014. *MMWR. Morbidity and Mortality Weekly Report*, 65(37), 993–998.
- Chien, J.-E., & Hsu, W.-L. (2018). Effects of dynamic perturbation-based training on balance control of community-dwelling older adults. *Scientific Reports*, 8(1).
- Gudnadottir, M., Thorsteinsdottir, T. K., Mogensen, B., Aspelund, T., & Thordardottir, E. B. (2018). Accidental injuries among older adults: An incidence study. *International Emergency Nursing*, 40, 12–17.

Mansfield, A., Wong, J. S., Bryce, J., Knorr, S., & Patterson, K. K. (2015). Does perturbation-based balance training prevent falls? Systematic review and meta-analysis of preliminary randomized controlled trials. *Physical Therapy*, 95(5), 700–709.

## Affiliations

<sup>1</sup> Department of Mechanical Engineering, Auburn University

<sup>2</sup> School of Kinesiology, Auburn University

# Investigating Late-Stage Polypeptide Diversification via Formation of Twisted Amides

Xavier Streety, Mahesh Sriram, Victor Adebomi, and Monika Raj

Peptides occupy a biomolecular niche between small molecules and proteins. Given that they can function not only as substrates in biochemical pathways but as signaling molecules, peptide therapy presents a unique opportunity for medicine to closely mimic natural pathways (Fosgerau & Hoffman, 2015). As new challenges such as mutant viral and bacterial strains with resistance arise, the need for modification of peptide therapeutics has increased. In recent years, the use of acyclic twisted amides as reactants for cross-coupling reactions has been investigated. These twisted amides feature a distorted amide bond which has reduced double bond character and thus allows for the incorporation of various functional groups (Liu & Szostak, 2017).

We sought to find a method to selectively introduce these twisted amides into peptides and test their reactivity toward cross coupling and nucleophilic acyl substitution reactions to introduce new functionalities. Amide bonds form the backbone of peptides and thus are a desirable synthetic handle for modification. Therefore, methodology to selectively modify the amide backbones of peptides leads to more possible peptide derivatives.

We started this process by investigating oxazolidinone and thiazolidinone, derivatives of serine and cysteine, respectively, using density functional theory (DFT) calculations to determine whether these structures exhibited a twisted amide bond. DFT is computational quantum mechanical modeling method used to investigate the electronic structure of large molecules. From these initial calculations we determined four potential moieties capable of twisting

the amide backbone of peptides: the aforementioned oxazolidinone and thiazolidinone structures in addition to their thiocarbonyl analogs.

Following the calculations, we moved to the synthesis of these moieties on small molecules before moving to the synthesis of these moieties on peptides. Following each step of synthesis, each product was purified using silica gel chromatography and confirmed by mass spectrometry and nuclear magnetic resonance (NMR). For small molecules, the methyl ester derivative of either serine or cysteine was used as a starting point. These small molecules with added carbonyl or thiocarbonyl groups were then reacted with benzoyl chloride to yield the desired potential twisted amide functionality. These potential twisted amides were tested as reactants in cross coupling and nucleophilic acyl substitution reactions.

Work on small molecules gave positive results as these molecules featuring twisted amide moieties were successfully used in transamidation, esterification, Suzuki-Miyaura coupling, and Friedel-Crafts acylation. These results support the formation of twisted amides as a method to introduce modifications to peptides.

The introduction of twisted amides to tripeptides is ongoing. The general scheme of this process is outlined in Figure 1. Once these twisted peptides are formed, they will be tested as reactants in the previously mentioned reactions to form modified peptide derivatives. Positive results with these twisted tripeptides support the application of twisting amide bonds as a method for late-stage peptide diversification.

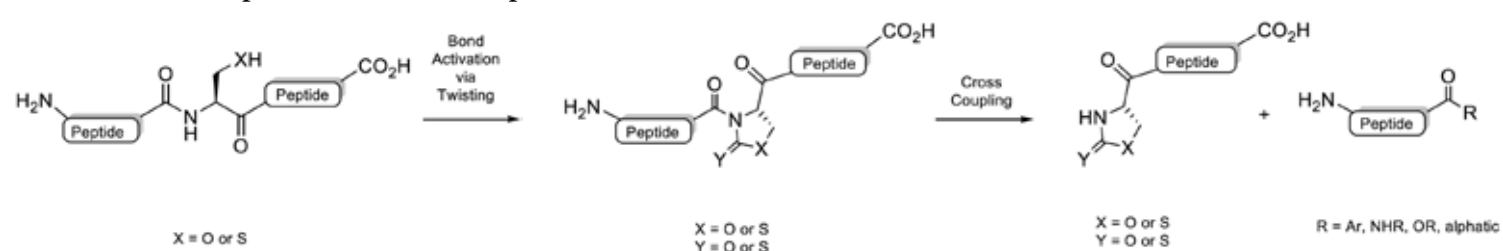


Figure 1. General scheme for peptide diversification using twisted amides.

## References

Fosgerau, K., & Hoffmann, T. (2015). Peptide therapeutics: Current status and future directions. *Drug Discovery Today*, 20 (1), 122–128. <https://doi.org/10.1016/j.drudis.2014.10.003>

Liu, C., & Szostak, M. (2017). Twisted amides: From obscurity to broadly useful transition-metal-catalyzed reactions by N–C amide bond activation. *Chemistry – A European Journal*, 23 (30), 7157–7173. <https://doi.org/10.1002/chem.201605012>

## Affiliations

Department of Chemistry and Biochemistry,  
Auburn University

# Auburn University and the United Nations' Sustainable Development Goals

*Hollen Terry and Alicia Powers*

As Auburn University continues to build its standing nationwide as an innovative and prestigious institution, multi-faceted, interdisciplinary scholarship is essential. The United Nations has outlined 17 Sustainable Development Goals (SDGs) that aim to enhance the quality of life for people worldwide by improving environmental, social, and economic conditions globally by 2030. The purpose of this project is to describe Auburn University's engagement with the United Nations' SDGs through teaching, research, and outreach from 2016 to 2018.

Teaching, research, and outreach includes all courses, majors, minors, graduate programs, departmental research, centers and institutes, and student organizations across the university. Using data and expertise from the Hunger Solutions Institute (HSI), Office of Sustainability (OOS), and Academic Sustainability Programs (ASP), researchers developed an inventory of sustainability-related teaching, research, and outreach within every college, school, and discipline. The data we used was collected by ASP for use in the triennial Association for the Achievement of Sustainability in Higher Education Sustainability Tracking, Assessment, and Rating System (AASHE STARS) report. HSI research assistants coded all inventory entries for the SDG with which it was most closely related. For example, the course *HUSC 2000: Hunger Causes, Consequences, and Responses* most closely aligns with the second SDG, to achieve zero hunger by 2030. Coding was cross-examined by a different HSI research assistant to ensure each sustainable development goal was appropriately paired with each inventory entry.

Based on how often each of the 17 SDGs related to inventory entries, we were able to discern the six SDGs that are the most represented and the four SDGs that are the least represented at Auburn.

The six SDGs which were most represented across all categories were goals 3, 12, 15, 10, 9, and 11. Those goals are described as follows.

- |  |   |
|--|---|
| 3: Good health and wellbeing               | 10: Reduced inequalities                    |
| 12: Responsible consumption and production | 9: Industry, innovation, and infrastructure |
| 15: Life on land                           | 11: Sustainable cities and communities      |

The four goals which were the least represented across all categories were goals 17, 1, 4, and 5. Those goals are described as follows,

- |                                   |                      |
|-----------------------------------|----------------------|
| 17: Partnerships to achieve goals | 4: Quality education |
| 1: No poverty                     | 5: Gender equality   |

While the data collection and coding process was thorough, we experienced some limitations which are to be expected of a report of this scale. The HSI research assistants who coded all teaching, research, and outreach did so with access only to course and program descriptions, research abstracts, and organizational mission statements. HSI team members did not always have access to syllabi or experiential knowledge of courses, programs, etc.

Our report may be used by university administration, faculty, and students to learn more about each of the 17 SDGs as well as gain insight into what the university

is already doing to support each goal. While there are four goals where the university can lend more attention, those four goals are represented in at least one category. By highlighting the four goals that are underrepresented, the university can celebrate those efforts that are already being made to support those goals. It is also important to prioritize increased attention to those underrepresented goals. The United Nations' SDGs are a common thread pulling the world forward together, and Auburn University can be proud of how well it has begun to direct its teaching, research, and outreach toward achieving a higher quality of life for people worldwide.

## Affiliations

Hunger Solutions Institute, Auburn University

# Effect of Different Inlet Velocity Profiles on Patient-Specific CFD Simulations of Healthy Trachea

Bipin Tiwari<sup>1</sup>, Tarun Kore<sup>2</sup>, Zhenglun Alan Wei<sup>3</sup>, Sandeep Bodduluri<sup>4</sup>, Surya P. Bhatt<sup>4</sup>, Vrishank Raghav<sup>1</sup>

Common Obstructive Pulmonary Disease (COPD) is a respiratory disease which is the third leading cause of death in the world. A recently discovered phenomenon Expiratory central airway collapse (ECAC) linked with COPD, defined by >50% collapse of large airways during expiration, resulting from either cartilaginous weakening or redundancy of the posterior membranous wall of the trachea, is an increasingly recognized disorder. Pathophysiology of ECAC is multifactorial and the biomechanics of airflow in the trachea could be an important factor resulting in the progression of the disease. As detail flow characteristics through airway will help in early diagnosis of the disease and its treatment, which could lead to improvement in quality of life. Thus, one of the viable methods to study detail flow characteristics is Computational Fluid Dynamics (CFD). So, this study is done with collaboration from University of Alabama at Birmingham (UAB) to do the preliminary CFD study with healthy patient-specific trachea. Hence, the objective of the present study is two-fold, 1) to simulate a) steady flow and b) nominal tidal flow simulation through trachea and 2) to study both steady and tidal flow case simulation using different inlet velocity profiles a) flat profile and b) parabolic profile and c) Womersley profile for inhalation phase. We aim to compute flow field metrics such as wall shear stress variations along with Time-Averaged Wall Shear Stress (TAWSS) from these simulations.

The 3D geometry of five patient-specific healthy tracheas obtained from the computed tomography (CT) scans were smoothed and clipped with 3D slicer (V4.8.1; www.slicer.org) as shown in Figure 1a. The processed model was saved into Standard Tessellation Language (STL) format. Then, Solidworks (solidworks corp., Waltham, USA) was used to simplify the inlet and outlet boundaries of the trachea model as shown in Figure 1b.

The trachea model was imported to ICEM CFD (ANSYS Inc., Pennsylvania, USA) where an unstructured mesh was generated with a mixture of prism and tetrahedral elements plus prism mesh method as shown in Figure 1c. Depending on the size of the trachea model, the number of elements was around 1.2 M and the element size was set around 1% of the inlet diameter. The file from ICEM CFD was exported to fluent format to conduct the flow simulations.

ANSYS-Fluent (ANSYS Inc., Pennsylvania, USA) flow solver was used for steady and transient simulation with SST K-omega flow model simulations. The boundary condition for the inlet portion which is near the mouth was given a velocity boundary condition and a pressure outlet condition accounting pressure drop due to resus. The velocity boundary condition was selected from the healthy adult data having tidal volume of 500ml with 12 breaths per minute (Qi et al., 2017). A pressure-based solver with a simple pressure-velocity coupling scheme and a second order spatial discretization of pressure and momentum was used for each simulation in ANSYS-Fluent. Continuity and velocity residuals values were set to  $1 \times 10^{-3}$  as a convergence criterion.

- The following results were observed from the study:
1. The spatial average WSS of the flat profile is 220% higher than other profile (Figure 2a)
  2. The spatial average TAWSS of the flat profile is 330% higher than other profile (Figure 2b)

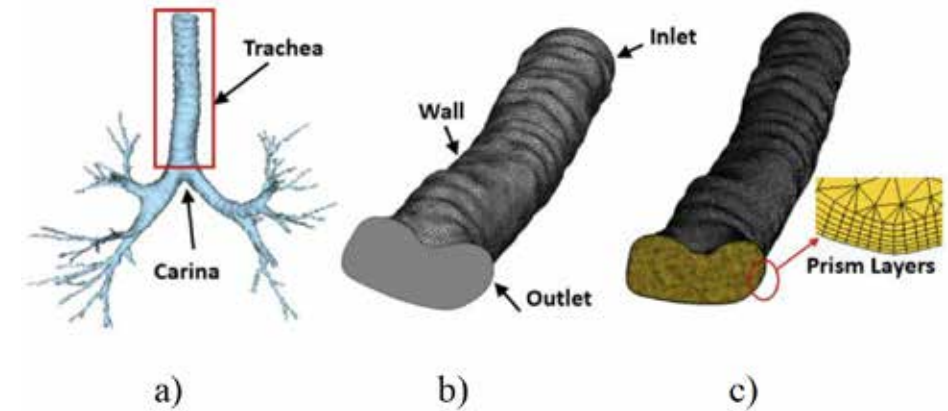


Figure 1. a) Smoothed and clipped trachea geometry with 3D slicer; b) Simplified geometry with Solidworks; c) Mixture of prism and tetrahedral elements

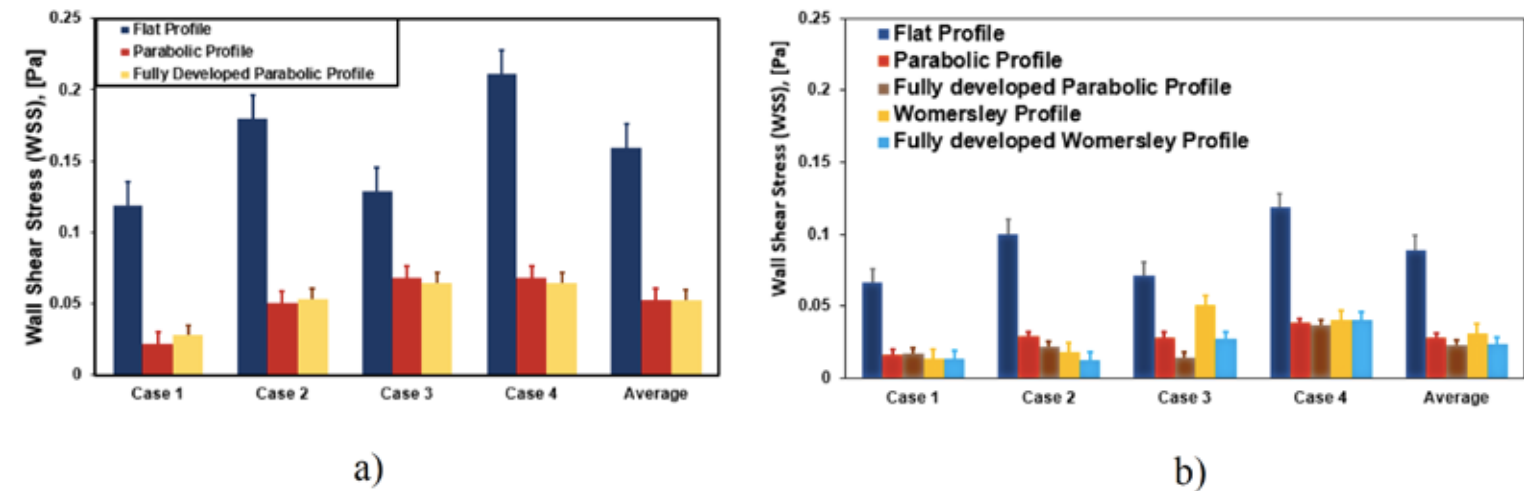


Figure 2. a) Comparison showing three different idealized velocity profile for steady flow b) Comparison showing TAWSS for all five idealized velocity profile

In this study, it is concluded that the use of a simplified velocity profile influences the WSS and TAWSS results for both steady and tidal flow cases

## References

Qi, S et al. (2017). *Computational and Mathematical Methods in Medicine*.

## Affiliations

<sup>1</sup> Department of Aerospace Engineering, Auburn University

<sup>2</sup> Department of Chemical Engineering, Auburn University

<sup>3</sup> Wallace H. Coulter School of Biomedical Engineering, Georgia Institute of Technology

<sup>4</sup> Department of Medicine, University of Alabama at Birmingham

# A Method of Containing Near-Source Undegraded Floating Plastic

Zachary Wadzinski<sup>1</sup> and Mark Dougherty<sup>2</sup>

Plastic packaging represents the majority of the macroscopic waste found in waterways around the globe. Only 14% of plastic packaging is collected for subsequent recycling. A recent modelling study has shown that between 0.41 and 4 million tons of plastic is sent to the ocean via rivers annually (Crippa et al., 2019). Plastic waste finds its way to the ocean in a multitude of ways. After starting in factories, it follows a chain of events from consumer to waterway and finally the ocean. The focus of this paper is on the rivers and streams that link to the ocean from said chain. A cylindrical obstruction was modeled in a stream to create a downstream vortex to capture in-stream plastic waste before it can be transported further downstream. To measure the effectiveness of modeled vortices two parameters were used; recirculation,  $\Gamma$  and recirculation length,  $l_c$ . Above parameters were tested using a variety of simulated, in-stream cylinder diameters, including 1 ft, 2 ft, 5 ft, and 10 ft.

Three different stream sizes were considered and modeled: Alabama River, Flint River, and Chewacla Creek. Each stream varies greatly in discharge rate, cross-sectional area, and velocity. Using values of velocity, area, and discharge rate for each stream, characteristics of vortex generation were determined. Computational results for each stream, cylinder, and recirculation vortex were quantified using Ansys<sup>TM</sup> Fluent<sup>TM</sup>. All simulations completed in this study were in two dimensions. The vortex recirculation ( $\Gamma$ ) and recirculation length ( $l_c$ ) was measured. Recirculation is defined as

$$\Gamma = \oint \mathbf{V} \cdot d\mathbf{l} \quad (1)$$

where  $\mathbf{V}$  is the fluid velocity on a small element defined curve and  $d\mathbf{l}$  is the differential length of the small element used. Recirculation length is defined as

$$l_c = \frac{l}{d} \quad (2)$$

where  $l$  is the length of the vortex and  $d$  is the diameter of the cylinder. An additional hypothetical river,

X-river, was added to demonstrate vortices shedding at a faster flowrate relative to the other streams evaluated. The X-river was simulated with a velocity of 8.9 ft/s compared to 0.56 ft/s in the Chewacla, 1.23 ft/s in the Alabama and 2.52 ft/s in the Flint.

As seen in Figure 1, recirculation,  $\Gamma$ , increased in strength with stream discharge rate and velocity. Thus, the faster the stream, the higher the recirculation value of the vortex. The recirculation length proved to be positively correlated with stream velocity; the faster the stream, the larger the recirculation length. Cylinder diameter was shown to decrease circulation length. This trend is more prevalent streams with higher velocity such as the Flint and X-river.

It was concluded that the oscillation frequency of the vortex is essential for vortex shedding (creation), as follows. Larger cylinders reduce the stability of the vortex resulting in lower recirculation lengths and recirculation. This is due to the increased area the water has to move around the cylinder for vortex shedding to occur. The Flint River proved to be the most suitable stream in this study for potential plastic capture due to it having the highest average discharge rate and velocity; which resulted in higher recirculation and recirculation length. After determining  $l_c$  and  $\Gamma$ , this study had planned to simulated plastic waste to determine the efficiency of capture in the circulation vortex,  $\eta_p$ . This research component however was removed, however, due to the arrival of COVID-19. Additional research into methods that are most beneficial for efficiency of capture in the circulation vortex could be explored using  $\eta_p$ .

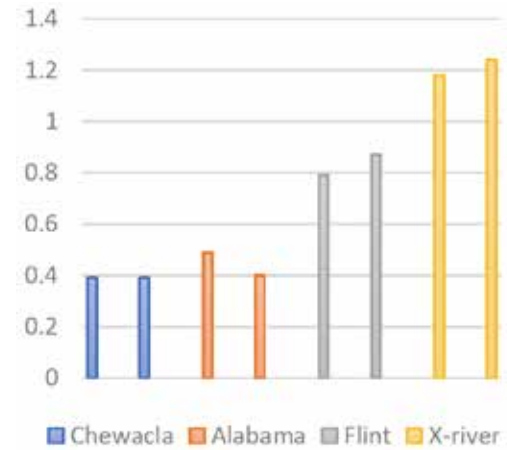


Figure 1. Two-Foot Diameter Recirculation Length  $l_c$  Compared at Varying Flow Rates

## References

Crippa, M., De Wilde, B., Koopmans, R., Leysens, J., Muncke, J., Ritschkoff A-C., Van Doorselaer, K., Velis, C., & Wagner, M. (2019). *A circular economy for plastics – Insights from research and innovation to inform policy and funding decisions*. (M. De Smet & M. Linder, Eds.) European Commission, Brussels, Belgium.

## Affiliations

<sup>1</sup> Department of Aerospace Engineering, Auburn University

<sup>2</sup> Department of Biosystems Engineering, Auburn University

# Biocidal Properties of Europa Lander Solid Rocket Motor Adhesive, Loctite® EA9394, Against *Hypsibius dujardini*

Natalie Williams, Mark Liles, and Morgan Sisk

An ice-covered moon of Jupiter, Europa, is a prime candidate as a potentially viable environment in NASA's search for extraterrestrial life. Since Europa is a viable celestial body unlike any NASA has explored before, new issues regarding forward contamination of Europa and sterility of the spacecraft arise. These novel problems that often accompany exploration of new frontiers must be solved in accordance with NASA planetary protection standards, and the launch of the Europa Lander is ultimately contingent upon the fulfillment of these criteria.

The Europa Lander Mission launch criteria requires spacecraft decontamination of terrestrial microorganisms to limit the probability of contaminating the surface of Europa. These standards include reducing microorganisms present on the lander by at least  $10^{-6}$  and a final European contamination probability of  $10^{-4}$  %. For the mission to be a success, the microbiome of certain spacecraft problem areas must be quantified, and the inherent antimicrobial or biocidal properties of native rocket motor materials must be characterized. We discovered that a frequently used rocket motor adhesive, Loctite® EA9394, can reduce the number of viable *Bacillus atrophaeus* vegetative cells by 10 million-fold, and spores by greater than 100-fold, after short term exposure. Though spore-forming bacteria have traditionally been the primary targets of planetary protection efforts, eukaryotic *Hypsibius dujardini* (i.e. tardigrades, or “water bears”) is the best animal model for planetary protection given their known resistance to radiation, desiccation, and space environments. This study evaluated susceptibility of *H. dujardini* to exposure to Loctite® EA9394.

Viability assays were performed with populations of active *H. dujardini* in water and several concentrations of water-soluble extracts of Loctite® EA9394, using 70% ethanol as a positive control and spring water as a negative control. Final concentrations of extracts in solution ranged from 1.6 mg/mL to 0.025 mg/mL. After 24

hours, each replicate was observed under a microscope at 100X magnification. Immobile tardigrades were classified nonviable while spontaneously mobile tardigrades were classified viable.

We found that increasing adhesive concentration correlated with an increase in tardigrade death. There was a statistically significant difference of percent viability from 1.6 to 0.8 mg/mL of extract when compared to negative control, corresponding to 100% and 94.9% viability reduction, respectively. In summary, active *H. dujardini* populations suffered an average of 100% viability loss when exposed to 1.6 mg/mL of desiccated water-soluble extracts for 24 hours. The minimum inhibitory concentration at which 50% viability was observed ( $MIC_{50}$ ) was approximately 0.2 mg/mL.

The results of this study suggest the risk posed by radiation and desiccation-resistant *H. dujardini* could be mitigated through the biocidal activity of Loctite® EA9394. These reductions can be incorporated into the launch risk assessment for the Europa Lander Mission. As this is an ongoing project, next steps include inducing anhydrobiosis in *H. dujardini* and testing these dormant, extremotolerant populations against Loctite® EA9394 to calculate percent viability reductions as done before, as well as identifying the sporicidal and tardigradicidal compounds in the adhesive through mass spectrometry.

## References

NASA HDBK 6022-Handbook for the Microbial Examination of Space Hardware. (2010).

National Research Council. (2000). *Preventing the Forward Contamination of Europa*. The National Academies Press.

## Affiliations

Department of Biological Sciences, Auburn University

# Determining How Images of Different Exercise Contexts Are Spontaneously Registered in the Brain of Non-Exercisers via Electroencephalography (EEG)

Victoria A. Zona, Juliana O. Parma, and Matthew W. Miller

Physical inactivity continues to be an issue in our world today. Regular participation in physical activity decreases the risk of obesity, heart disease, depression, and many other diseases that result from physical inactivity. In the field of exercise psychology, exercise images are commonly used to evaluate how participants perceive and evaluate exercise and can be used to promote exercise behavior and well-being. People's spontaneous evaluations of exercise can influence their likelihood of engaging in exercise; thus, it is important to determine what kind of exercise stimuli are spontaneously evaluated as positive so that such stimuli can be used to promote exercise. In recent studies, spontaneous (implicit) processing of exercise images has been shown to differ from explicit ratings of exercise images in regular exercisers and non-exercisers alike. The implicit processing of images as a function of exercise type and setting is yet to be determined. To address this, we used an electroencephalographic (EEG) oddball paradigm in order to evaluate whether non-exercisers implicitly prefer certain exercise contexts over others.

Nineteen participants engaged in an oddball paradigm that presented images of different exercise contexts interspersed randomly within series of positive, negative, and neutral images. The different exercise contexts presented were indoor gym-type exercise, indoor sport-type exercise, outdoor-gym type exercise, and outdoor-sport type exercise. Participants (explicitly) rated images in terms of whether they thought the images shown were positive or negative by making selections on a keyboard, with the number 1 denoting positive and 2 denoting negative. Implicit evaluations were assessed using the amplitude of the P3b component of participants' electroencephalography (EEG)-derived event-related potentials (ERPs) evoked by the exercise images. Crucially, P3b amplitude reflects implicit affective processing such that small P3b amplitudes

indicate the exercise image is processed like the other images in the series. For example, if an exercise image is presented in a series of positive images and evokes a small P3b, then the exercise image is implicitly processed as positive.

Results suggest that non-exerciser participants had similar implicit and explicit affective associations with the different types of exercise images, but the participants allocated more neural resources to processing outdoor images and gym-type images. Thus, outdoor and gym-type exercise images may elicit greater cognitive processing than indoor and sport-type images when used to promote exercise. In conclusion, the context of exercise images may influence the magnitude of implicit cognitive processing of the images, but not the implicit or explicit affective processing of the images.

Explicit ratings results (shown in Figure 1) showed that participants rated exercise images as positive a similar percentage of time irrespective of setting or type.

## Affiliations

School of Kinesiology, Auburn University

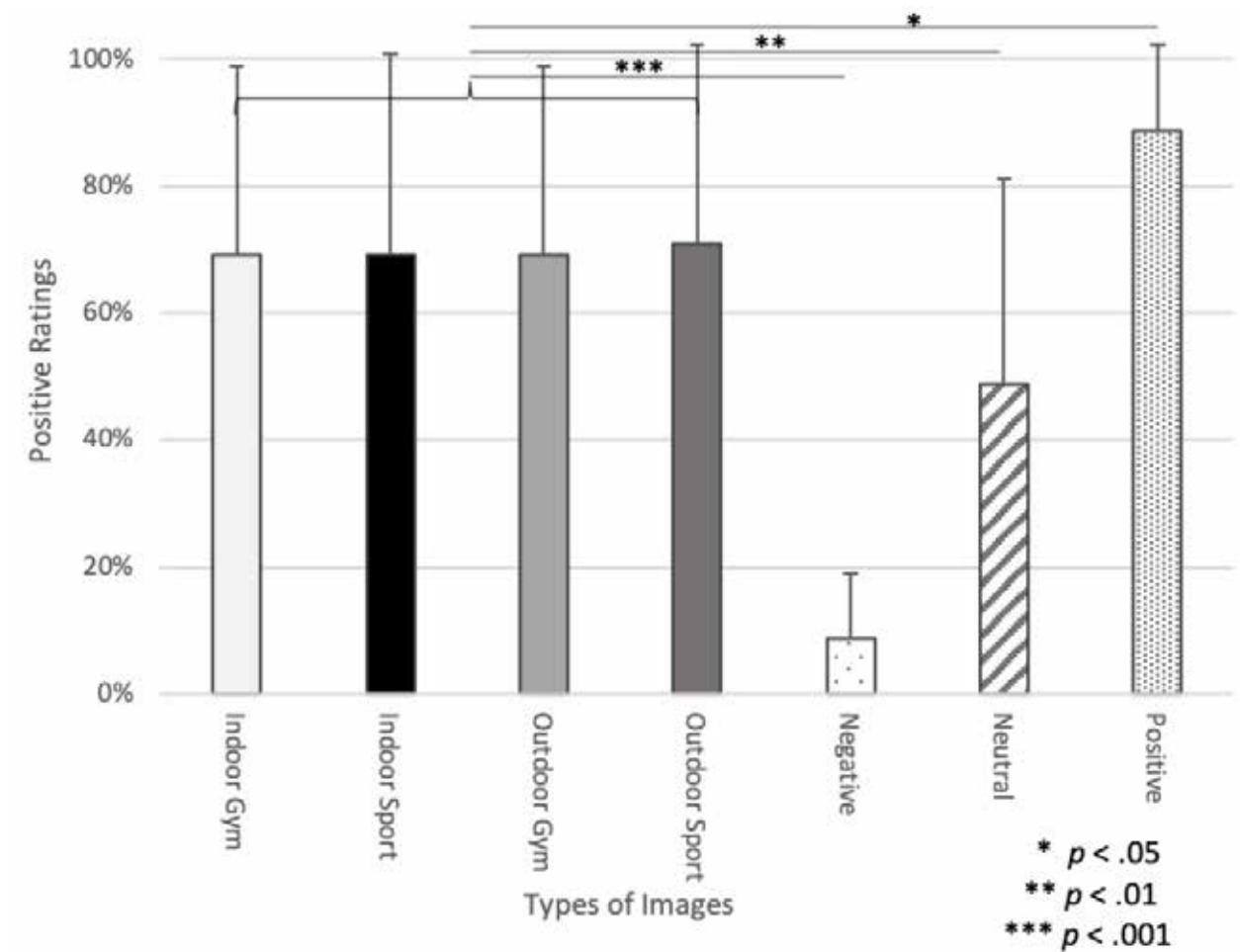


**Figure 1.** Participants rated exercise images as positive significantly more often than they rated negative or neutral images as positive ( $p_s < .001$  and  $p \leq .039$ , respectively), and significantly less often than they rated positive images as positive ( $p_s \leq .016$ ). The error bars denote standard deviation.



AUBURN  

---

UNIVERSITY

**Undergraduate Research**  
206 Cater Hall  
Auburn, AL 36849  
[aub.ie/researchstudentsymposium](http://aub.ie/researchstudentsymposium)